LOW-FREQUENCY CHARACTERIZATION OF SWITCHED dc-dc CONVERTERS

Thesis by

Gene Ward Wester

In Partial Fulfillment of the Requirements

for the Degree of

Doctor of Philosophy

California Institute of Technology

Pasadena, California 91109

1972

(Submitted May 12, 1972)

To

Marge, Janice, and David

ACKNOWLEDGMENTS

For continuing encouragement and advice throughout the course of this work, the author wishes to convey his deepest appreciation to Dr. R. D. Middlebrook. Unrestricted use of an analog computer was generously provided by Dr. R. E. Kaplan at the Hybrid System Simulation Laboratory at the University of Southern California. The typing dexterity of K. Ellison is to be commended.

Financial support by way of Teaching Assistantships from the California Institute of Technology and National Science Foundation Fellowships is gratefully acknowledged.

ABSTRACT

Techniques are developed for the approximate representation of switched dc-dc converters by time-averaged models. Simple analytical expressions in terms of the circuit components are derived for the characteristic transient and frequency responses of averaged power-stage models for use in designing and understanding the behavior of the actual switched power stages. High-order systems can be analyzed by the averaging technique without a commensurate increase in complexity.

Two functional blocks are necessary to construct a switched converter: the switch controller, which is relatively well understood, and the power stage. When concreteness is necessary, a particular pulse-width modulator is chosen for the switch controller and is thoroughly analyzed. The output of representative power stages (buck, boost, and buck-boost) is a complicated nonlinear function of the switch controller and source input, and since conventional methods of nonlinear analysis are shown to be intractable or uninterpretable, attention is focused on the challenge of obtaining useful design equations.

The difficulty encountered in the nonlinear analysis of switched power stages is successfully surmounted by the semiheuristic development of a continuous power-stage model. Since the characteristic response times of state variables in the switched power stage are invariably large with respect to the switching period, discontinuous forcing functions in the equivalent circuits are averaged over a time interval comparable with the switching period without appreciably affecting the nature of

the response. Consequently, the averaged model is limited to response times greater than the averaging interval. Equivalent circuits and analytic expressions for the transient and frequency response of each power-stage type are then derived from the averaged models. A linearized control-input transfer function, obtained for small amplitude variations of the averaged control, reveals a dependence of effective circuit component values upon the switch duty ratio, and the possible existence of a positive real zero.

The unusual behavior predicted above is confirmed by an analog computer simulation of both the switched and averaged power stages. It is also shown experimentally that closed-loop stability of the switched power stage is adequately predicted by the averaged model. The averaging technique is thus a powerful analytical tool for exposing inherent characteristics of switched circuits.

TABLE OF CONTENTS

LIST OF ILLUSTRATIONS

Chapter 1

INTRODUCTION

Electrical loads often require a dc voltage at some particular value, even though the only available dc source voltage has a different value: for example, the mélange of electrical equipment in a space vehicle is powered by a single dc source. The functional block which transforms voltage from a dc input value to a different dc output value is called a dc-dc converter and fulfills the need expressed above. The degree of dc-dc conversion should be controllable to adjust for possible variations in the source voltage or load current; in some applications another system consideration is conversion efficiency, which is defined as the ratio of converter output power to input power. Thus the need emerges for a dc-dc converter with the auxiliary features of control and high conversion efficiency.

Two dc-dc converters in common usage are shown symbolically in Fig. 1.1. The variable resistor exercises continuous conversion control, either by dropping source voltage with the series configuration shown in Fig. 1.1(a), or by shunting current from the load as in Fig. 1.1(b). Two important limitations are a direct consequence of the method used for conversion and control: output voltage must be less than the input voltage, and conversion efficiency may be low because conversion and control functions are obtained at the expense of power dissipation.

Switched dc-dc converters can overcome the limitation on efficiency which arises from dissipative conversion methods. The observation that

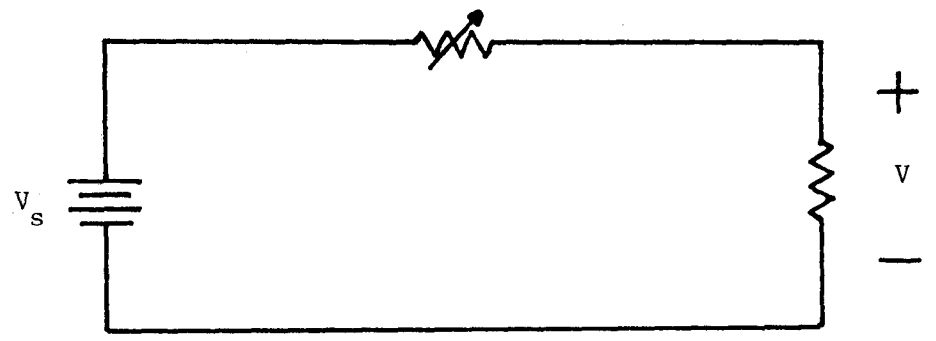

(a)

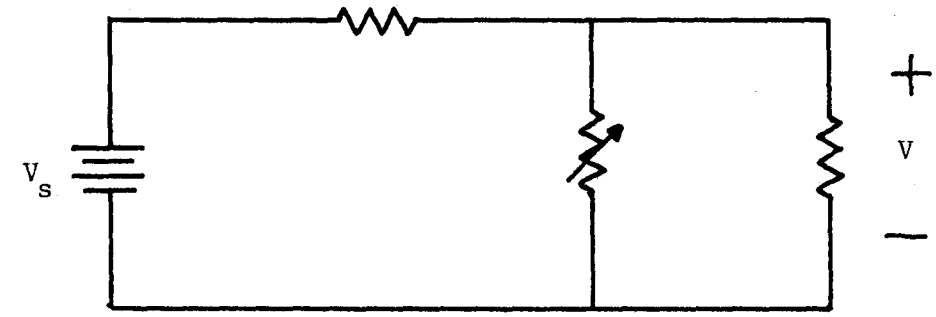

(b)

Fig. 1.1 Conventional dc-dc converters: (a) series control, (b) shunt control.

periodic pulse waveforms have an average value which varies with the ratio of pulse width to pulse period, as illustrated in Fig. 1.2, is the basis underlying switched control. Figure 1.3 shows how the average value of a pulse waveform generated from the source voltage with an ideal switch can be extracted by a low-pass filter (lossless for high efficiency) whose cut-off frequency is less than the switching frequency. Since no power is dissipated in ideal switches[1] or lossless filters, the theoretical conversion efficiency of switched dc-dc converters is 100 percent. A consequence of low filter cut-off frequency is slow filter response: output variations, with the exception of ripple at the switching frequency caused by incomplete filter cut-off, occur on a time scale greater than the switching period. As a practical matter, the use of a high switching frequency permits a reduction of size and weight of the passive filter components; however, switch and filter losses which increase with frequency force the adoption of an upper bound on frequency in order to maintain high conversion efficiency.

Switched dc-dc converters consist of two distinct subblocks: the basic power stage contains those circuit components, essential for the conversion operation, through which the power flows; and the controller determines the degree of dc-dc conversion in the power stage. Typical characteristics of each subblock are expanded upon in the following discussion.

---

[1] Either the current through or the voltage across an ideal switch is always zero.

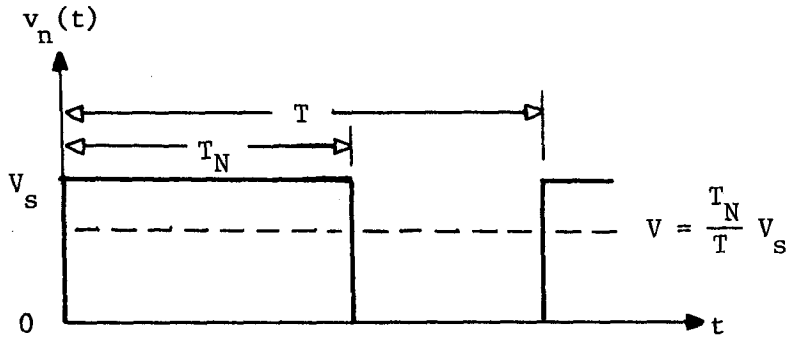

Fig. 1.2 Dependence of a switched waveform average upon relative pulse width.

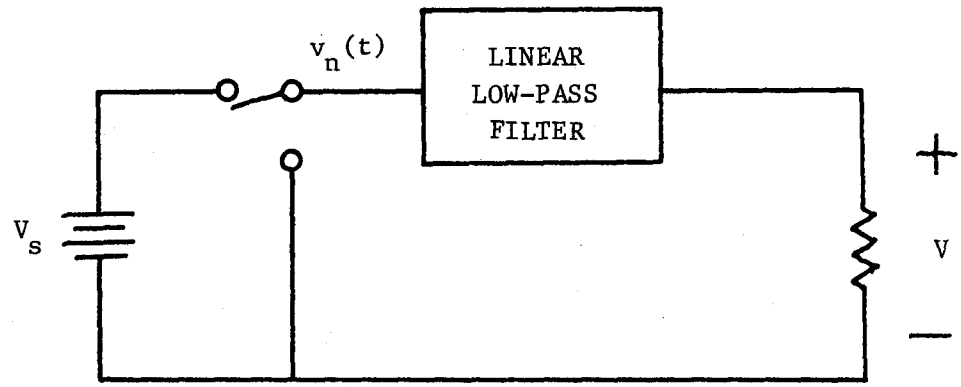

Fig. 1.3 Conceptual implementation of a switching dc-dc converter.

A generalized control mechanism for varying the dc value of the converter output is the switch duty ratio D, which is defined as the fraction of time that the switch is closed: the correspondence between switch state and pulse waveform is evident in Figs. 1.2 and 1.3. A controller determines the switch duty ratio by generating from an analog controller input ε a digital (two-level) switch-drive d which uniquely defines the switch state (open or closed); thus the switch controller is functionally an analog-to-digital (A/D) converter as depicted in Fig. 1.4(a). The controller output consists of constant-amplitude pulses whose duration T_N and spacing T_F are determined by the controller input. Without loss of generality one can choose unity and zero (corresponding to closed and open switch states, respectively) for the two output levels; consequently, D is numerically equal to the dc component of d. Typical controller output waveforms are shown in Figs. 1.4(b) and 1.4(c) for two values U and U' of dc controller input and are periodic in time, with periods $T = T_N + T_F$ and $T' = T_N' + T_F'$, respectively.

For a dc controller input U, the duty ratio associated with the static output waveform may or may not be a linear function of U, depending on the specific controller; however, the instantaneous controller output d is always a nonlinear function of the instantaneous input ε for a variety of reasons. If superposition were valid for the controller, then the output resulting from N inputs could have any integer value between 0 and N inclusively, which is contrary to the assumed output levels of 0 and 1. Also, the Fourier series expansion of the periodic

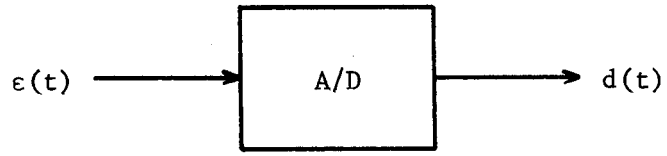

(a)

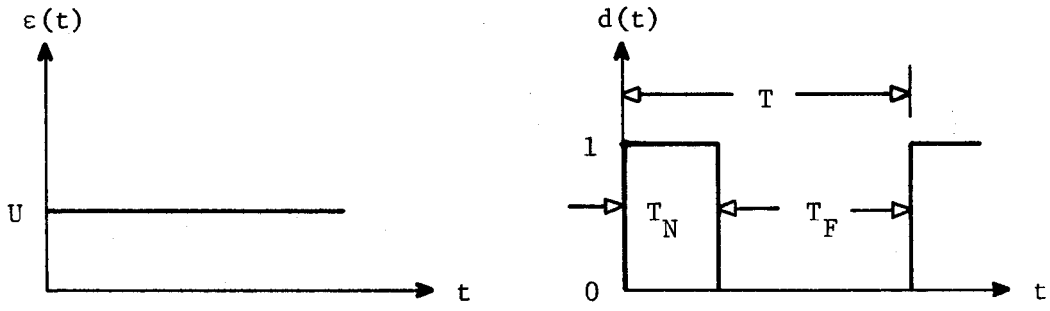

(b)

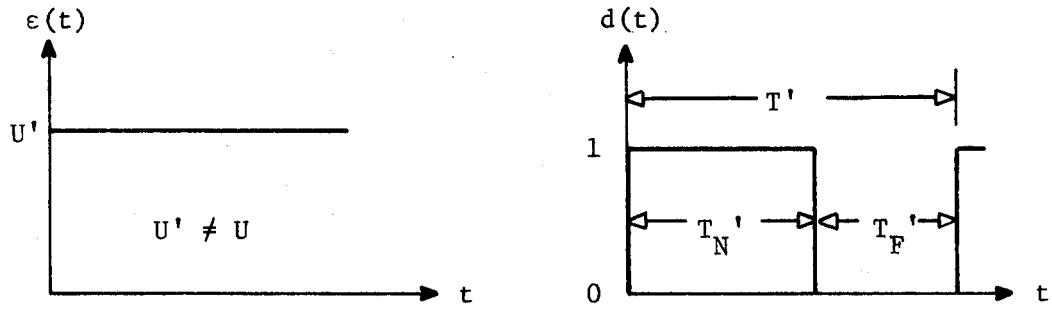

(c)

Fig. 1.4 Description of a switch controller: (a) functional block diagram; (b), (c) possible input-output relationships.

output which results from a constant input has an infinite number of frequencies that were not present in the input. Furthermore, the instantaneous controller output may depend on the input through samples only, which again precludes the use of superposition, but for an independent reason.

Figure 1.5(a) shows the functional relationship between the power-stage output v and the two inputs: source voltage and digital switch drive d. Since v is analog and d is digital, the power stage appears as a digital-to-analog (D/A) converter to the control input; however, the analog source voltage is digitized by switch action within the power stage, so the power stage effects an analog-to-digital-to-analog (A/D/A) transformation of the source voltage. For a particular power stage, Fig. 1.5(b) shows a possible steady-state output waveform, including the ripple component with period T, which corresponds to a static digital control input whose duty ratio is D. If driven by a static control input whose duty ratio is different, the same power stage may produce the steady-state output waveform illustrated in Fig. 1.5(c).

Though the switching power stage in Fig. 1.3 provides good efficiency, the output voltage can be only less than the source voltage. Variations of the switching power-stage configuration have been evolved which not only retain the inherent efficiency, but also overcome the stated conversion limitation. The operation and circuit diagram for each of three typical power-stage types will be described briefly in the following paragraphs. Source voltage V_s and load resistance R are included in the description since they are essential for proper operation of the power

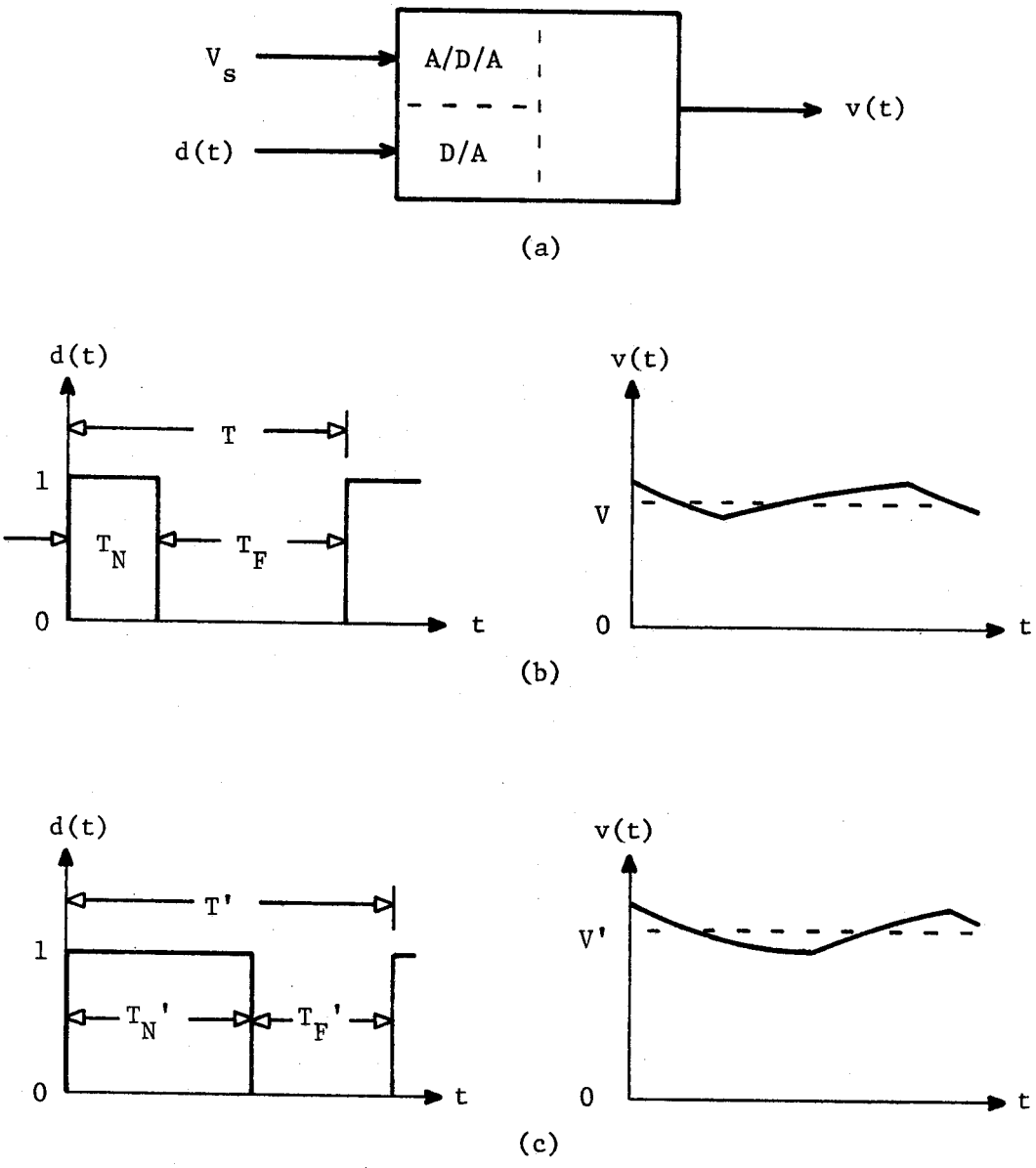

Fig. 1.5 Description of a power stage: (a) functional block diagram; (b), (c) possible input-output relationships.

stage. It is assumed here that the digital control signal causes two complementary switches, S and S', to operate synchronously but in opposite states as described by Eq. (1.1),

$$d(t) = \begin{cases} 1; \text{ S closed, S' open} \\ 0; \text{ S open , S' closed} \end{cases} . \qquad (1.1)$$

A buck, or chopper, power stage is used to buck the source voltage down to a lower load voltage. The buck circuit and relevant steady-state waveforms are shown in Fig. 1.6. The digital switch-drive waveform d in Fig. 1.6(b) represents the output of the controller. During the time interval T_N, switch S clamps voltage v_n to the source voltage V_s as shown in Fig. 1.6(c). The positive voltage across inductor L is V_s-v(t) and is nearly constant because the output low-pass filter is chosen to make the ripple component of v small, so the inductor current increases approximately linearly with time as shown in Fig. 1.6(d). During T_F, switch S' makes voltage v_n zero, so the voltage across the inductor is -v(t), which is negative and almost constant; thus the inductor current decreases approximately linearly. Output voltage, shown in Fig. 1.6(e), is obtained by smoothing the inductor current with a low-pass RC filter designed to make the switching ripple small.

A boost power stage, shown in Fig. 1.7(a), is capable of boosting the source voltage to some higher load voltage. The digital switch drive d again determines the length of T_N and T_F as illustrated in Fig. 1.7(b). During T_N, Fig. 1.7(c) shows that the voltage v_n is zero and the source voltage V_s is applied across the inductor, so inductor

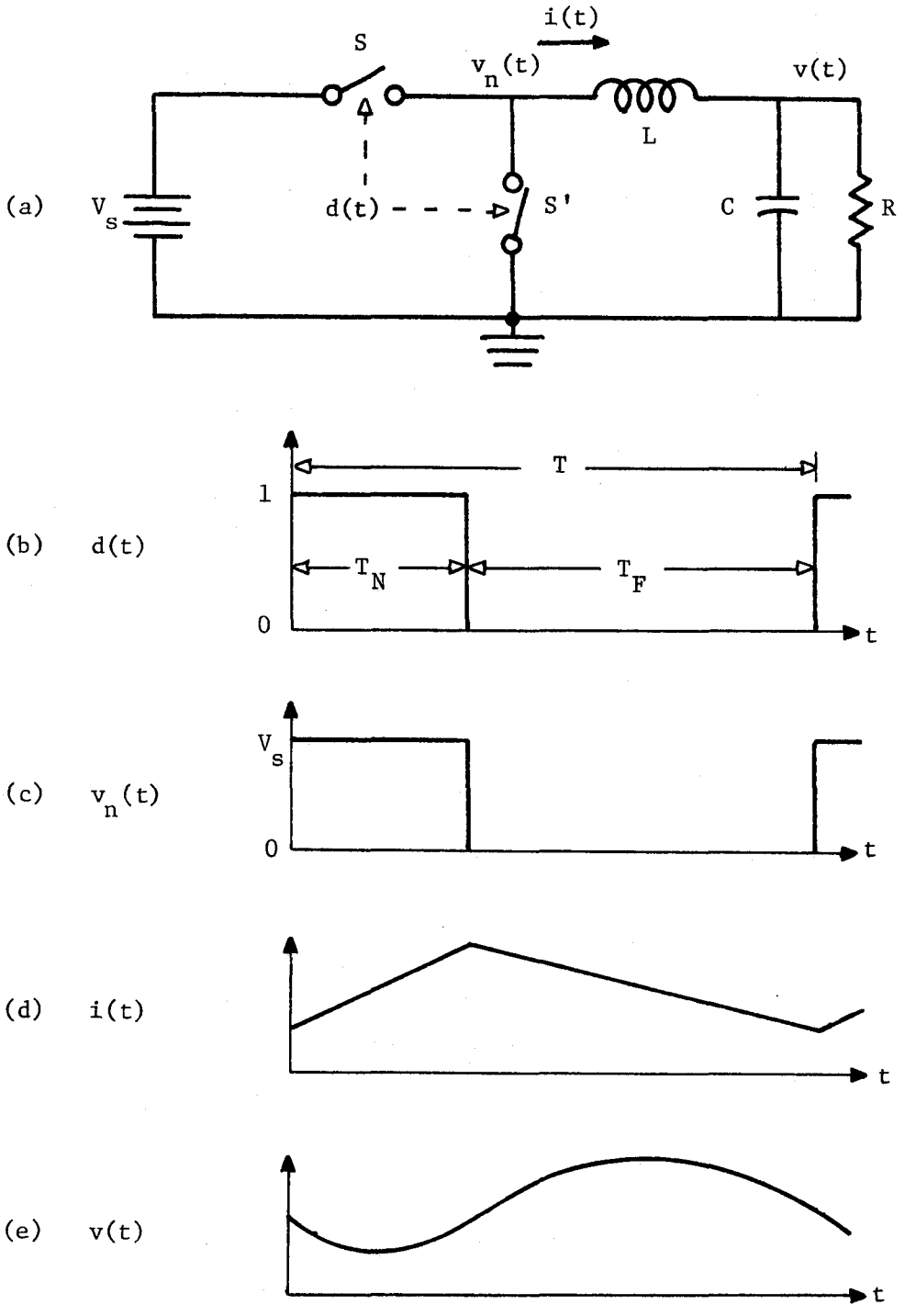

Fig. 1.6 Basic buck power stage: (a) circuit diagram; (b) to (e), circuit waveforms.

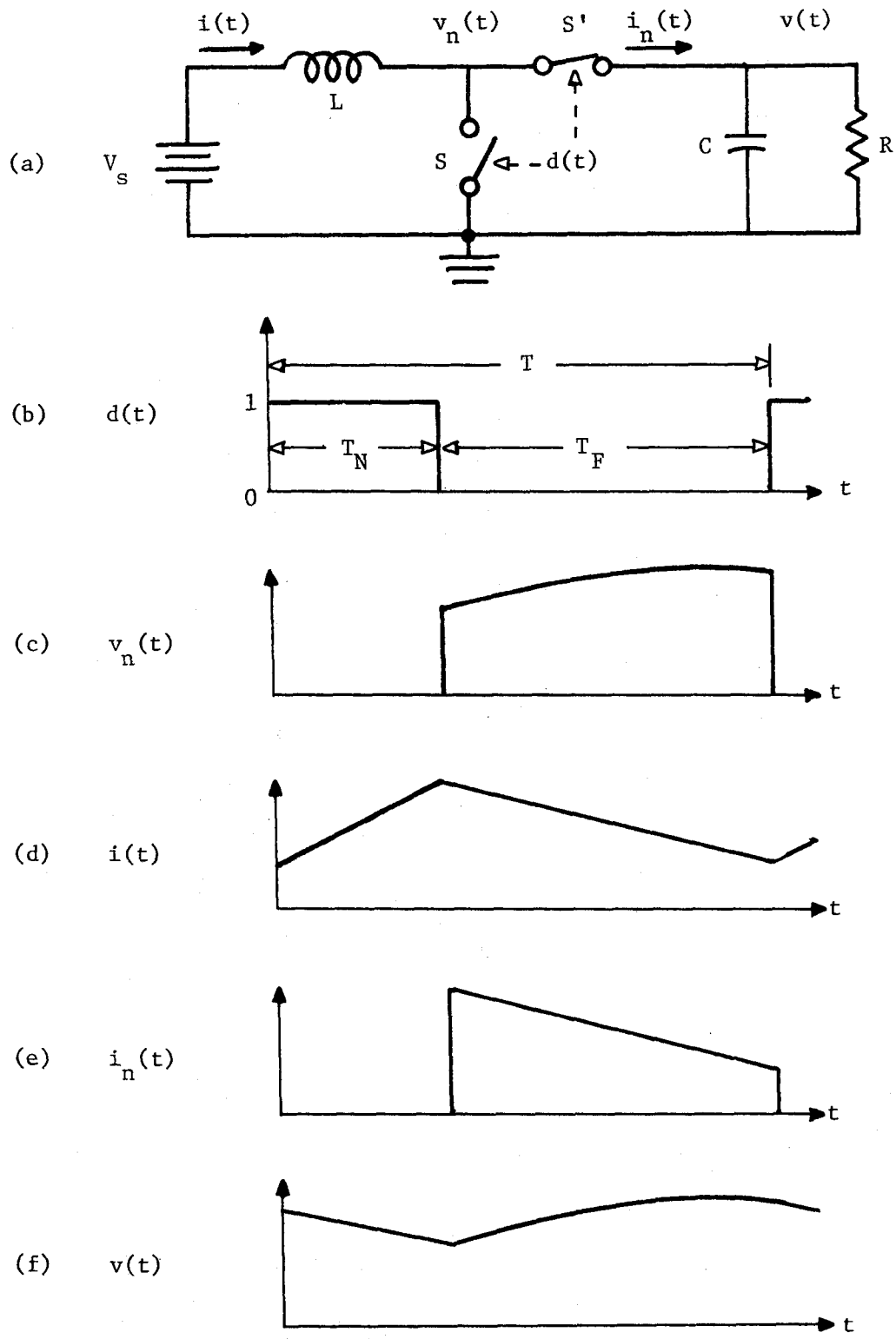

Fig. 1.7 Basic boost power stage: (a) circuit diagram; (b) to (f), circuit waveforms.

current increases linearly as seen in Fig. 1.7(d). Throughout T_F, the switches assume their opposite states. The resultant inductor voltage V_s-v(t) is negative and almost constant so the inductor current decreases nearly linearly. Only the inductor current that occurs during T_F, see Fig. 1.7(e), is low-pass RC filtered to produce the smoothed output voltage shown in Fig. 1.7(f).

The buck-boost, or modified flyback, power stage can produce an output voltage that is either higher or lower than the source voltage, depending on the relative length of the T_N and T_F periods. Figure 1.8(a) shows a circuit realization having a single inductor, but whose output voltage polarity is negative: positive or floating output voltage can be obtained by using a transformer in place of the inductor, but the simpler model of Fig. 1.8(a) will be used exclusively for the comparative purposes at hand. Switch action is governed through Eq. (1.1) by the periodic digital switch-driving signal shown in Fig. 1.8(b). During T_N, inductor voltage, see Fig. 1.8(c), is constant at the positive source voltage so inductor current increases linearly as in Fig. 1.8(d). When the switch states reverse during T_F, a nearly constant negative output voltage appears across the inductor, which causes inductor current to decrease in an approximately linear fashion. The inductor current that occurs during T_F, shown in Fig. 1.8(e), is averaged by a low-pass RC filter to produce the smoothed output voltage shown in Fig. 1.8(f).

A properly designed power-stage filter makes the output ripple negligible with respect to the average output component, so the output voltage is approximately constant. Values of L and C are chosen to satisfy

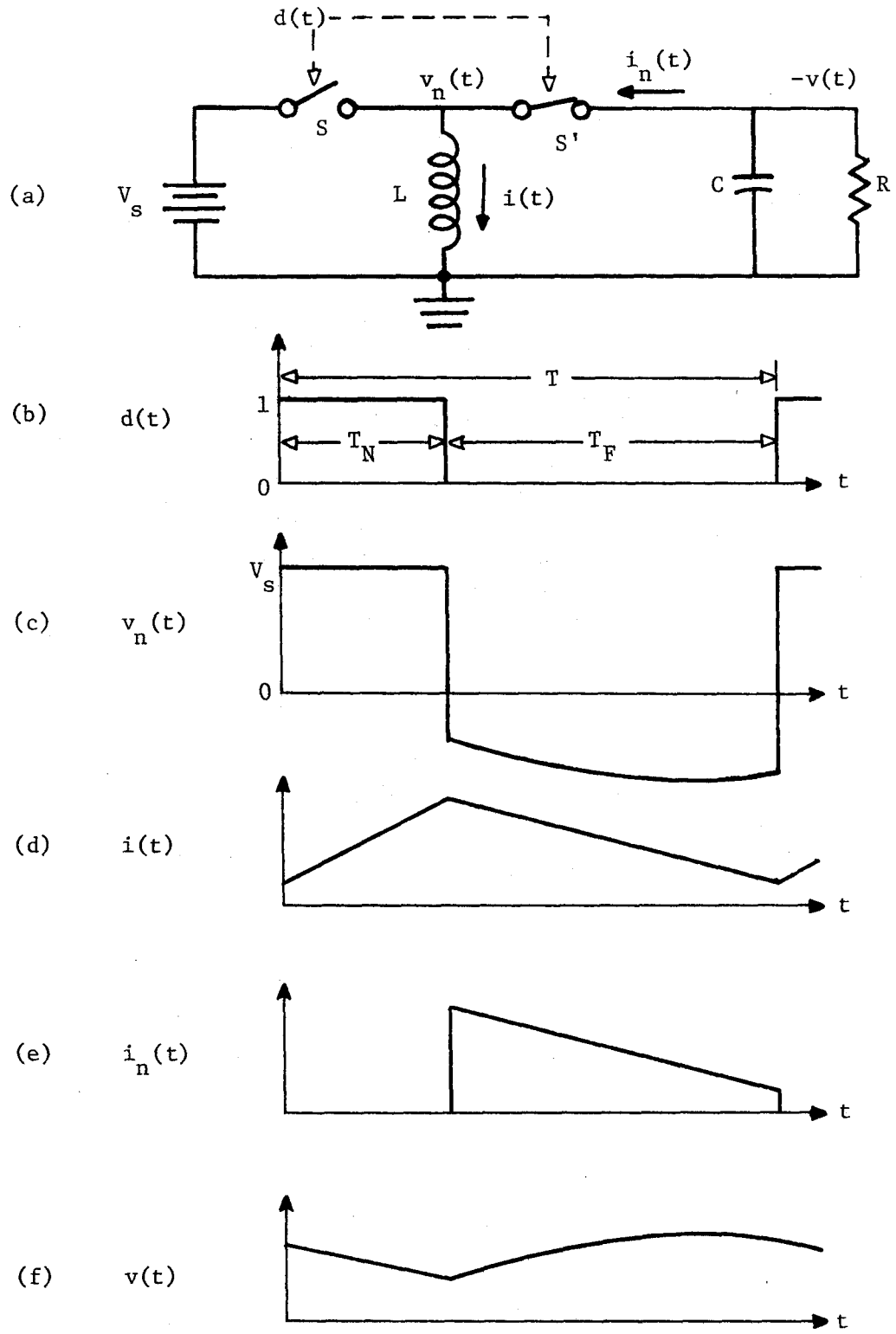

Fig. 1.8 Basic buck-boost power stage: (a) circuit diagram; (b) to (f), circuit waveforms.

design constraints placed on such quantities as output voltage ripple, size, weight, and power.

In a practical system the digital switch-driving signals may be simplified by using one switch in such a way that its state depends on the state of the other switch; only a single switch-drive signal is required for such a configuration. Switch labels have been chosen in the preceding three circuit examples to allow replacement of switch S' by a diode. The use of a diode will be clarified by using the buck power stage in Fig. 1.6(a) for an example. If switch S' is replaced by an ideal diode whose characteristic is illustrated in Fig. 1.9, the circuit for the buck power stage is as given in Fig. 1.10. When switch S is closed, the diode voltage v_d is negative, $v_d = - V_s$, so there is no diode current. The diode appears as an open circuit, so inductor current increases almost linearly as explained in the text accompanying Fig. 1.6(d). Immediately after switch S is opened, the inductor current i starts decreasing at a rapid rate and induces a negative voltage across the inductor, as described by Faraday's Law:

$$v_L = L \frac{di}{dt} \tag{1.2}$$

However, v_L is also constrained by the loop voltage equation $v_L = -v_d - v$, so the diode clamps to zero the voltage $v_L + v$ as it starts to go negative. Thereafter the diode appears as a short circuit until either S is closed or i decreases to zero, whichever occurs first. The inductor thus plays an important role in forcing the diode to behave as

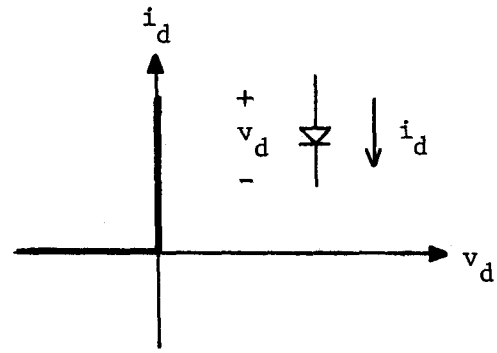

Fig. 1.9 Ideal diode characteristic.

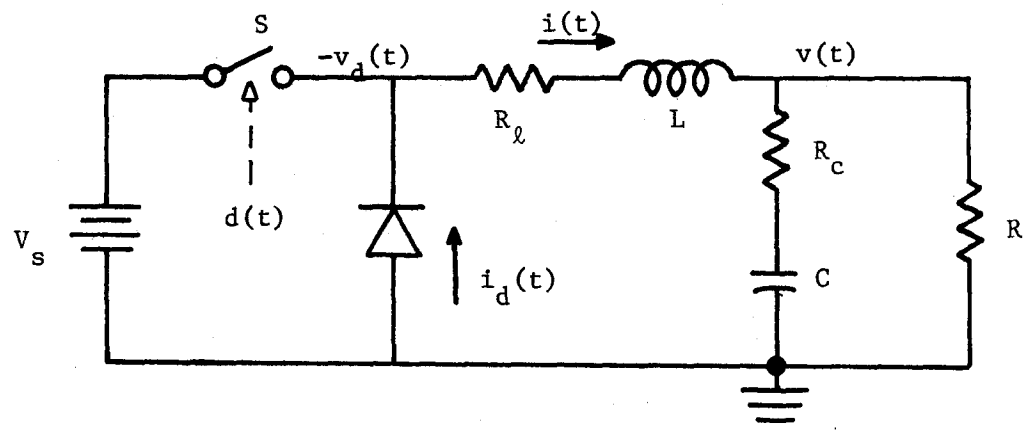

Fig. 1.10 Replacement of switch S' by a diode, buck power stage.

a switch in synchronism with the switch S. If inductor current is always positive, then the action of two switches is duplicated by a single switch and a diode for all three power-stage types, although, for simplicity, the use of two ganged switches will be continued in subsequent discussions.

Switching converters look very promising at this point for use as efficient dc-dc converters, so the next logical step is an attempt to characterize their dynamic behavior. Converter performance can often be improved by the application of negative feedback in a closed-loop configuration, such as that shown in Fig. 1.11, to form a switching regulator. The error ε between the (possibly compensated) regulator output v and a reference v_r changes the duty ratio as necessary to maintain a constant output voltage; however, feedback systems always require a careful consideration of stability.

System stability is, in a broad sense, a description of the feedback system's resistance to perturbations. Stability analysis involves tracing a disturbance signal around the feedback loop to determine whether the disturbance is reinforced or attenuated. The effects of a disturbance eventually disappear if the returned signal is attenuated; however, if successive traversals of the feedback loop make the disturbance larger, then the final result is system destruction or a self-sustained oscillation, either of which is undesirable. It seems reasonable then to use a sinusoidal test signal for stability analysis.

Before one attempts the stability analysis of a switching regulator, one must know how suitable test signals at the controller input ε affect

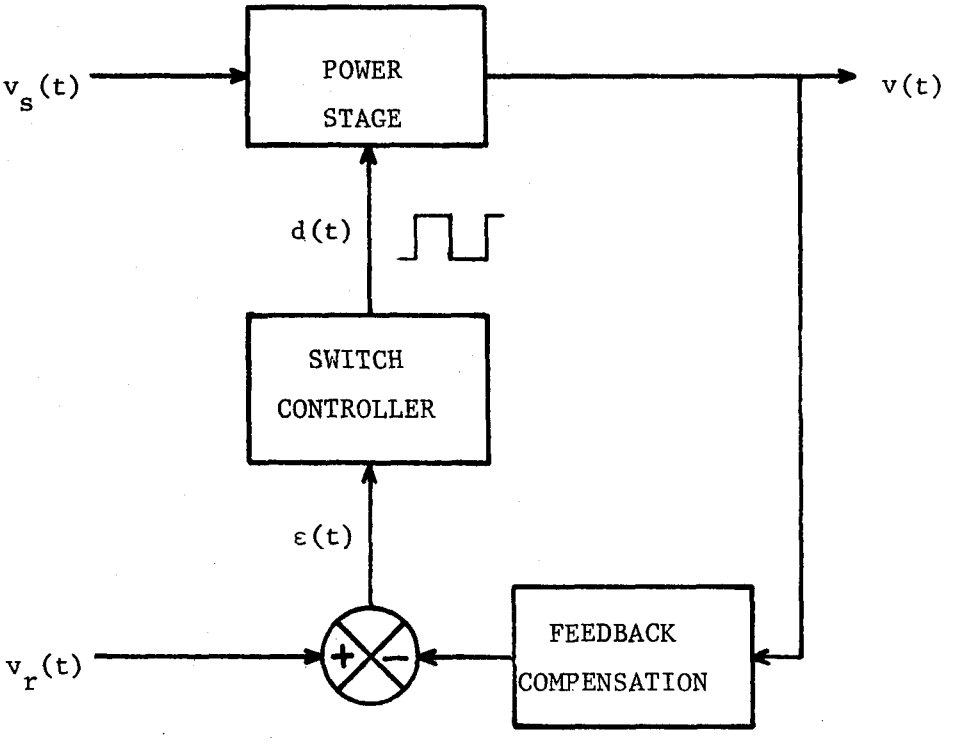

Fig. 1.11 Block diagram of a switching converter in a closed-loop regulator configuration.

the power-stage output v. One can separate this process into two distinct transformations which correspond to the controller and power stage. The transformation of each block must be known independently to permit the analytical evaluation of various controller and power-stage combinations.

The controller determines the ε to d transformation; that is, the dependence of digital switch drive on controller input. The controller input of interest in stability study is a sinusoidal disturbance superimposed on a dc signal; however, it is necessary to consider only sinusoidal frequencies less than the lowest switching frequency because the inherent low-pass filter characteristic which attenuates switching ripple in the power stage output also reduces the gain of the feedback loop at higher frequencies. All digital controllers are nonlinear, as indicated earlier in the discussion; even so, the output frequency spectrum of some controllers can be obtained exactly for an input consisting of dc plus sinusoid.

The d to v transformation is governed by the power stage. For the buck power stage, one observes from Fig. 1.6 that v is a linear function of the filter input voltage v_n, which in turn is a linear[2] function of the instantaneous switch-drive d; unfortunately, though, no circuit variables appear to be linear functions of d for the boost or buck-boost power stages. The fact that the current waveform smoothed by the RC filter in the boost and buck-boost power stages depends both on duty ratio and

---

[2] If only the values zero and unity are permitted for d(t) as defined in Eq. (1.1), then $v_n(t) = v_s(t)\, d(t)$, where $v_s(t)$ is the instantaneous source voltage.

on power-stage state variables makes the dynamic analysis of the nonlinear d to v transformation a very difficult, unsolved problem.

Static analysis of a power stage is much easier to achieve than dynamic analysis because the inputs are not allowed to vary (the digital input continues to switch, but the duration and spacing of all pulses are constant). For static conditions, the analysis of ideal (lossless) power stages is particularly simple: Faraday's Law, Eq. (1.2), relates the voltage v_L across an inductor to the current i through the inductor, so the integral of v_L over a switching period T is proportional to the net change in inductor current, which is zero for steady-state operation;

$$\int_0^T v_L \, dt = L \int_{i(0)}^{i(T)} di$$

$$= L[i(t) - i(0)]$$

$$= 0, \text{ steady state} \quad . \qquad (1.3)$$

Applied to the ideal buck power stage in Fig. 1.6(a), Eq. (1.3) yields

$$V_s T_N - V\,T = 0 \quad , \text{ buck} \quad , \qquad (1.4)$$

where V is the static (dc) output voltage of interest. For each type of ideal power stage, equations similar to Eq. (1.4) are easily derived and solved for the static output V:

$$V = \frac{T_N}{T} V_s = D V_s \quad , \text{ buck} \tag{1.5}$$

$$V = \frac{T}{T_F} V_s = \frac{V_s}{1 - D} \quad , \text{ boost} \tag{1.6}$$

$$V = \frac{T_N}{T_F} V_s = \frac{D V_s}{1 - D} \quad , \text{ buck-boost} \quad , \tag{1.7}$$

where $D = \frac{T_N}{T}$ is the duty ratio. Equations (1.5) to (1.7) are plotted in Fig. 1.12 to show the variation of V with respect to D: notice that the output voltage is a nonlinear function of the digital input for the boost and buck-boost power stages, even for static analysis. The capability of boost and buck-boost power stages to provide an output voltage greater than the source voltage was anticipated, but apparently carries a penalty of nonlinear complication. Kossov[1] extended the static analysis to include the parasitic resistance associated with the inductor.

The absence of dynamic analysis of switched power stages presents a challenging problem. To be useful, any method proposed for the nonlinear analysis of switched power stages must be simple enough to lend insight into system design. Before accepting the above challenges one should review potentially useful analytic methods and compare their relative merits.

Computers can simulate very complex nonlinear systems. The resultant simulation for any particular system is devoid of insight into such questions as parameter sensitivity, stability, compensation, and design if the system is slightly modified: even extensive numerical and graphical results often fail to provide a design model. Computer simulation should therefore be limited to the investigation of a particular

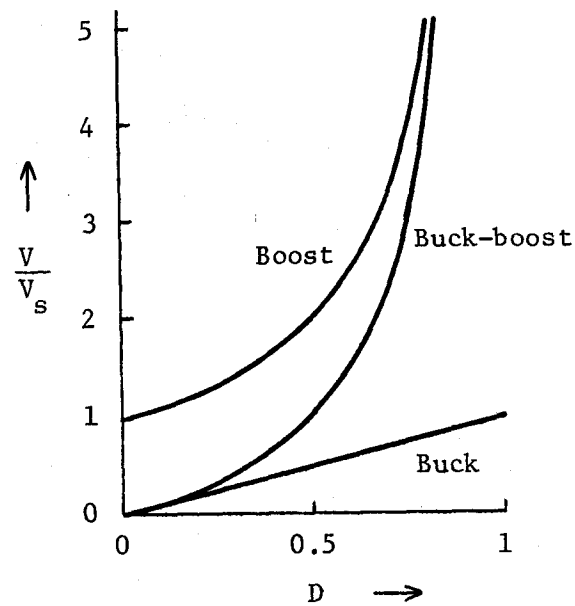

Fig. 1.12 Dc output voltage V versus duty ratio D for static conditions in ideal power stages.

system after initial design has been completed.

Few closed-form solutions exist for systems described by nonlinear differential equations, even when the system is second-order or less. Most other nonlinear systems in general, and switching regulators in particular, cannot be forced into any of the standard differential equation formulations which have known exact solutions.

Stability information for a nonlinear system can occasionally be obtained from a knowledge of the initial conditions, input, and system equations, without an actual solution of the system equations. Lyapunov's Direct Method indicates stability if a scalar positive-definite function can be found which has a negative time derivative in the vicinity of the phase space surrounding the initial condition; however, failure to find such a scalar implies absolutely nothing about system stability. Since there is no algorithm to provide a suitable trial function for nonlinear systems, efforts to use the Direct Method of Lyapunov often go unrewarded.

The system trajectory in state space gives useful dynamic properties, but methods for obtaining the dynamic path are not feasible unless the system is second-order or less. The resulting graphical approach, or phase-plane solution, may give the response for simple input functions but is limited in practice to the low-order system.

Perturbation techniques attempt to express the dynamic response of a system as a series expansion around an assumed solution in terms of some, hopefully small, parameter. The dominant issue of such expansions concerns their convergence, which depends on the assumed solution. Rapid

convergence occurs only when the solution is nearly that of either an exact nonlinear system or a linear system, but the nonlinearity is neither type for the majority of pulse-controlled regulators.

Sampled-data systems can often be treated using the linear theory of z-transforms. Though switching regulators bear some resemblance to sampled-data systems, their nonlinear aspects rule out the exclusive use of linear theory.

Nonlinear systems can often be linearized by assuming that only small variations occur in the state variables. The operating point must be known a priori. The resultant linear system can then be studied using the numerous methods of linear analysis and design. Unless the response of the linearized model is in the assumed range of small variations, there may be no correlation between the nonlinear system and its model. The linearization method breaks down if the operating point is near a discontinuity of the nonlinearity response characteristic.

In quasi-linearization, a waveform is assumed for the nonlinearity input, that part of the output which has the same waveform as the input is found in some way and is related to the input waveform by an equivalent linear transfer function called the describing function (DF). Although the describing function itself is linear, the gain and phase of the describing function may be a nonlinear function of the input waveform parameters. The principal advantages of describing functions are the straightforward design applicability and analytic system insight which result from a linear transfer function. Valid describing functions may be derived for arbitrary input variations and discontinuous

nonlinearity characteristics. Describing functions are not without their limitations, most of which arise as a consequence of operation in a feedback loop: restrictions, such as low-pass loop filtering, are necessary to circumvent the problem created by the interdependence of model upon input signal and input signal upon model, and there is no analytic measure of the accuracy of results based on the describing function. Of course, analytic describing-function conclusions apply only when the assumed nonlinearity input signal is actually present.

Consideration of the analysis alternatives leads one to conclude that the describing function is the most suitable choice for nonlinear design and stability analysis. Since necessary and sufficient stability criteria can be derived for purely linear feedback systems, it is reasonable to expect "almost necessary" stability conditions when nonlinearities are replaced by a linear transfer function. One is now ready to examine qualitatively the application of describing-function analysis to switching dc-dc converters.

As indicated in a previous discussion, the appropriate control input to assume for stability analysis is a sinusoidal modulation superimposed on a dc component; for such an input, the describing function DF of a nonlinearity is evaluated as the ratio of the modulation-frequency component in the output to the corresponding component in the input, where both are expressed as complex exponentials. Figure 1.13(a) portrays a controller input whose dc level is U: the symbols M_ε and ϕ_ε represent, respectively, the sinusoid's peak amplitude and phase with respect to a time reference which has been chosen arbitrarily to coincide with the

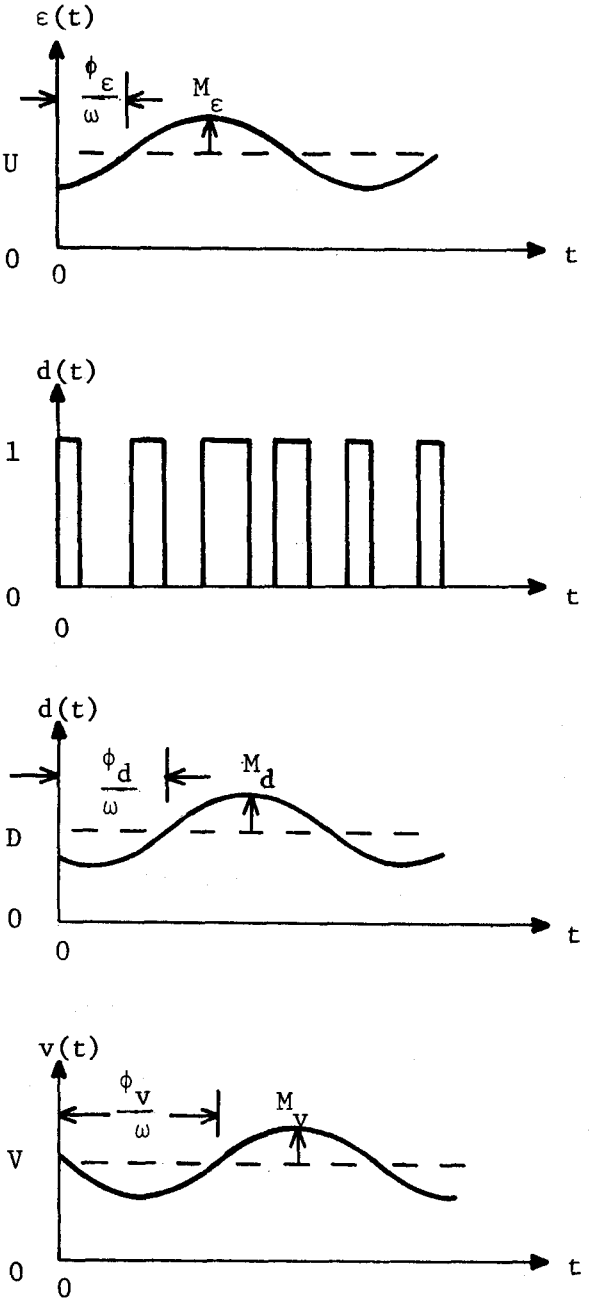

Fig. 1.13 Representative converter waveforms for a modulated controller: (a) controller input, (b) controller output, (c) dc and fundamental components of controller output, (d) dc and fundamental components of power-stage output.

leading edge of a controller output pulse. The modulated digital controller output (power-stage input) shown in Fig. 1.13(b) is composed of a dc component D and modulation-frequency component as shown in Fig. 1.13(c): components whose order or frequency is higher than that of the modulation are neglected to simplify the picture. The modulation-frequency component of d, which has a peak amplitude M_d and phase ϕ_d with respect to the same time reference used to determine ϕ_ε, causes a similar component to appear in the power-stage output as shown in Fig. 1.13(d): the higher-order and higher-frequency components are again omitted for simplicity. The modulation-frequency output component is characterized by phase ϕ_v, with respect to the previously established time reference, and peak amplitude M_v. The describing functions of the controller, power-stage, and converter are now given by the expressions $M_d\, e^{j\phi_d}/(M_\varepsilon\, e^{j\phi_\varepsilon})$, $M_v\, e^{j\phi_v}/(M_d\, e^{j\phi_d})$, and $M_v\, e^{j\phi_v}/(M_\varepsilon\, e^{j\phi_\varepsilon})$, respectively; for stability analysis, the converter is replaced by an equivalent linear gain $\frac{M_v}{M_\varepsilon}$ with phase shift $\phi_v - \phi_\varepsilon$.

One ultimately needs separate describing functions for the controller and power stage in order to optimize or examine the stability of any combination. Describing functions of switch controllers can be evaluated approximately without undue difficulty, and the buck power stage is actually trivial to treat because its output is a linear function of the switch control signal.

Unfortunately, serious problems arise when one attempts to evaluate analytically the control-input describing functions for boost and buck-boost power stages. The principal difficulty is caused by the nonlinear

discontinuous manner in which the output depends on the switch control: the modulation-frequency output component is analytically intractable for the digital switch drive depicted in Fig. 1.13(b); yet, switches can only be closed or open, so the power-stage switch-control waveform shown in Fig. 1.13(c) lacks interpretation. Poulo and Greenblatt[2] derived a continuous nonlinear time-varying differential equation to characterize power stages, but could not produce simple equivalent circuits or tractable describing functions. Landsman[3] obtained a linear equivalent circuit which is useful for source variations of the boost power stage; however, the equivalent circuit he proposed for control variations is sadly inadequate, as evidenced by the poor correlation between his theoretical and experimental results.

The objective of the present endeavor is to extend the static description of power stages by developing a relatively simple, and hence useful, method which can be used to analyze dynamic responses (e.g., transient and frequency) caused by variations in either of the two power-stage inputs; in essence, one must obtain the effective transfer functions which relate source voltage and digital switch control to the power-stage output, even though the power stage is switched and may be nonlinear.

Treated as an example in Chap. 2 is one of the few switch controllers for which an exact spectrum analysis of the modulated output is possible. The modulation-frequency component of the controller output is extracted from the spectrum to form an exact describing function. A simpler derivation of the linearized transfer functions is demonstrated which should be generally useful when the describing function is relatively

insensitive to modulation frequency or amplitude. Since the buck power stage is linear, a description of the controller output also characterizes the power-stage output.

Based on the observation that power-stage response times are invariably slow with respect to the period of switch operation, continuous nonlinear power-stage models are developed in Chap. 3 by an averaging technique. Since switches are eliminated, power-stage input waveforms of the type shown in Fig. 1.13(c) can now be interpreted; thus a significant contribution to the potential analysis of power stages is contained in this chapter.

Approximate linear equivalent circuits and simple analytical expressions for the transient and frequency responses of all three power-stage types are derived in Chap. 4 from the averaged (continuous) models. Novel conclusions include the modification of effective filter component values by the switch duty ratio, and the possible existence of a real positive zero in the linearized control-input transfer function. Based on open-loop power-stage and controller describing functions, critical closed-loop stability factors are predicted.

The credence of any hypothesis is immeasurably strengthened if conclusions drawn from the postulate can be verified by experiment, so this idea is pursued in Chap. 5 by the experimental simulation of both averaged and switched power-stage models for each type of power stage. Excellent correlation is observed between the theoretical expressions and the experimental data for the frequency response of averaged power-stage models; in turn, data from simulations of the averaged power-stage

models agrees well with that from simulations of the switched power stages. Finally, the experimental stability of switched power stages in a negative-feedback configuration supports the analytical predictions based on the open-loop averaged power-stage models.

Deduced from the results summarized in Chap. 6 is the conclusion that the averaging technique is a powerful analytical tool for the tractable analysis and useful design of switching power stages.

Chapter 2

EXACT ANALYSIS OF A BUCK CONVERTER

2.1 Introduction

The purpose of the present chapter is to provide an exact spectrum analysis of a switching converter with a modulated control input. The exact analysis will serve as a comparison standard for approximate procedures which are developed in later chapters.

Chapter 1 discussed qualitatively the significance with respect to stability of dc plus ac (sinusoidal) modulation input to the switch controller. Describing functions were acknowledged as likely candidates for the stability analysis and design of switching converters, so attention will also be focused in Chap. 2 on the extraction of the describing function from the exact frequency spectrum.

Section 2.2 reviews the characteristics of three power-stage types and concludes that only the buck power stage is amenable to exact frequency analysis. A linear transfer function is derived for the buck power stage to relate the digital switch drive to the converter output; a knowledge of the controller output spectrum leads directly to the frequency spectrum of the buck converter output.

A specific controller is analyzed in Sec. 2.3 for the output spectrum which results from a modulated input. The controller specimen has been chosen because it permits an exact output spectrum analysis for a modulated input, although in general, exact spectrum analysis of a switch controller is rarely tractable and invariably difficult. Describing-function analysis is universally more feasible than exact

spectrum analysis so first an approach which yields an approximate describing function of the controller is suggested and demonstrated in Sec. 2.3.1. The exact frequency spectrum of the controller output is then given in Sec. 2.3.2 and leads to the exact describing function. Comparisons between the exact and approximate describing functions show that the simpler procedure yields a useful transfer function for most modulation situations.

In Sec. 2.4 the exact controller output spectrum is transformed by the linear operation in the buck power stage to produce the exact frequency spectrum of the buck converter. Finally, the converter describing function is shown to be the product of controller and power-stage describing functions.

2.2 Power Stage

Three basic power stages for a switching dc-dc converter were introduced in Chap. 1; namely, buck, boost, and buck-boost. Description of the basic power stages and their associated waveforms accompanied Figs. 1.6 to 1.8. Some of the observations previously discussed will be emphasized here because of their relevance to the present considerations.

It is obvious from Fig. 1.6(a) that for the buck power stage the instantaneous output voltage $v(t)$ is a linear function of the instantaneous switched voltage $v_n(t)$. The linear theory of Laplace transforms can be used to express the Laplace transform of the instantaneous output voltage $V(s)$ as a superposition of the Laplace transform of the instantaneous switched voltage $V_n(s)$ and appropriate

initial conditions, where s is the complex Laplace frequency variable. The transfer function $G_f(s)$ of the RLC filter is defined in Eq. (2.1) as the ratio $V(s)/V_n(s)$ when initial conditions are neglected:

$$G_f(s) \equiv V(s)/V_n(s)\Big|_{\text{zero initial conditions}} \text{, filter transfer function .} \qquad (2.1)$$

Figures 1.6(b) and 1.6(c) show that for a constant source voltage V_s the instantaneous switched voltage $v_n(t)$ is related to the instantaneous digital switch drive d(t) by

$$v_n(t) = V_s\, d(t), \quad \text{if } V_s \text{ is constant .} \qquad (2.2)$$

The overall power-stage transfer function G(s) is defined by Eq. (2.3), where D(s) is the Laplace transform of d(t)

$$G(s) \equiv V(s)/D(s)\Big|_{\text{zero initial conditions}} . \qquad (2.3)$$

Equation (2.4) shows the overall transfer function of the buck power stage which results when Eq. (2.2) is Laplace transformed and substituted with Eq. (2.1) into Eq. (2.3)

$$G(s) = V_s\, G_f(s) \text{ , buck power stage .} \qquad (2.4)$$

Unfortunately, a simple expression, such as Eq. (2.4), for G(s) is possible only for the buck power stage. Its unique simplicity occurs because connections between the RLC components do not change when the switch states reverse; hence the RLC components form a filter whose characteristics are invariant with respect to instantaneous switch positions. The boost and buck-boost power stages illustrated in Figs. 1.7 and 1.8 do not share the feature just mentioned: their RLC components form a time-varying filter whose properties depend on the instantaneous switch states and whose input voltage or current cannot even be identified. Stated another way, the power-stage transfer function G(s) is independent of D(s) for the buck but changes with D(s) for the other types of power stage.

Based on the above comments, the choice of power stage to be used for exact analysis must be the buck type. The basic buck power stage is extended in Fig. 2.1 to include in the analysis the parasitic effects exposed by large currents in physical circuit components. Both inductors and capacitors are more accurately modeled by the inclusion of effective resistances R_ℓ and R_c, respectively, in series with the ideal components.

The filter transfer function can be written by inspection of the practical buck power stage shown in Fig. 2.1. The resulting gain is given in Eq. (2.5), first as a voltage divider ratio and then as a ratio of polynomials in s:

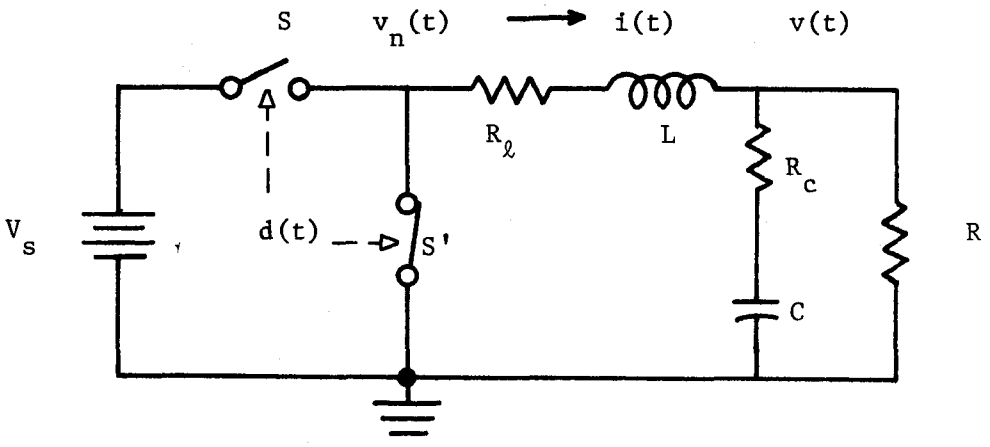

Fig. 2.1 Buck power stage with parasitic resistances R_ℓ and R_c.

$$G_f(s) = \frac{R \,\|\, (R_c + 1/sC)}{R_\ell + sL + [R \,\|\, (R_c + 1/sC)]}$$

$$= \frac{R}{R + R_\ell} \; \frac{1 + sCR_c}{1 + s[C(R_c + R\|R_\ell) + \frac{L}{(R + R_\ell)}] + s^2 \, LC \frac{(R + R_c)}{(R + R_\ell)}} \; , \tag{2.5}$$

Parallel vertical lines are used to denote a parallel impedance combination; for example, the equivalent impedance consisting of an impedance Z_1 in parallel with an impedance Z_2 is symbolized by $Z_1 \,\|\, Z_2$.

If R_ℓ and R_c had been omitted in the buck power stage, the only significant change in the nature of Eq. (2.3) for typical numerical values would be the removal of the zero in the numerator of $G_f(s)$. The magnitude and phase angle of $G_f(j\omega)$ represent the gain and phase shift which an input sinusoid of frequency ω undergoes in passing through the filter; thus, a filter input given by Eq. (2.6) produces the output described by Eq. (2.7):

$$v_n(t) = A \sin(\omega t + \phi) \tag{2.6}$$

$$v(t) = A|G_f(j\omega)| \sin (\omega t + \underline{/G_f(j\omega)} + \phi) \; . \tag{2.7}$$

The collective display of a transfer function's phase shift and logarithmic magnitude, as a function of logarithmic frequency, is called the Bode plot. A typical Bode plot which corresponds to the buck power-stage transfer function obtained by substitution of Eq. (2.5) into

Eq. (2.4) is shown in Fig. 2.2. Bode plots provide complete design and stability information for linear systems. Notice that the amplitude of the filter transfer function shown in Fig. 2.2(a) does indeed have the characteristic of a low-pass filter.

The describing function was introduced in Chap. 1 as a tool which can approximately characterize nonlinearities, but it can also be used for linear systems. Since superposition holds for linear systems by definition, a sinusoidal input at a frequency ω produces an output sinusoid at the same frequency which is related to the input sinusoid by the linear transfer function, regardless of what other input signals are present. Thus the describing function of a linear system is simply the linear transfer function and is independent of sinusoidal amplitude. For example, the describing function DF of the buck power stage is given by Eq. (2.8)

$$DF = G(j\omega) = V_s \, G_f(j\omega) \ . \tag{2.8}$$

The linearity of the buck power stage gives its transfer function yet another useful interpretation. The output frequency spectrum is completely specified when the input frequency spectrum and the linear transfer function are given. The power-stage input is just the switch-controller output, so the exact frequency spectrum of the buck converter can be found once the frequency spectrum of the controller output is obtained.

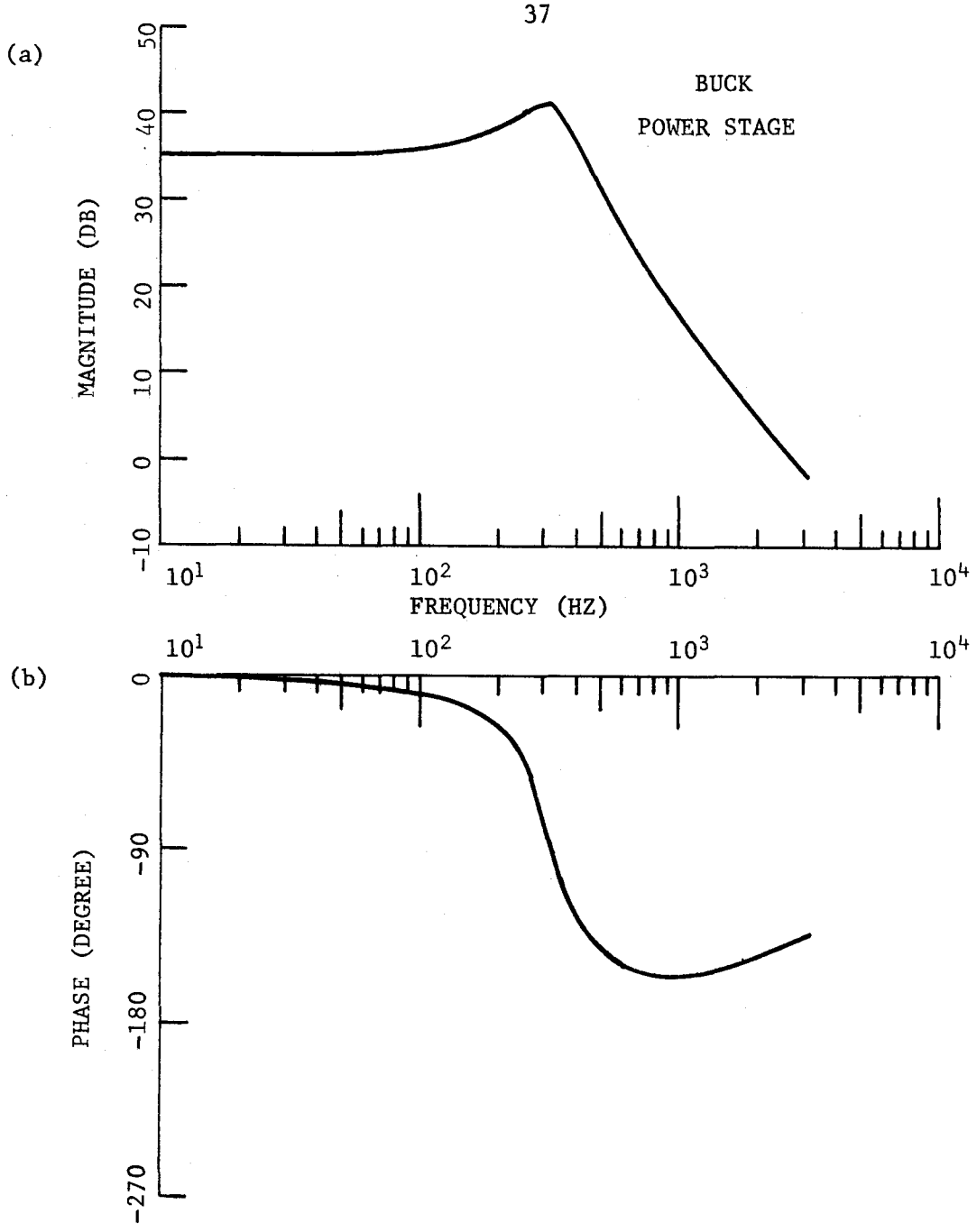

Fig. 2.2 Bode plot of buck power-stage transfer function.

2.3 Controller

In order to find the exact frequency spectrum of the buck converter, one must be able to compute the frequency spectrum of the switch controller. A suitable dimensionless control input, from the viewpoint of stability analysis, consists of a dc and an ac signal given by Eq. (2.9)

$$\varepsilon(t) = U + u \sin(\omega t - \phi) \ . \qquad (2.9)$$

The modulation amplitude u and frequency ω, the phase lag ϕ of the sinusoid with respect to a time reference, and the dc level U completely specify the modulated input to the controller.

The immediate objective is to select a possible controller for which, with an input of the form described by Eq. (2.9), the exact frequency spectrum of its output can be obtained analytically. Although proof is deferred until Sec. 2.3.2, a controller which meets the above objective will be described here.

The switch controller which will be used exclusively in the remainder of this thesis is a uniformly-sampled, linear-lead, pulse-width-modulator (PWM). This controller uses input samples, which are obtained at uniform time intervals T, to modulate the widths of a sequence of unity-amplitude pulses. One pulse is positioned at the leading or initial portion of each interval T; its width T_N, within the constraint $0 \leq T_N \leq T$, varies linearly with the input sample as shown in Fig. 2.3.

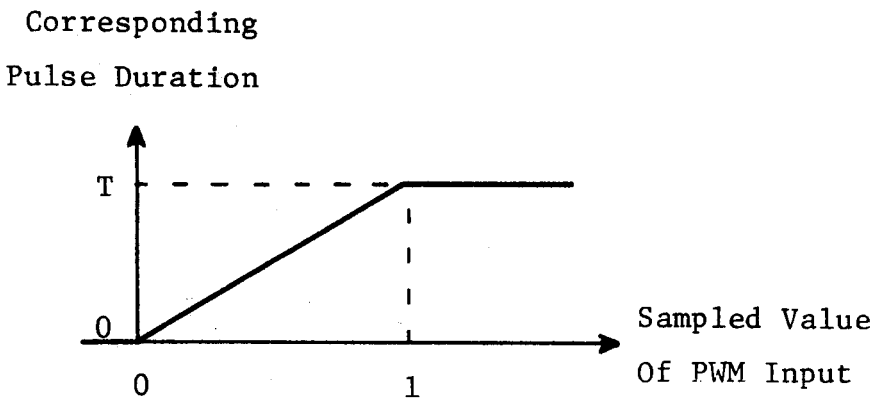

Fig. 2.3 Saturation characteristic of PWM.

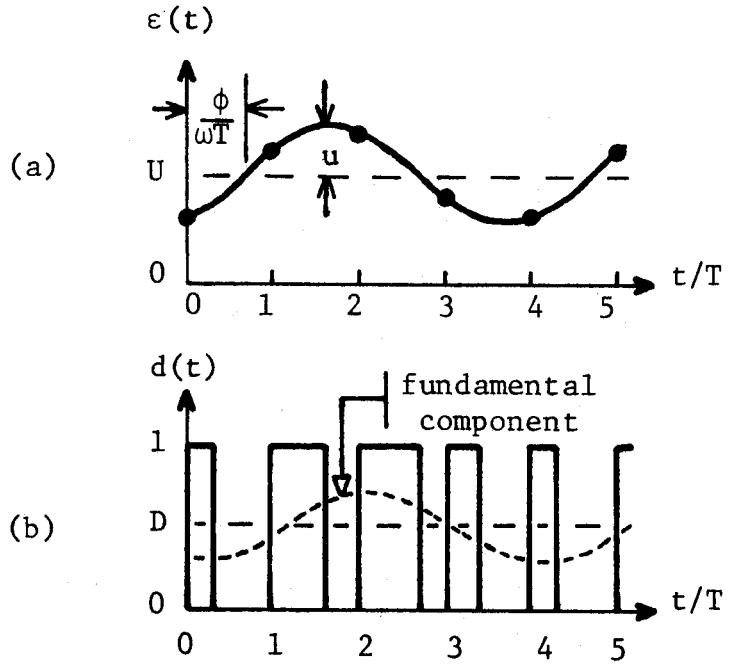

Fig. 2.4 PWM response to sinusoidal modulation;
(a) input, (b) output.

Figure 2.4 illustrates the operation of a PWM for a control input given by Eq. (2.9). The time origin is chosen for convenience to coincide with the reference sampling-instant which gives values of ϕ/ω between 0 and T. The continuous input and the resulting sampled values are shown in Fig. 2.4(a), whereas Fig. 2.4(b) shows the rectangular output waveform with unity-amplitude pulses whose leading edges occur every T seconds and whose trailing edges are modulated, in accordance with Fig. 2.3, by the sampled input values. Constraints on u and U are imposed in Eq. (2.10) to avoid additional conceptual complexity caused by saturation effects; Eq. (2.10) also reflects a restriction on ϕ determined by the choice of time reference

$$\left.\begin{aligned} &0 \leq U \leq 1 \\ &u \leq \min(U,\ 1-U) \leq \frac{1}{2} \\ &0 \leq \phi \leq \omega T \quad . \end{aligned}\right\} \tag{2.10}$$

Now that the controller has been specified, one is ready to find the frequency spectrum of the modulated output shown in Fig. 2.4(b). The task is admittedly difficult when the modulation frequency ω and switching frequency, $\omega_s \equiv 2\pi/T$, are independent. A qualitative discussion of the expected frequencies and their relative amplitudes follows, and is intended to make plausible the use of a simplified approach based on the describing function. The statements are presented here without proof, but will be demonstrated in Sec. 2.3.2.

If the PWM input is unmodulated, the remaining dc input causes a

square wave of period T to be generated at the controller output. The frequency spectrum of this output has components at all integer multiples of the switching frequency ω_s, as shown in Fig. 2.5(a). The amplitude of the m^{th} switching harmonic, or multiple, is attenuated, when compared with the amplitude of the fundamental switching frequency, by a factor of 1/m.

Consider now the modulated input and output that were shown in Fig. 2.4. Recalling an earlier observation that all switch controllers are inherently nonlinear, one expects not only the fundamental modulation frequency ω in the output, but also all higher harmonics of ω. In addition, harmonics of ω appear as sidebands around all the harmonics, including the fundamental, of ω_s. If u is the amplitude of a sinusoidal input to an arbitrary nonlinearity, then the amplitude of the n^{th} harmonic in the output is of order u^n. Not only the n^{th} modulation harmonic, but also the n^{th} sidebands of each switching harmonic in the output, have amplitudes which are limited to the order of u^n for the modulated PWM under consideration. Figure 2.5(b) illustrates the amplitude spectrum of the modulated PWM; for the sake of clarity, the case is shown where ω is much less than ω_s. Since the effective cut-off frequency of the filter in a well-designed converter is less than ω_s, one is concerned primarily about modulation frequencies less than ω_s:

$$\omega < \omega_s \quad . \tag{2.11}$$

If the modulation amplitude u is small with respect to U, then the

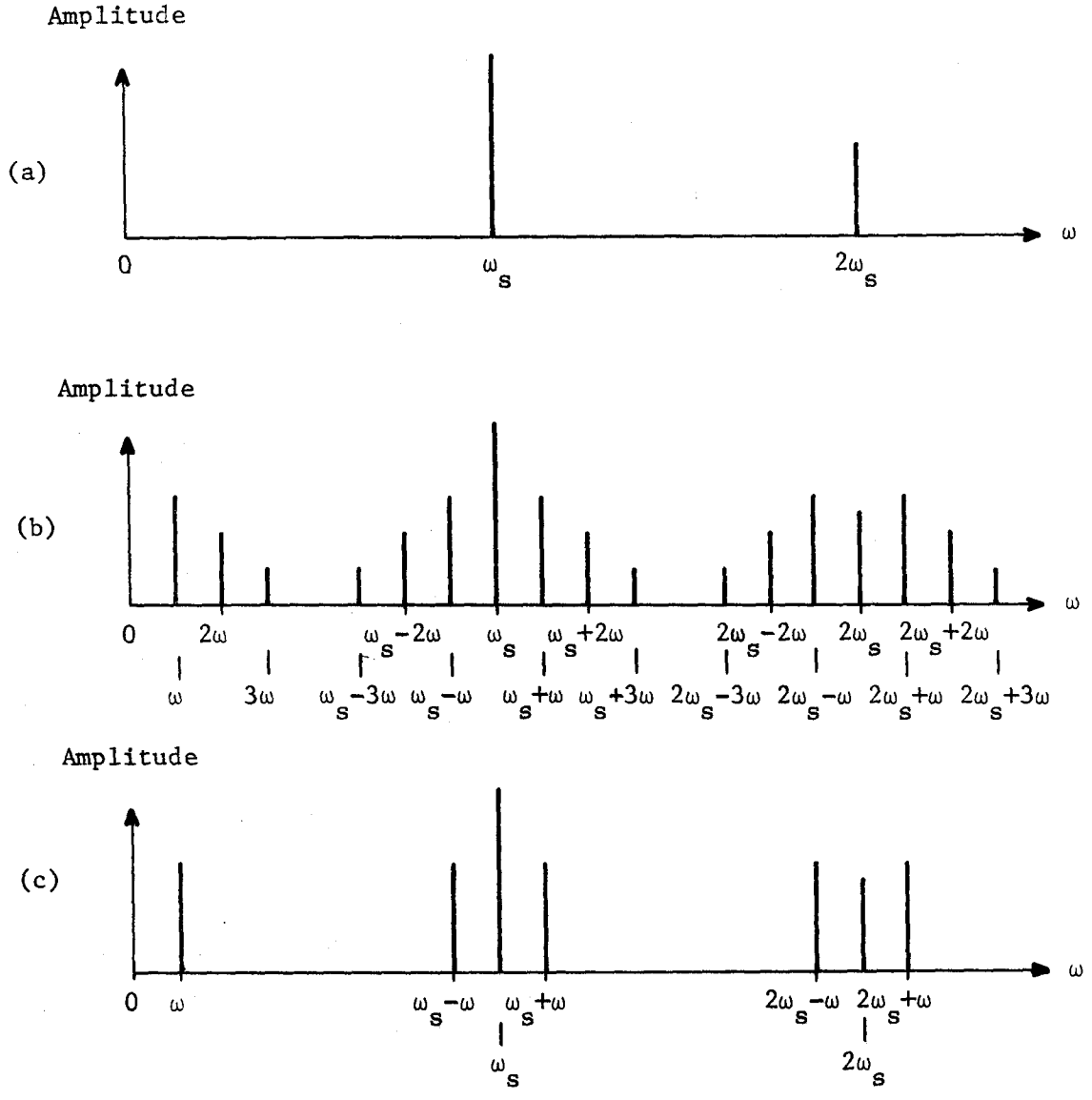

Fig. 2.5 Representative frequency spectrum of controller output: (a) unmodulated, (b) modulated, (c) modulated with small amplitude.

amplitudes of the higher-order harmonics of ω and sidebands of switching harmonics in the output are negligible with respect to the amplitude of the fundamental modulation frequency. The remaining frequency components are shown in Fig. 2.5(c). Since the PWM output passes through a low-pass filter whose cutoff frequency is intentionally chosen less than ω_s, one can assume that frequencies which are inclusively higher than ω_s do not contribute to the converter output spectrum as effectively as frequencies lower than ω_s. Of the two frequencies, ω and $\omega_s-\omega$, that can possess appreciable amplitudes in the converter output, the first one can be accounted for by the describing function. The following section treats a special class of modulation in order to derive a simple describing function for the PWM, although the method is applicable to general switch controllers.

2.3.1 Linearized Describing-Function Analysis

The preceding paragraph justified the importance of two frequency components in the spectrum of the PWM output when its input is modulated at a frequency ω. These two frequencies, ω and $\omega_s-\omega$, are distinct except for the case $\omega = \omega_s/2$ where special care is necessary to evaluate the net effect of the ω and $\omega_s-\omega$ components. It should be a foregone conclusion that a single frequency component of the output should be easier to compute than the complete output spectrum. The describing function DF of the PWM defines the output component at frequency ω in terms of the input modulation, so is a logical analytical tool for obtaining a quantitative description of first-order behavior. Though it portrays an incomplete picture of the output spectrum, DF analysis is

generally tractable, whereas the exact spectrum of arbitrary switch controllers may be analytically impossible to obtain. It is the purpose of this section to derive the describing function of the PWM.

The modulation input of the PWM is given by Eq. (2.9), subject to the restrictions in Eq. (2.10) which prohibit saturation of the pulse widths in the output. Equation (2.12) focuses attention on the output component at frequency ω, where ϕ_d and M_d denote, respectively, its phase lag with respect to the time origin at one of the sampling instants, and its magnitude:

$$d(t) = M_d \sin(\omega t - \phi_d) + (\text{other frequency components}) \ . \qquad (2.12)$$

Once M_d and ϕ_d have been determined, it is straightforward to evaluate the DF as shown in Eq. (2.13)

$$DF_m = \frac{M_d \, e^{-j\phi_d}}{u \, e^{-j\phi}} = G_m \, e^{j\phi_m} \ , \qquad (2.13)$$

where

$$G_m \equiv |DF_m| = \frac{M_d}{u}$$

$$\phi_m \equiv \underline{/DF_m} = \phi - \phi_d \ .$$

The subscript "m" refers to modulator parameters: DF_m, G_m, and ϕ_m are, respectively, the describing function, equivalent gain, and equivalent phase shift of the modulator. One must now find M_d and ϕ_d for the

given controller.

Recall the fact that a periodic function in time can always be expanded, either analytically or numerically, into a Fourier series. For the modulated input given by Eq. (2.9) and illustrated in Fig. 2.4(a), one can obtain a necessary and sufficient condition which insures that d(t) is periodic in Fig. 2.4(b). In particular, if the phase shift of $\varepsilon(t)$ after some integral number N of sample intervals is an integral multiple M of 2π, then the sequence of sampled input values, and hence d(t), is periodic. The periodicity condition for d(t) is given by Eq. (2.14),

$$\omega NT - \phi = 2\pi M - \phi \quad , \tag{2.14}$$

or, equivalently, since $\omega_s = 2\pi/T$, by Eq. (2.15):

$$\omega/\omega_s = M/N < 1 \quad . \tag{2.15}$$

The inequality arises from Eq. (2.11).

Two frequencies are said to be commensurable if both are integral multiples of a common frequency; otherwise, they are incommensurable. Suppose ω_1 and ω_2 were commensurable, as expressed by $\omega_1 = \ell\ \omega_x$ and $\omega_2 = q\ \omega_x$, where ω_x is the common frequency factor and ℓ and q are integers which have no common factor. The ratio of commensurable frequencies ω_1/ω_2 is the integer fraction ℓ/q, which is the same form as Eq. (2.15). Thus d(t) is periodic if and only if the modulation and

and switching frequencies are commensurable.

If d(t) is periodic, then ω and ω_s are related by Eq. (2.15). Let ω_x be the common factor of the commensurable frequencies, and let T_x be its period, as defined in Eq. (2.16):

$$\begin{aligned} \omega_x &\equiv \omega_s/N = \omega/M \\ T_x &\equiv 2\pi/\omega_x = NT \quad . \end{aligned} \tag{2.16}$$

The Fourier series expansion of d(t) is given by Eq. (2.17),

$$d(t) = \sum_{p=-\infty}^{\infty} A_p \, e^{jp\omega_x t} \quad , \tag{2.17}$$

where the complex amplitude coefficient A_p is given by the integral in Eq. (2.18)

$$A_p = \frac{1}{T_x} \int_0^{T_x} d(t) \, e^{-jp\omega_x t} \, dt \quad . \tag{2.18}$$

Since the amplitude coefficient is evaluated by a finite integral, one has some hope for a simple analytic result; on the other hand, an infinite integral must be performed to evaluate the frequency spectrum when d(t) is aperiodic . In the interest of simplicity, only commensurable modulation of the PWM will be considered in the remainder of this section.

The describing function concerns only the output component at the modulation frequency ω so one examines Eqs. (2.17) and (2.18) for the

values $p = \pm M$ (see Eq. (2.16)). Observe from Eq. (2.18) that since $d(t)$ is real, A_{-p} is the complex conjugate A_p^* of A_p, as shown in Eq. (2.19):

$$A_{-p} = A_p^* = \text{complex conjugate of } A_p \quad . \tag{2.19}$$

One feels intuitively that, when ω and ω_s are commensurable, the magnitude and phase shift of the describing function are both dependent on the modulation phase lag ϕ with respect to sampling instants.

The introductory remarks of Sec. 2.3.1 included a warning to treat with special care the situation $\omega = \frac{\omega_s}{2}$ which corresponds to the values $M = 1$ and $N = 2$ in Eq. (2.15). This case will now be examined in its entirety for the associated DF and will illustrate the possible dependence on ϕ. The PWM input and output waveforms are shown for two values of ϕ in Figs. 2.6(a) and 2.6(b). For $\phi = 0$, the first figure shows a complete absence of output component at ω; the second figure shows a large modulation-frequency component in the output for $\phi = \frac{\pi}{2}$.

Consider $\frac{M}{N} = \frac{1}{2}$ and evaluate Eq. (2.18) for $p = M = 1$. For an input given by Eq. (2.9) and (2.10), the PWM output is given, in conjunction with Fig. 2.3, by Eq. (2.20).

$$d(t) = \begin{cases} 1, & kT \leq t < kT + T \cdot \varepsilon(kT) \\ & \qquad\qquad\qquad\qquad , \; k = \text{integer} \\ 0, & kT + T \cdot \varepsilon(kT) \leq t < kT + T \end{cases} \tag{2.20}$$

From Eqs. (2.18) and (2.20), one can evaluate A_1 as:

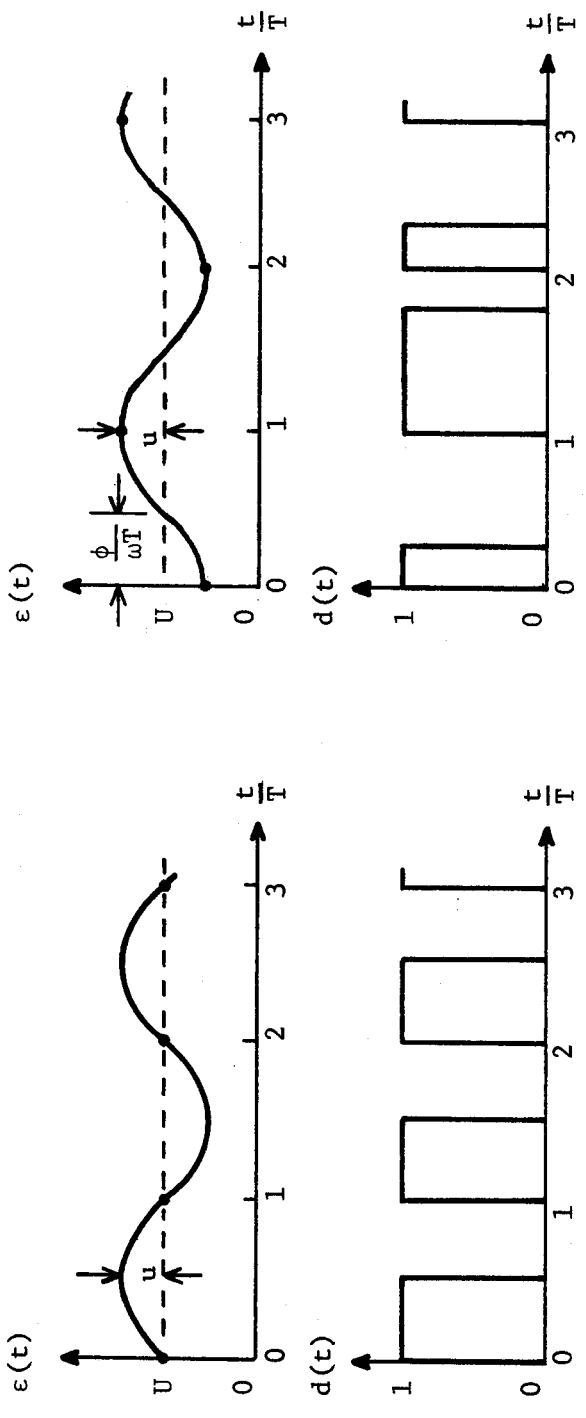

Fig. 2.6 Dependence of PWM output upon input phase when modulation and switching frequencies are commensurable ($\omega/\omega_s = 1/2$): (a)$\phi = 0$, (b)$\phi = \pi/2$.

$$A_{-1} = \frac{1}{T_x} \int_0^{NT} d(t)\, e^{-j\omega_x t}\, dt$$

$$= \sum_{k=0}^{N-1} \int_{kT}^{kT + T\,\varepsilon(kT)} \frac{1}{T_x} e^{-j\omega_x t}\, dt$$

$$= \frac{1}{-j\omega_x T_x} \sum_{k=0}^{1} \left[e^{-j\omega_x T\left(k + U + u \sin\left[\frac{2\pi k}{N} - \phi\right]\right)} - e^{-j\omega_x kT} \right]$$

$$= \frac{1}{-j2\pi} \left[e^{-j\pi\left(U + u \sin\left[-\phi\right]\right)} - 1 + e^{-j\pi\left(1 + U + u \sin\left[\pi - \phi\right]\right)} - e^{-j\pi} \right]$$

$$= \frac{e^{-j\pi U}}{-j2\pi} \left[e^{ju\pi \sin\phi} - e^{-ju\pi \sin\phi} \right]$$

$$= \frac{1}{\pi} \sin\left(u\pi \sin\phi\right) e^{-j\pi(U + 1)} \quad . \tag{2.21}$$

Equation (2.19) is used with Eq. (2.21) to obtain A_{-1} in Eq. (2.22)

$$A_{-1} = \frac{\sin(u\pi \sin\phi)}{\pi}\, e^{j\pi(U + 1)} \quad . \tag{2.22}$$

One can now rewrite Eq. (2.17) as Eq. (2.23)

$$d(t) = A_1 e^{j\omega t} + A_{-1} e^{-j\omega t} + \sum_{p \neq \pm 1} A_p e^{jp\omega_x t}$$

$$= \frac{\sin(u\pi \sin\phi)}{\pi} \left[e^{j(\omega t - \pi U - \pi)} + e^{-j(\omega t - \pi U - \pi)} \right]$$

$$+ \sum_{p \neq \pm 1} A_p e^{jp\omega_x t}$$

$$= \frac{2}{\pi} \sin(u\pi \sin\phi) \sin(\omega t - \pi U - \frac{\pi}{2}) + \sum_{p \neq \pm 1} A_p e^{jp\omega_x t} , \qquad (2.23)$$

which is the same form as Eq. (2.12), so one can identify M_d and ϕ_d:

$$\left.\begin{aligned} M_d &= \frac{2}{\pi} \sin(u\pi \sin\phi) \\ \phi_d &= \pi U + \frac{\pi}{2} \end{aligned}\right\} , \quad \frac{\omega}{\omega_s} = \frac{1}{2} . \qquad (2.24)$$

Equation (2.24) now allows one to evaluate exactly the amplitude and phase of the modulator DF in accordance with Eq. (2.13):

$$\left.\begin{aligned} G_m &= \frac{2}{u\pi} \sin(u\pi \sin\phi) \\ \phi_m &= \phi - \pi U - \frac{\pi}{2} \end{aligned}\right\} , \quad \frac{\omega}{\omega_s} = \frac{1}{2} . \qquad (2.25)$$

Equation (2.25) gives the exact DF of the PWM for the special case $\frac{\omega}{\omega_s} = \frac{1}{2}$. It shows that both G_m and ϕ_m are functions of ϕ as expected. Notice that u and U influence only G_m and ϕ_m, respectively; although both G_m and ϕ_m will generally be functions of u. The modulator gain G_m is strongly dependent on ϕ, but is relatively insensitive to the value of u.

The linearized describing function DF_{mo} is defined in Eq. (2.26) as the limit of DF_m for vanishing modulation amplitude:

$$DF_{mo} \equiv \lim_{u \to o} DF_m = \text{linearized describing function}$$

$$= G_{mo} e^{j\phi_{mo}} \quad , \tag{2.26}$$

where

$$G_{mo} \equiv |DF_{mo}|$$

$$\phi_{mo} = \underline{/DF_{mo}} \quad .$$

The removal of the u parameter from the DF exposes the predominate effects of other more influential modulation paramters, ϕ and U. Because DF_m is only slightly sensitive to the value of u, the linearized describing function should yield good DF predictions, yet it is easily derived analytically. To obtain DF_{mo}, one needs to determine only the leading term in the expansion about u = 0 of the controller output components at the modulation frequency. For simplicity, the leading term in u can be resolved as soon as it is practical to do so.

In anticipation of more difficult, or impossible, analytical evaluation of the exact DF for $\frac{\omega}{\omega_s} \neq \frac{1}{2}$ where the linearized DF may be advantageous, one should find the linearized DF in the present situation for comparative purposes. Because ϕ_m is independent of u, it is straightforward to obtain from Eqs. (2.26), (2.13), and (2.25) the linearized describing function,

$$DF_{mo} = 2 \sin \phi \; e^{j(\phi - \pi U - \frac{\pi}{2})}$$

$$= e^{-j\pi U} (1 - e^{j2\phi}) \quad , \frac{\omega}{\omega_s} = \frac{1}{2} \quad , \tag{2.27}$$

which is plotted in Fig. 2.7. Notice the strong dependence of DF_{mo} upon the modulation phase with respect to the sampling instant which was chosen as the time origin.

Since exact and linearized describing functions have been found for the special case $\frac{\omega}{\omega_s} = \frac{1}{2}$, one can now examine other values of M and N in Eq. (2.15). For simplicity, only the linearized DF will be derived here. From Eq. (2.18), one follows the procedure exemplified by Eq. (2.21) to obtain the complex Fourier coefficient for the output component at the modulation frequency:

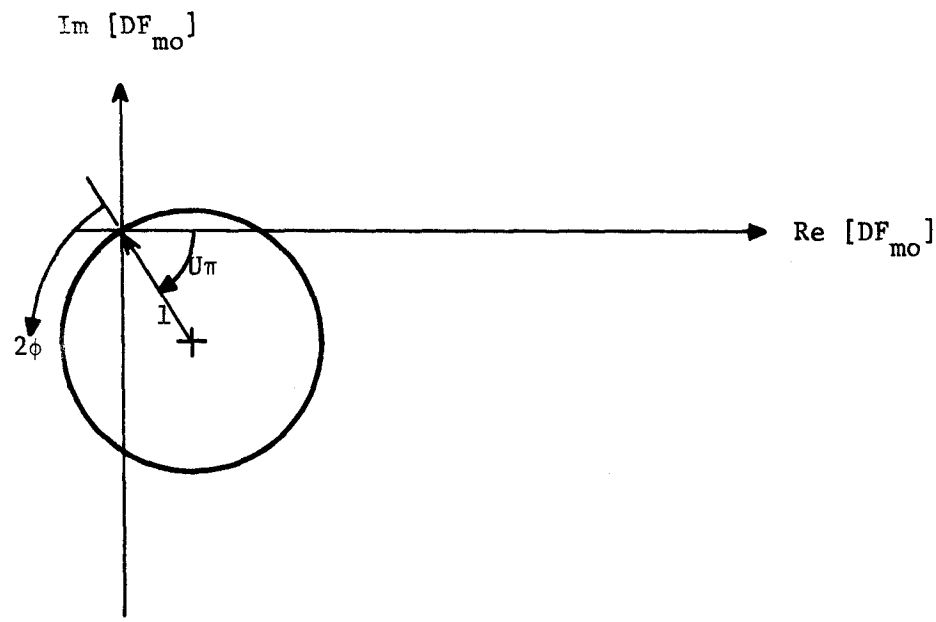

Fig. 2.7 Linearized PWM describing function, $\omega/\omega_s = 1/2$.

$$A_M = \frac{1}{T_x} \int_0^{T_x} d(t)\, e^{-jM\omega_x t}\, dt$$

$$= \frac{1}{T_x} \sum_{k=0}^{N-1} \int_{kT}^{kT + T\varepsilon(kT)} e^{-jM\omega_x t}\, dt$$

$$= \frac{1}{-jM\omega_x T_x} \sum_{k=0}^{N-1} \left[e^{-jM\omega_x T(k + U + u \sin[Mk\omega_x T - \phi]} - e^{-jM\omega_x kT} \right]$$

$$= \frac{1}{-jM2\pi} \sum_{k=0}^{N-1} \left[e^{-j \frac{2\pi M}{N}(k + U + u \sin[\frac{2\pi M}{N} k - \phi])} - e^{-j \frac{2\pi M}{N} k} \right]$$

$$= A_M(u) \quad . \tag{2.28}$$

Since the linearized DF is desired, expand A_M as a Taylor series in u

$$A_M(u) = A_M(0) + u\, A_M'(0) + \frac{u^2}{2!} A_M''(0) + \ldots \quad , \tag{2.29}$$

where a prime indicates the derivative of A_M with respect to u. One finds $A_M(0)$ from Eq. (2.28):

$$A_M(0) = \frac{1}{-jM2\pi} \left(e^{-j \frac{2\pi M}{N} U} - 1 \right) \sum_{k=0}^{N-1} e^{-j \frac{2\pi M}{N} k} \quad . \tag{2.30}$$

As an aside, one can do the summation in Eq. (2.30) by recalling

the geometric progression:

$$\sum_{k=0}^{N-1} z^k = \begin{cases} \dfrac{1 - z^N}{1 - z}, & z \neq 1 \\ N, & z = 1 \end{cases} \tag{2.31}$$

where z is an arbitrary complex variable. Let $z = e^{\pm j 2\pi \frac{M}{N}}$ in Eq. (2.31); observe that $z = 1$ if and only if $\frac{M}{N}$ is an integer, whereas $z^N = 1$ for any M and N values.

$$\sum_{k=0}^{N-1} e^{\pm j\frac{2\pi M}{N} k} = \begin{cases} 0, \frac{M}{N} \text{ not an integer} \\ N, \frac{M}{N} \text{ an integer} \end{cases} \tag{2.32}$$

Continuing the evaluation of $A_M(0)$, one concludes, from Eqs. (2.30), (2.32), and (2.15) that $A_M(0) = 0$. This is a general result and can be qualitatively justified as follows: if $u = 0$, then the input is unmodulated and the output has no component at ω (unless ω is some multiple of ω_s).

A comparison of Eqs. (2.12) and (2.17) shows that $A_M(u)$ is necessary to obtain $M_d(u)$ and $\phi_d(u)$;

$$\begin{aligned} M_d \sin(\omega t - \phi_d) &= A_M e^{j\omega t} + A_{-M} e^{-j\omega t} \\ &= A_M e^{j\omega t} + A^*_M e^{-j\omega t}, \end{aligned} \tag{2.33}$$

however, Eq. (2.28) cannot be evaluated in general by a closed form. In an effort to determine DF_{mo}, consider expanding Eq. (2.33) as a series in

u by substituting Eq. (2.29) for $A_M(u)$, where $A_M(0) = 0$,

$$M_d(u)\sin[\omega t - \phi_d(u)] = [u\,A_M'(0) + \frac{u^2}{2!}A_M''(0) + \ldots]\,e^{j\omega t}$$

$$+[u\,A_M'(0) + \frac{u^2}{2!}A_M''(0) + \ldots]^*\,e^{-j\omega t}$$

$$= u\;2\left|A_M'(0)\right|\cos\left[\omega t + \underline{/A_M'(0)}\right] + \sigma(u^2)$$

$$= u\;2\left|A_M'(0)\right|\sin(\omega t + \underline{/A_M'(0)} + \tfrac{\pi}{2}) + \sigma(u^2)\ . \tag{2.34}$$

Thus as u approaches zero

$$\left.\begin{aligned}\lim_{u\to o} M_d(u) &\equiv M_{do} = 2\,u\left|A_M'(0)\right| \\ \lim_{u\to o} \phi_d(u) &\equiv \phi_{do} = -\underline{/A_M'(0)} - \frac{\pi}{2}\end{aligned}\right\}\ , \tag{2.35}$$

so the linearized describing function defined in Eq. (2.26) is given by

$$DF_{mo} = \frac{M_{do}\,e^{-j\phi_{do}}}{u\,e^{-j\phi}}$$

$$= G_{mo}\,e^{j\phi_{mo}}\ , \tag{2.36}$$

where

$$G_{mo} = 2\left|A'_M(0)\right| \tag{2.37}$$

$$\phi_{mo} = \phi + \underline{/A'_M(0)} + \frac{\pi}{2} \quad . \tag{2.38}$$

Equation (2.28) is used to evaluate $A'_M(0)$:

$$A'_M(u) = \sum_{k=0}^{N-1} \left[\frac{1}{N} \sin\left(\frac{2\pi M}{N} k - \phi\right) e^{-j \frac{2\pi M}{N} \left(k + U + u \sin\left[\frac{2\pi M}{N} k - \phi\right]\right)} \right] \tag{2.39}$$

$$A'_M(0) = \frac{1}{N} \sum_{k=0}^{N-1} \sin\left(\frac{2\pi M}{N} \kappa - \phi\right) e^{-j \frac{2\pi M}{N} (k + U)}$$

$$= \frac{e^{-j \frac{2\pi M}{N} U}}{2jN} \left[Ne^{-j\phi} - e^{j\phi} \sum_{k=0}^{N-1} e^{-j\, 2\pi \frac{2M}{N} k} \right] \quad . \tag{2.40}$$

The summation in Eq. (2.40) is given by Eq. (2.32) and is zero for all M and N values ($0 < M < N$) except $\frac{M}{N} = \frac{1}{2}$.

$$A'_M(0) = \begin{cases} \frac{1}{2} e^{-j(\phi + \frac{2\pi M}{N} U + \frac{\pi}{2})} & , \ \frac{M}{N} \neq \frac{1}{2} \\ \sin\phi \; e^{-j(\pi U + \pi)} & , \ \frac{M}{N} = \frac{1}{2} \quad . \end{cases} \tag{2.41}$$

Substitute Eq. (2.41) into Eqs. (2.37) and (2.38) to get

$$DF_{mo} = \begin{cases} 1 \; e^{-j \frac{2\pi M}{N} U} & , \ \frac{M}{N} \neq \frac{1}{2} \\ 2 \sin\phi \; e^{j(\phi - \pi U - \frac{\pi}{2})} & , \ \frac{M}{N} = \frac{1}{2} \quad . \end{cases} \tag{2.42}$$

Equation (2.42) is the linearized describing function of the PWM when ω and ω_s are commensurable. The leading term in the expansion of A_M as a function of u is sufficient to completely specify DF_{mo}; as a result, DF_{mo} is much easier to evaluate than the exact DF_m. Notice the comforting correlation between Eqs. (2.27) and (2.42) which give DF_{mo} for the special case $\frac{\omega}{\omega_s} = \frac{1}{2}$. For $\frac{\omega}{\omega_s} \neq \frac{1}{2}$, DF_{mo} is particularly simple: its magnitude is unity and its phase angle is independent of ϕ and is a linear function of U. The magnitude and phase of DF_{mo} are shown as a function of ω in Fig. 2.8; any resemblance to a Bode plot is superficial since the frequency scale is linear, instead of logarithmic. Dots are used for data points as a mnemonic device for remembering the frequency restrictions $\frac{\omega}{\omega_s} = \frac{M}{N}$.

The analysis has considered only commensurable frequencies to this point; the treatment of incommensurable frequencies, $\frac{\omega}{\omega_s} \neq \frac{M}{N}$, is a logical extension. One does not expect the nature of the DF to change suddenly as ω varies continuously through the frequency range $0 < \omega < \omega_s$, so the linearized describing function for incommensurable frequencies should conceptually fill in the spaces between dots in Fig. 2.8. When ω and ω_s are incommensurable, the phase shift in the modulation sinusoid after any number of sampling periods is never a multiple of 2π, so there is no periodicity in the output of the PWM. The DF in this situation should be independent of ϕ regardless of the sampling instant chosen as time reference. The aperiodicity of the PWM output makes exact DF evaluation difficult since the straightforward Fourier series formulation no longer applies. The following section is concerned with incommensurable frequencies.

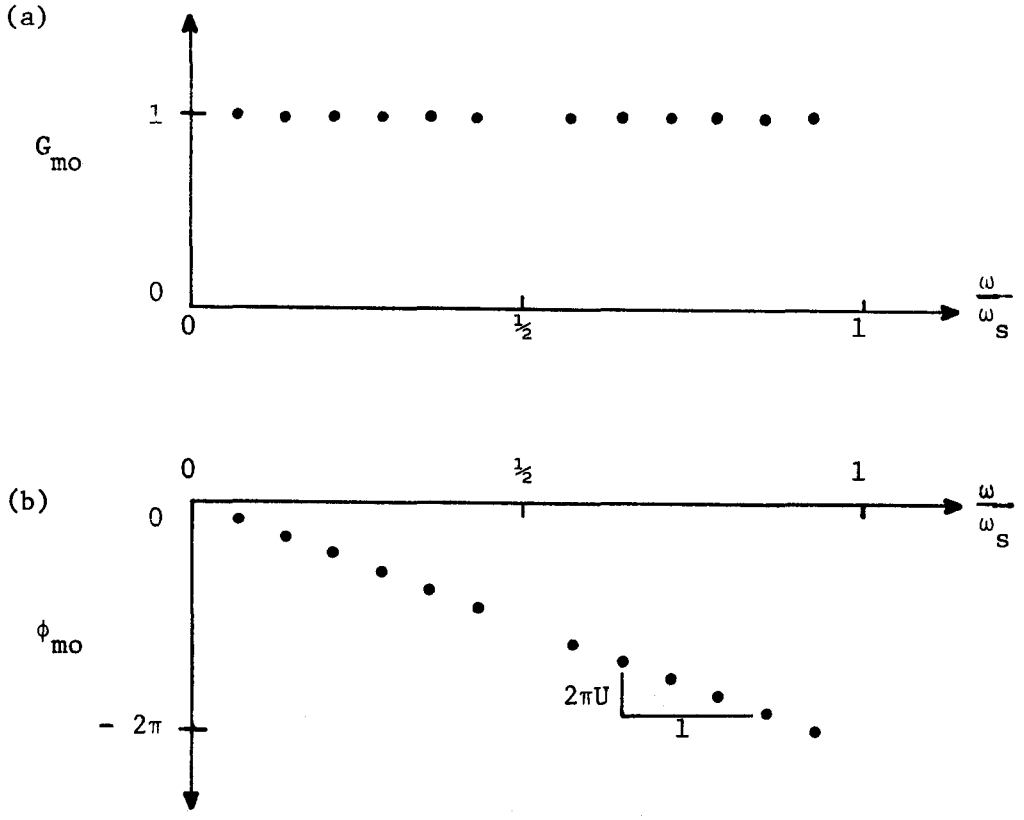

Fig. 2.8 Linearized PWM describing function for commensurable frequencies, $\omega/\omega_s = M/N \neq 1/2$ $(0 < M < N)$; (a) magnitude, (b) phase.

2.3.2 Exact Output Spectrum of Controller

Section 2.3.1 treated special cases of modulation in order to illustrate analytic procedures which are generally applicable to nonlinear switch controllers. The output spectrum of a PWM was discussed qualitatively and the approximate first-order output component at frequency ω was obtained for an input which results in a periodic output. A necessary and sufficient condition for a periodic PWM output is commensurable frequencies, $\frac{\omega}{\omega_s} = \frac{M}{N}$.

Here the DF for incommensurable frequencies is sought. This problem can be imbedded within a larger problem that seeks the PWM output spectrum which occurs when ω and ω_s are independent. The solution for independent frequencies can be examined at will for either commensurable or incommensurable frequencies, but it is rarely analytically tractable. Fortunately, the solution can be found for the PWM with an input consisting of dc plus sinusoid.

The exact frequency spectrum of the PWM output is presented in this section and then is reduced to show the spectrum corresponding to incommensurable and commensurable frequencies. Comparisons are drawn where appropriate between the results of the present section and the corresponding equations of Sec. 2.3.1. Finally, a linearized transfer characteristic emerges which is valid for modulation frequencies less than $\frac{\omega_s}{2}$.

The successful derivation of the modulated output spectrum hinges upon the existence of a bivariate function g which satisfies Eqs. (2.43) and (2.44)

$$g(x,y) = g(x + 2\pi m,\ y + 2\pi n),\ m \text{ and } n \text{ are arbitrary integers} \qquad (2.43)$$

$$g(\omega_s t,\ \omega t) = d(t) \quad . \qquad (2.44)$$

Since g(x,y) is doubly periodic, it can be written as a double Fourier series,

$$g(x,y) = \sum_{m=-\infty}^{\infty} \sum_{m=-\infty}^{\infty} A_{m,n}\ e^{j(mx + ny)} \quad , \qquad (2.45)$$

where

$$A_{m,n} = \frac{1}{(2\pi)^2} \int_0^{2\pi} \int_0^{2\pi} g(x,y)\ e^{-j(mx + ny)}\ dx\ dy \quad . \qquad (2.46)$$

Once $A_{m,n}$ is known, then the desired spectrum of d is given by substitution of Eq. (2.45) into Eq. (2.44)

$$d(t) = \sum_{m} \sum_{n} A_{m,n}\ e^{j(m\omega_s + n\omega)t} \quad . \qquad (2.47)$$

Evaluation of a modulated spectrum by means of a two-dimensional approach was first suggested by Bennett[4], and later elucidated by Black[5] and Rowe[6]. Details in the computation of $A_{m,n}$ are presented in Appendix A; the resultant spectrum shows in Eq. (2.48) that d(t) is composed of a dc term, harmonics of ω, harmonics of ω_s, and sidebands of all ω_s harmonics:

$$d(t) = U + \sum_{m\neq 0} \frac{1}{jm\omega_s T} e^{jm\omega_s t}$$

$$- \sum_{m} \sum_{n} e^{-jn(\phi + \pi)} \frac{J_n[uT(m\omega_s + n\omega)]}{jT(m\omega_s + n\omega)} e^{j(m\omega_s + n\omega)(t - UT)},$$

$$m\omega_s + n\omega \neq 0 \qquad (2.48)$$

where $J_n(z)$ is a Bessel function of the first kind.

The nature of this spectrum was qualitatively depicted in Fig. 2.5(b). One could, if interested, plot the amplitude of the n^{th} harmonics and sidebands versus n with u and ωT as parameters. It is sufficient here to observe that, since $J_n(z)$ is of order z^n, these n^{th}-order components decrease in amplitude as u^n so are usually negligible when compared to the fundamental.

Incommensurable Frequencies. The spectrum in Eq. (2.48) can be rewritten as in Eq. (2.49) to show explicitly the various harmonics and sidebands which occur at distinct frequencies when ω and ω_s are incommensurable. Each subscript pair (m,n) refers to a unique frequency; for example, no sideband of ω_s or its harmonics can coincide in frequency with a harmonic of ω,

$$d(t) = U + \sum_{m\neq 0} \left[1 - e^{-j2\pi mU} J_o(u2\pi m)\right] \frac{e^{jm\omega_s t}}{j2\pi m}$$

$$- \sum_{n\neq 0} J_n(un\omega T)\, e^{-jn(\phi + \pi)} \frac{e^{jn\omega(t - UT)}}{jn\omega T}$$

$$- \sum_{m\neq 0} \sum_{n\neq 0} e^{-jn(\phi + \pi)} J_n[uT(m\omega_s + n\omega)] \frac{e^{j(m\omega_s + n\omega)(t-UT)}}{j(m\omega_s + n\omega)\, T}$$

(2.49)

Equation (2.49) is easily arranged into the form of Eq. (2.12) in order to identify the amplitude and phase lag, with respect to the time origin, of the fundamental modulation frequency in the output

$$\left.\begin{aligned} M_d &= \frac{2}{\omega T} J_1(u\omega T) \\ \phi_d &= \phi + U\omega T \end{aligned}\right\} . \tag{2.50}$$

Substitute Eq. (2.50) into Eq. (2.13) to get the exact DF for incommensurable frequencies:

$$DF_m = \frac{2}{u\omega T} J_1(u\omega T)\, e^{-j\omega UT} . \tag{2.51}$$

The magnitude G_m and phase ϕ_m of DF_m are plotted in Figs. 2.9(a) and 2.9(b) with dashed lines to represent the restriction to incommensurable frequencies $\frac{\omega}{\omega_s} \neq \frac{M}{N}$. Observe that both G_m and ϕ_m are independent of ϕ as anticipated; also, G_m and ϕ_m can be independently varied as either u or U is changed.

The plot of G_m versus u is the same shape as Fig. 2.9(a) since u and ωT appear as a product in G_m; thus, G_m is relatively insensitive to the value of u for $u << \frac{1}{2}$. This condition is necessary for the linearized describing function to be meaningful. Equations (2.51) and (2.26) yield DF_{mo}

$$DF_{mo} = 1\, e^{-j\omega UT} = 1\, e^{-j2\pi U \frac{\omega}{\omega_s}} , \tag{2.52}$$

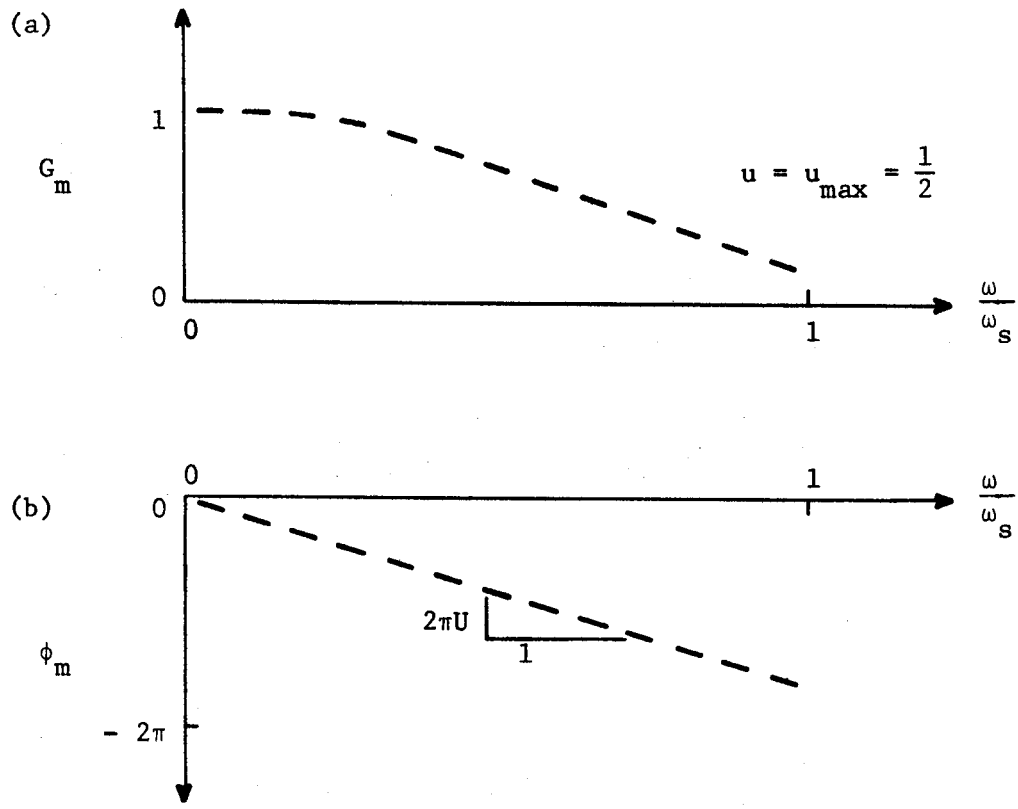

Fig. 2.9 Exact PWM describing function for incommensurable frequencies, $\omega/\omega_s \neq M/N$; (a) magnitude, (b) phase.

which is sketched in Fig. 2.10.

Comparison of Figs. 2.8 and 2.10 reveals the gratifying conclusion that DF_{mo} is a continuous function of ω, except for the special case $\frac{\omega}{\omega_s} = \frac{1}{2}$, regardless of whether ω and ω_s are incommensurable or commensurable. This observation substantiates the intuitive expectation stated in the final paragraph of Sec. 2.3.1 concerning the continuous nature of the DF. Attention will be turned now to the exact treatment of commensurable frequencies.

Commensurable Frequencies. Section 2.3.1 derived the linearized describing function of the PWM when ω and ω_s are commensurable. The present analysis attempts to formulate the exact DF for the same situation in an effort to remove the restrictions on u which result from linearization.

Suppose that ω_x is the common factor in the commensurable frequencies, as defined in Eq. (2.16). The frequency factor,

$$m\omega_s + n\omega = (mN + nM)\omega_x = r\omega_x \quad , \tag{2.53}$$

in the general series expansion of the modulator output, Eq. (2.48), shows that commensurable frequencies result in the interaction or superposition of many orders of harmonics and sidebands. Thus, there are an infinite number of m and n values which produce an output component at $r\omega_x$. In particular, if the indices (m_r, n_r) produce a component at $r\omega_x$, then so do the indices $(m_r - qM, n_r + qN)$ for any integer q. The components at frequency $r\omega_x$ can be grouped by summing over the index q; the resulting

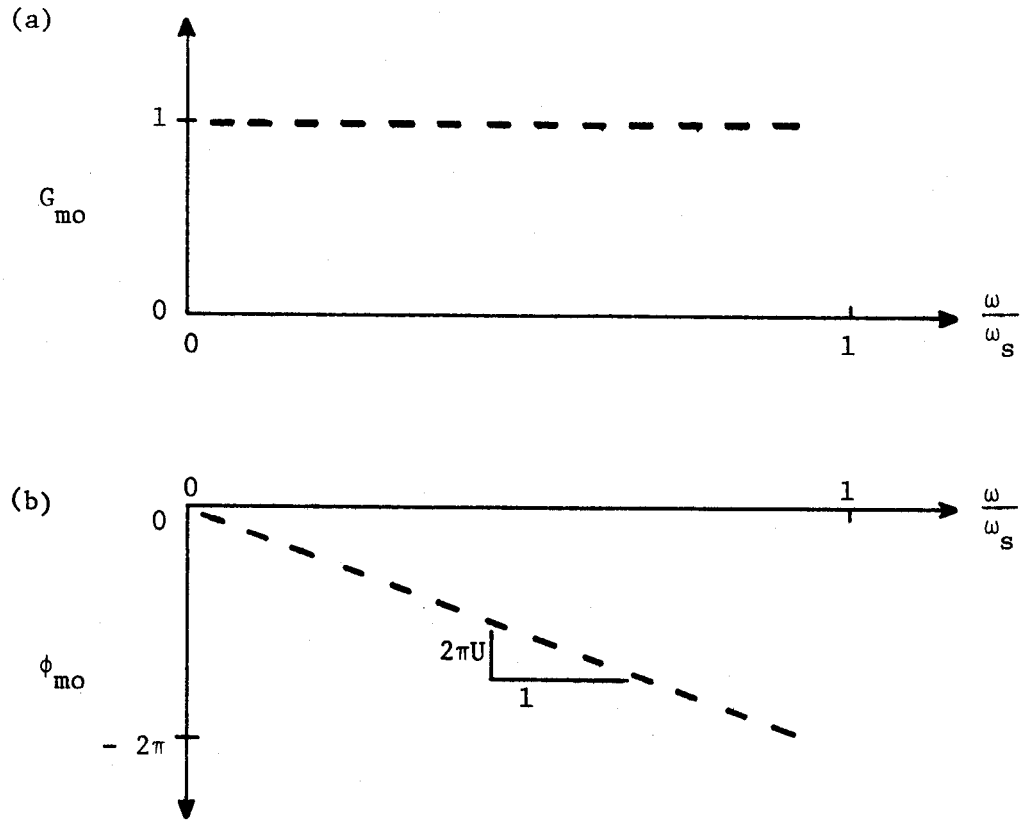

Fig. 2.10 Linearized PWM describing function for incommensurable frequencies, $\omega/\omega_s \neq M/N$; (a) magnitude, (b) phase.

specialization of Eq. (2.48) for commensurable frequencies is given by Eq. (2.54)

$$d(t) = U + \sum_{m\neq 0} \frac{1}{j2\pi m} e^{jm\omega_s t} - \sum_{r\neq 0} \sum_{q} \frac{Ne^{j(n_r + qN)(\phi + \pi)}}{j2\pi r} J_{n_r + qN}(ur\frac{2\pi}{N})\, e^{jr\omega_x(t-UT)} . \tag{2.54}$$

The components of d(t) which occur at frequency $r\omega_x = \pm \omega = \pm M\omega_x$ determine the amplitude and phase of the sinusoid defined in Eq. (2.12). Equation (2.55) shows the $r = \pm M$ terms of Eq. (2.54); observe from Eq. (2.53) that the appropriate m and n indices are $(m_r, n_r)_{r = \pm M} = (0, \pm 1)$,

$$M_d \sin(\omega t - \phi_d) = - \sum_{q} \frac{N}{\pi M} J_{1 + qN}(u\frac{2\pi M}{N}) \sin(\omega t - \frac{2\pi M}{N} U - (1 + qN)(\phi+\pi)) \tag{2.55}$$

Unfortunately, Eq. (2.55) shares the same fate as an earlier analysis of commensurable frequencies which culminated in Eqs. (2.28) and (2.33); namely, a summation has been encountered that cannot be summed analytically in a closed form. Equation (2.28) was derived from a simple Fourier series expansion whereas Eq. (2.55) is based on a double Fourier series expansion in two independent variables and arises when the two

variables are linearly related; however, it can be shown that both methods lead to precisely the same result for commensurable frequencies, as follows.

Substitute into Eq. (2.28) the expansion (see Ref. (7), Eq. 9.1.41):

$$e^{\pm jz \sin\theta} = \sum_{m=-\infty}^{\infty} (e^{\pm j\theta})^m J_m(z) \quad . \tag{2.56}$$

The second exponential in the square bracket of Eq. (2.28) sums to zero by virtue of Eq. (2.32) so the remaining terms in A_M become

$$A_M = \frac{1}{-jM2\pi} \sum_{k=0}^{N-1} e^{-j\frac{2\pi M}{N}(k+U)} \; e^{-j\frac{2\pi M}{N} u \sin(\frac{2\pi M}{N} k - \phi)}$$

$$= \frac{-1}{jM2\pi} \sum_{k=0}^{N-1} e^{-j\frac{2\pi M}{N}(k+U)} \sum_{m} e^{-jm(\frac{2\pi M}{N} k - \phi)} J_m(\frac{2\pi M}{N} u)$$

$$= \frac{-e^{-j\frac{2\pi M}{N} U}}{j2\pi M} \sum_{m} e^{jm\phi} J_m(u\frac{2\pi M}{N}) \sum_{k=0}^{N-1} e^{-j\frac{2\pi M}{N}(1+m)k}$$

$$= \frac{-e^{-j\frac{2\pi M}{N} U}}{j2\pi M} \sum_{m} e^{-jm(\phi+\pi)} J_m(u\frac{2\pi M}{N}) \sum_{k=0}^{N-1} e^{-j\frac{2\pi M}{N}(1-m)k} \quad . \tag{2.57}$$

The k summation is the geometric progression evaluated in Eq. (2.31) and has the value N for $1 - m = pN$, p any integer; otherwise it is zero. By summing over p, all values of $m = 1 - pN$ which contribute to the series are accounted for:

$$A_M = \frac{e^{-j\frac{2\pi M}{N}U}}{-jM2\pi} \sum_p e^{-j(1-pN)(\phi+\pi)} J_{1-pN}(u\frac{2\pi M}{N})\,N$$

$$= \frac{-N\,e^{-j\frac{2\pi M}{N}U}}{jM2\pi} \sum_p e^{-j(1+pN)(\phi+\pi)} J_{1+pN}(u\frac{2\pi m}{N})\,. \tag{2.58}$$

When Eq. (2.58) is substituted into Eq. (2.33), the result is identical with Eq. (2.55).

It has been shown for commensurable frequencies that two methods give equivalent expressions for the describing function, but that these expressions cannot be evaluated in closed form. When the exact DF is linearized by restricting u, an analytic approximation DF_{mo} results, as given by Eq. (2.42). At the other extreme, incommensurable frequencies can only be analyzed by the method that assumes the frequencies are independent. The linearized DF is continuous as ω varies through both commensurable and incommensurable frequencies, except for the special case $\frac{\omega}{\omega_s} = \frac{1}{2}$ which can be accounted for by restricting ω to the range $0 < \omega < \omega_s/2$; thus , one should use the simplest possible derivation (one-dimensional Fourier series for commensurable frequencies) when seeking DF_{mo}. The frequency restriction on ω is not unrealistic since if ω were in the range $\omega_s/2 < \omega < \omega_s$, then an output component of comparable amplitude would lie in the lower half-band at $\omega_s - \omega$ and would not be accounted for by the describing function.

The (linearized) describing function of the PWM which emerges from two restrictions is given by Eq. (2.52). It is valid to first-order approximation for both commensurable and incommensurable modulation

frequencies in the range

$$0 < \omega < \omega_s/2 \quad , \tag{2.59}$$

and for sufficiently small modulation amplitude,

$$0 < u << \frac{1}{2} \quad . \tag{2.60}$$

The simple form of DF_{mo} makes it particularly useful for analytic insight into complex switching systems.

2.4 Converter

Since the buck power stage and PWM switch controller have been individually analyzed, one can now consider the converter which results from their interconnection. The exact frequency spectrum of the PWM output d is given by Eq. (2.48) and consists of a superposition of sinusoids and dc. Since the buck power stage is linear, Eqs. (2.2), (2.6), and (2.7) show that the power-stage output v is given by,

$$\frac{v(t)}{V_s} = G_f(0)\ U + \sum_{m\neq 0} \frac{G_f(jm\omega_s)}{jm\omega_s T}\ e^{jm\omega_s t}$$

$$- \sum_m \sum_n e^{-jn(\phi+\pi)}\ \frac{J_n[uT(m\omega_s+n\omega)]}{jT(m\omega_s+n\omega)}\ G_f[j(m\omega_s+n\omega)]\ e^{j(m\omega_s+n\omega)(t-UT)} \quad ,$$

$$m\omega_s + n\omega \neq 0 \tag{2.61}$$

which again is a superposition of sinusoids and dc. The filter transfer function $G_f(j\omega)$, given by Eq. (2.5), is a complex variable whose characteristics are independent of modulation parameters. Thus Eq. (2.61) shows that the converter DF is the product of the PWM and power-stage describing functions for either incommensurable frequencies or first-order linearization of the modulation amplitude.

The exact analysis of the control path for a specific dc-dc converter has thus been completed. By no means can these results be generalized to other converters, since the buck power stage was the only type for which the transfer function was known. A method which is capable of obtaining the DF for boost and buck-boost power stages will be developed in the following chapter. The results of the present chapter can be used as a comparison standard for evaluating proposed methods of analysis.

Chapter 3

DEVELOPMENT OF AVERAGING METHOD AND AVERAGED POWER-STAGE MODELS

3.1 Introduction

In view of the absence of simple circuit models for the boost and buck-boost power stages, attention is directed now to the establishment of suitable models. Unlike the buck power stage, the circuit topology of the filter components in the boost and buck-boost power stages is changed when the switch states reverse. Filter characteristics of the basic power stages have thus been obscured by lack of a model which could account for the change in circuit topology, and yet lead to useful transfer functions.

A major part of the original contributions in this theis is presented in the present chapter. Section 3.2 provides a plausible basis for the concept of slowly-varying time averages, from which an averaging procedure is developed. Next, an appropriate model which includes typical parasitic components is developed for a representative (boost) converter power stage as an example of the averaging method, and illustrates inherent assumptions and limitations. Finally, circuit models are presented in Sec. 3.3 for the two remaining power-stage types.

3.2 Example Treatment of Boost Power Stage

Because it is sufficiently general to elucidate the procedure which applies for other circuit configurations, the boost power stage is considered here in detail to illustrate the method that is developed in this

chapter. Consider the slightly modified version shown in Fig. 3.1 of the boost power stage which was originally introduced in Fig. 1.7(a). The equivalent series resistances of the capacitor and the inductor are included since these small, but unavoidable, parasitic parameters may influence both efficiency and frequency response. Since practical switches have nonzero "on"-resistance, R_ℓ represents not only the inductor resistance, but also the source output resistance in series with weighted averages of the switch resistances. In general, the switch model may also include an "offset" voltage when the switch is in the "on" state. More accurate switch models were disregarded, in the interest of simplicity, after it was discovered through simulation that typical component values in the switch models cause only second-order effects.

Equations (3.1) and (3.2) describe the exact circuit of Fig. 3.1. The right-hand side of the circuit equations are identified as driving functions,

$$L \frac{di(t)}{dt} + R_\ell \, i(t) = v_s(t) - v_n(t) \quad , \qquad (3.1)$$

$$C \frac{dv_c(t)}{dt} + \frac{1}{R + R_c} \, v_c(t) = \frac{R}{R + R_c} \, i_n(t) \quad . \qquad (3.2)$$

Subsidiary equations are:

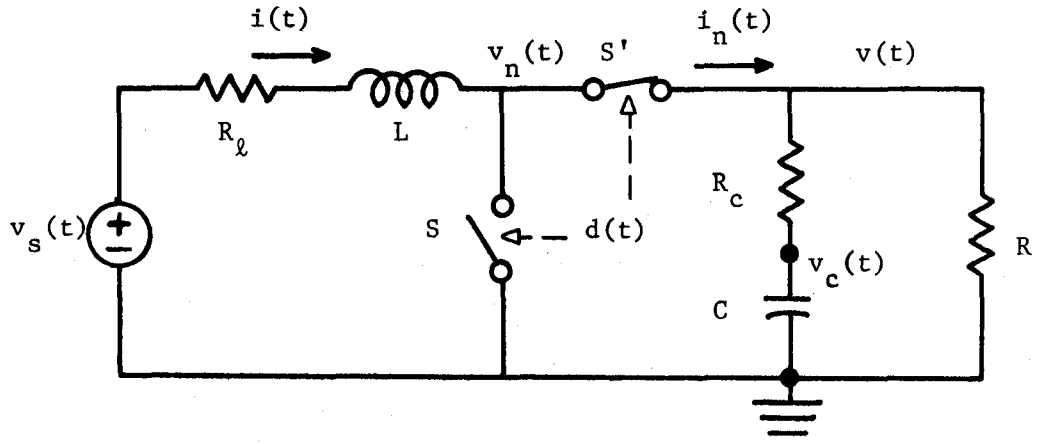

Fig. 3.1 Boost power stage with parasitic resistances R_ℓ and R_c.

$$v(t) = \frac{R}{R + R_c}\, v_c(t) + \frac{R \cdot R_c}{R + R_c}\, i_n(t) \tag{3.3}$$

$$v_n(t) = \begin{cases} 0; \text{ S closed, S' open} \\ v(t); \text{ S open , S' closed} \end{cases} \tag{3.4}$$

$$i_n(t) = \begin{cases} 0; \text{ S closed, S' open} \\ i(t); \text{ S open , S' closed} \end{cases} . \tag{3.5}$$

Notice that v_n and i_n can be expressed, in view of Eq. (1.1), as a function of the switch-drive signal d, so that Eqs. (3.4) and (3.5) can be replaced by:

$$v_n(t) = [1 - d(t)]\, v(t) \tag{3.6}$$

$$i_n(t) = [1 - d(t)]\, i(t) . \tag{3.7}$$

Equations (3.6) and (3.7), together with the following definitions,

$$\tau_i \equiv \frac{L}{R_\ell} \tag{3.8}$$

$$\tau_v \equiv (R + R_c)C , \tag{3.9}$$

allow Eqs. (3.1) - (3.3) to be rewritten as:

$$\frac{di(t)}{dt} + \frac{1}{\tau_i}\, i(t) = \frac{1}{L}\,\{v_s(t) - [1 - d(t)]\, v(t)\}\ , \qquad (3.10)$$

$$\frac{dv_c(t)}{dt} + \frac{1}{\tau_v}\, v_c(t) = \frac{R}{\tau_v}\,[1 - d(t)]\, i(t)\ , \qquad (3.11)$$

$$v(t) = \frac{R}{R + R_c}\, v_c(t) + R \| R_c [1 - d(t)]\, i(t)\ . \qquad (3.12)$$

It is evident from the above equations that Fig. 3.2 is an exact equivalent circuit for the power stage shown in Fig. 3.1. The notational convention adopted here used circles for independent sources, squares for dependent sources, and rectangles for impedances. The factor 1-d(t) is a time-variable gain of the dependent current and voltage generators and is the principal cause of analytic difficulty.

The following discussion is intended to demonstrate the converter insensitivity to fast variations of the driving functions in Eqs. (3.10) and (3.11). Consider the time interval T_N when switch S is closed and S' is open and assume $v_s(t)$ is a constant V_s. The exact solutions are easily derived,

$$\left.\begin{aligned} i(t) &= \frac{V_s}{R_\ell} - \left[\frac{V_s}{R_\ell} - i(0)\right] e^{-t/\tau_i} \qquad (3.13) \\ v_c(t) &= v_c(0)\, e^{-t/\tau_v} \qquad (3.14) \end{aligned}\right\} \quad 0 \le t \le T_N \ ,$$

and can be used to determine typical design restrictions on the time constants τ_i and τ_v. Intolerable power dissipation would occur if the inductor current were allowed to approach the value $\frac{V_s}{R_\ell}$ so a limitation,

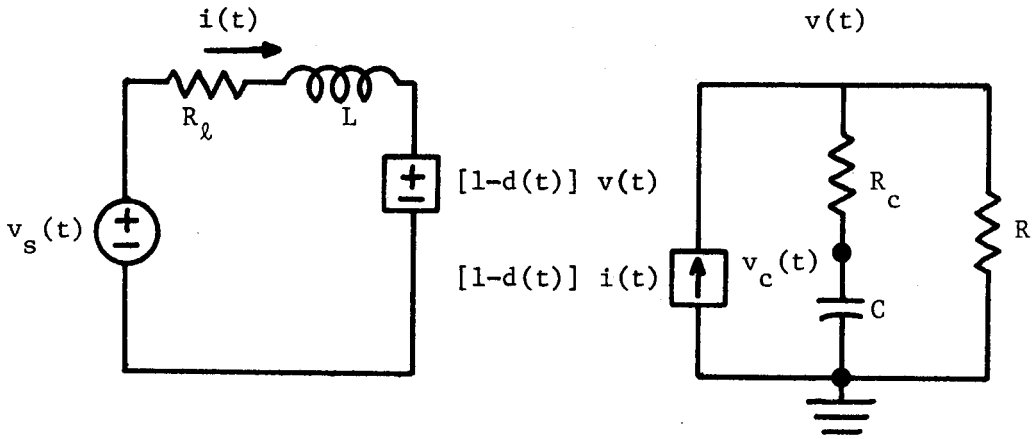

Fig. 3.2 Equivalent boost power stage.

$R_\ell\ i(T_N) << L \left.\frac{di}{dt}\right|_{T_N}$, on the instantaneous resistive power requires the restriction $\tau_i >> T_N$. Output voltage ripple can be constrained by imposing the condition $v_c(0) - v_c(T_N) << v_c(0)$, which results in the requirement $\tau_v >> T_N$. Since T_N varies between 0 and T, the constraints on power dissipation and ripple are always satisfied if

$$\tau_i,\ \tau_v >> T \quad . \tag{3.15}$$

Useful converters invariably satisfy Eq. (3.15) or suffer the consequences of large output ripple and poor efficiency. Because the time constants of i and v_c in Eqs. (3.10) and (3.11) are much greater than the switching period, variations in the driving functions which occur during a time interval T are effectively averaged by the power stage. This very important observation is the underlying basis for ensuing assumptions which engender a tractable analytic method.

The foregoing comments suggest that an averaging method of some kind is a suitable operational procedure for analyzing the approximate low-frequency response of a switched power stage. The precise algorithm chosen for the averaging process is not important as long as it is reasonably defined. Equation (3.16) describes a moving time-average of a function g over a time interval T and is one possible algorithm:

$$\langle g \rangle(t) \equiv \frac{1}{T} \int_{t-T}^{t} g(\tau)\ d\tau \quad . \tag{3.16}$$

One should inquire into the question of how the averaging operation defined by Eq. (3.16) affects the signal components of g. Suppose g is a sinusoid represented by the exponential phasor $e^{j\omega t}$; then, the average of g

$$\langle e^{j\omega t} \rangle = \frac{1}{j\omega T} [e^{j\omega t} - e^{j\omega(t-T)}]$$

$$= e^{j\omega(t-\frac{T}{2})} \frac{\sin(\omega T/2)}{\omega\ T/2} \quad , \qquad (3.17)$$

is simply g with an amplitude attenuation of $\sin(\omega T/2)/(\omega T/2)$ and a phase delay of $\omega T/2$. The averaging operator is, in essence, a low-pass filter with cut-off frequency $\omega_s = 2\pi/T$; thus, $\langle g \rangle$ is an acceptable approximation of g only for quasi-static frequencies, i.e., $\omega \leq \omega_s$. Notice that sinusoidal components of g at harmonic frequencies of 1/T do not appear in $\langle g \rangle$; also, $\langle g \rangle$ is continuous, even though g may be discontinuous.

It is easily shown from Eq. (3.16) that the average of the derivative equals the derivative of the average;

$$\langle \frac{dg}{dt} \rangle (t) = \frac{d\langle g \rangle}{dt}(t) \quad , \qquad (3.18)$$

hence, the result of applying the averaging operator to Eqs. (3.10) - (3.11) is a new set of filtered state variables with no ripple components,

$$\frac{d\langle i \rangle}{dt} + \frac{1}{\tau_i} \langle i \rangle = \frac{1}{L} (\langle v_s \rangle - \langle (1 - d)v \rangle) \qquad (3.19)$$

$$\frac{d\langle v_c\rangle}{dt} + \frac{1}{\tau_v}\langle v_c\rangle = \frac{R}{\tau_v}\langle (1 - d)i\rangle \quad , \tag{3.20}$$

where

$$\langle v\rangle = \frac{R}{R + R_c}\langle v_c\rangle + R \| R_c \langle (1 - d)i\rangle \quad . \tag{3.21}$$

The equivalent circuit corresponding to Eqs. (3.19) - (3.21) is shown in Fig. 3.3.

Interpretation is now clouded by the product averages, <id> and <vd>, which hinder the quest for a simple equivalent system in terms of <i> and <v>. One would like to find the conditions necessary in order to make assertions of the form <vd> = <v> <d>, etc. The average product

$$\langle vd\rangle = \frac{1}{T}\int_{t-T}^{t} v(w)\, d(w)\, dw \quad , \tag{3.22}$$

can be simplified if one of the factors is quasi-continuous over the integration interval; e.g.,

$$\left|\frac{v(t) - \langle v\rangle(t)}{v(t)}\right| << 1 \quad . \tag{3.23}$$

A possible variation of v, which satisfies Eq. (3.23), is shown in Fig. 3.4. Let F be the difference between the instantaneous voltage over an interval T and the average voltage associated with that interval:

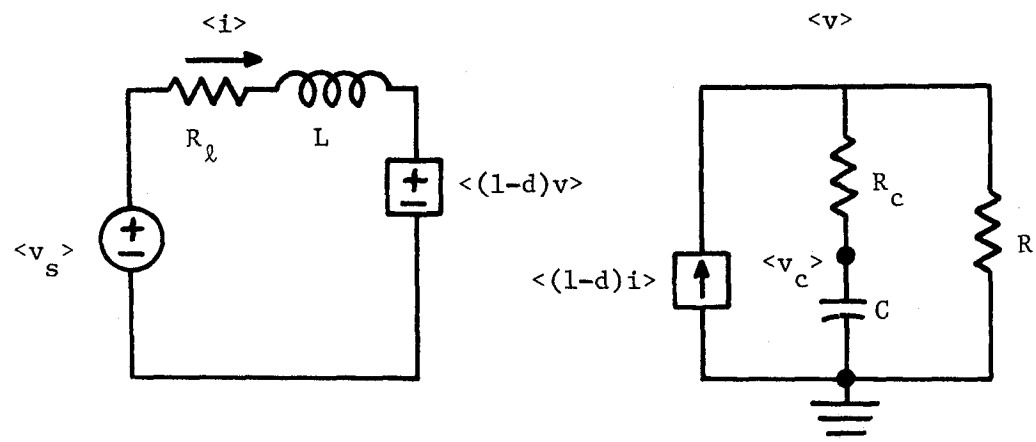

Fig. 3.3 Intermediate averaged model of the boost power stage.

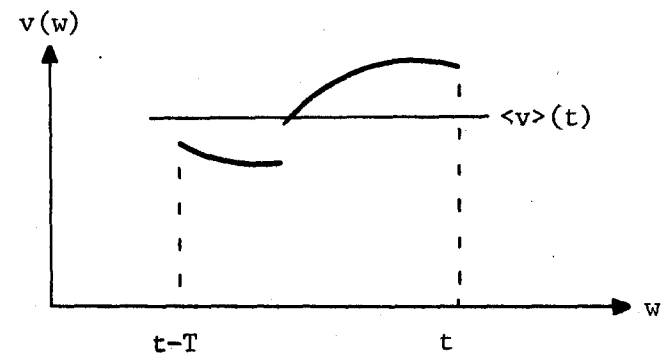

Fig. 3.4 Example of a quasi-continuous time-dependent variation.

$$F(w) \equiv v(w) - \langle v \rangle(t) \quad , \tag{3.24}$$

where $t-T \leq w \leq t$. Substitute Eq. (3.24) into Eq. (3.22) to get

$$\langle vd \rangle = \frac{1}{T} \int_{t-T}^{t} [\langle v \rangle(t) + F(w)]\, d(w)\, dw$$

$$= \langle v \rangle \langle d \rangle + \langle Fd \rangle \quad , \tag{3.25}$$

which, because the averaging operator is linear, can be rearranged as:

$$\langle v \rangle \langle d \rangle = \langle (v - F)d \rangle \quad . \tag{3.26}$$

Since $|F(t)| << |v(t)|$ by virtue of Eq. (3.23), Eq. (3.26) becomes

$$\langle v \rangle \langle d \rangle \doteq \langle vd \rangle \quad , \tag{3.27}$$

which, to a good approximation, is the anticipated result.

The sole requirement necessary for an approximation such as that in Eq. (3.27) is that one of the parameters be quasi-continuous, as expressed by Eq. (3.23). Strict continuity is not demanded; for example, a discontinuity Δv does not invalidate Eq. (3.27) if $|\Delta v| << |v|$. A similar approximation results for the average of id

$$\langle id \rangle \doteq \langle i \rangle \langle d \rangle \quad , \tag{3.28}$$

if i is quasi-continuous:

$$\left|\frac{i(t) - \langle i\rangle(t)}{i(t)}\right| \ll 1 \quad . \tag{3.29}$$

When the approximations exhibited in Eqs. (3.27) and (3.28) can be utilized in Eqs. (3.19) - (3.21), the averaged model is described by:

$$\frac{d\langle i\rangle}{dt} + \frac{1}{\tau_i}\langle i\rangle = \frac{1}{L}\left[\langle v_s\rangle - \langle 1 - d\rangle\langle v\rangle\right] \tag{3.30}$$

$$\frac{d\langle v_c\rangle}{dt} + \frac{1}{\tau_v}\langle v_c\rangle = \frac{R}{\tau_v}\langle 1 - d\rangle\langle i\rangle \tag{3.31}$$

$$\langle v\rangle = \frac{R}{R + R_c}\langle v_c\rangle + R \| R_c \langle 1 - d\rangle\langle i\rangle \quad . \tag{3.32}$$

The equivalent circuit of the boost power stage for these conditions is shown in Fig. 3.5. The interpretation of effects caused by the switch-drive d is now readily apparent: even though the factor $\langle 1 - d\rangle$ is a time-variable gain for both the dependent voltage and current generators, the averaged generator gains, in contrast with the switched gains in Fig. 3.2, are continuous variables and any changes must occur slowly with respect to the switching frequency. As a consequence of quasi-static driving functions $\langle v_s\rangle$ and $\langle d\rangle$, the state variables $\langle i\rangle$ and $\langle v\rangle$ have no switching ripple; thus, the relationship expected between a switched state variable and its analog in the averaged model is as shown in Fig. 3.6.

It may be well at this point to state an assertion invoked in the

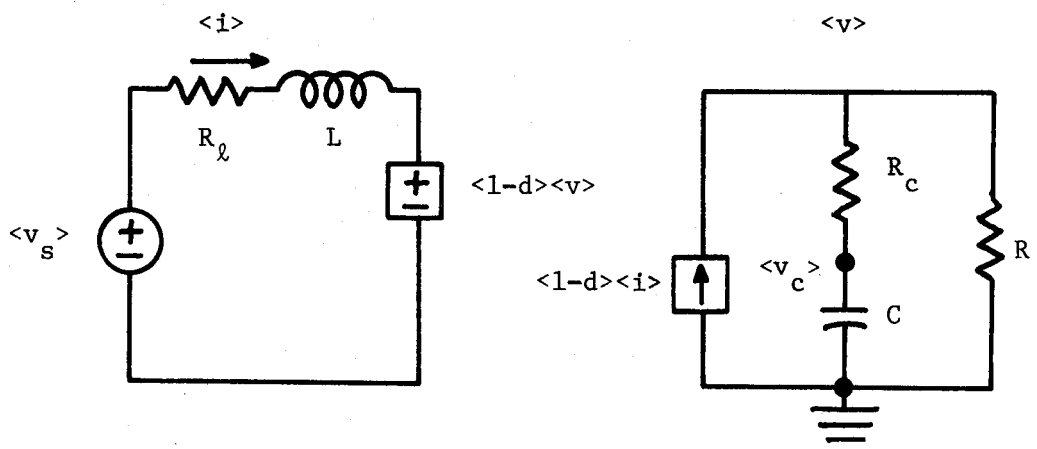

Fig. 3.5 Averaged model of the boost power stage.

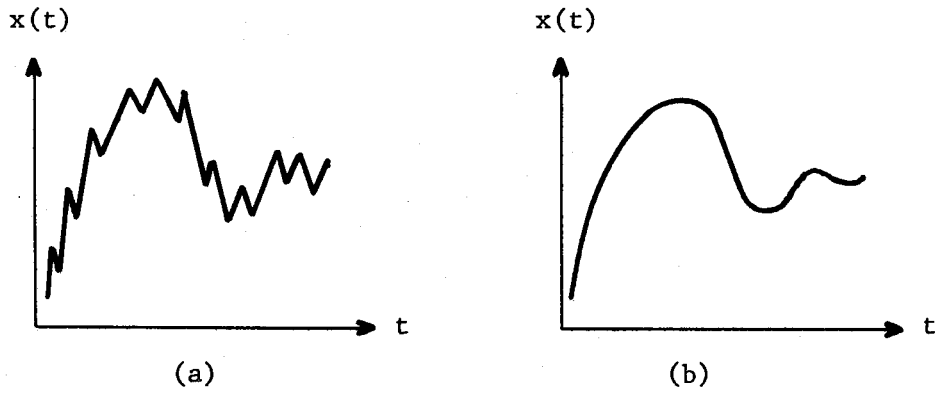

Fig. 3.6 Corresponding state variables in (a) the switched power-stage model, and (b) the averaged power-stage model.

usage of the averaged models. Given a switching power stage whose output voltage, inductor current, and source voltage are quasi-continuous, one merely asserts without proof that quasi-static transfer functions and responses are acceptably simulated by the averaged power-stage model. Figure 3.7(a) illustrates a switching power stage whose transfer function $G(j\omega)$ is unknown; however, the transfer function $G^*(j\omega)$ of the averaged power stage in Fig. 3.7(b) is alleged to be analytically tractable and representative of $G(j\omega)$ for quasi-static power-stage inputs and quasi-continuous state variables.

The principal achievement of this section has been the development of an approximate averaged model of the boost power stage. The model, illustrated in Fig. 3.5, is subject to certain restrictions which, although unavoidable, do not seriously limit the usefulness of results. The quasi-static restriction, which arises from the use of averages, means that analysis of sinusoidal variations must be confined to those frequencies which are small with respect to the switching frequency. Since the response times associated with filters inherent in properly-designed power stages are much greater than the switching period, the quasi-static constraint is not unduly restrictive. If the state variables v and i satisfy Eqs. (3.23) and (3.29), then they are quasi-continuous in the sense that instantaneous values are comparable with averages; when such is the case, the averaged power-stage models should adequately represent the approximate low-frequency behavior of switched power stages. Small discontinuities are admissible. For example, the step of v in Fig. 3.4, which occurs with the switched

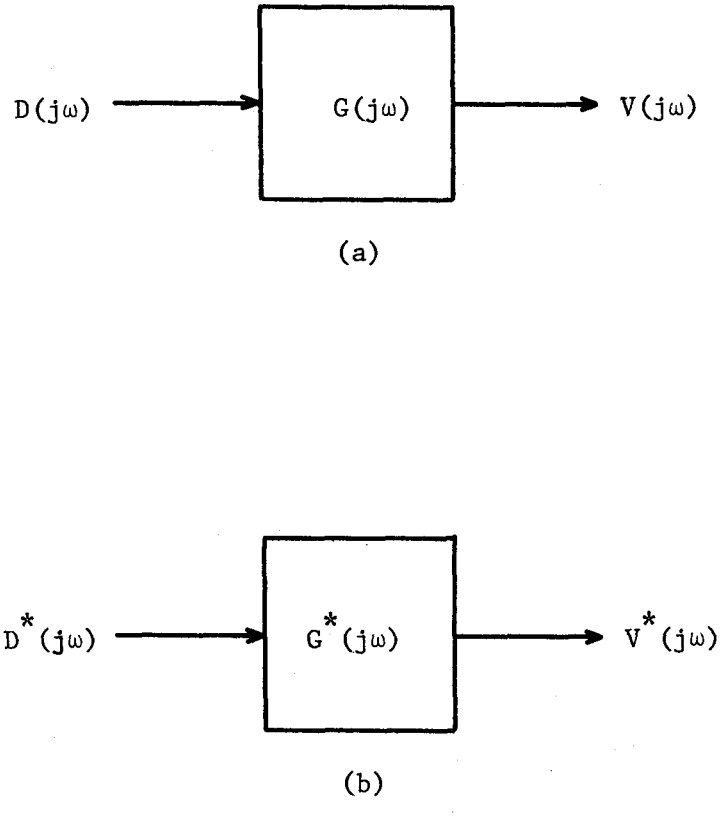

Fig. 3.7 Transfer function of (a) a switched power stage, approximated by that of (b) an averaged power stage.

current $(1 - d)i$ for nonzero R_c, is small if $|R_c\ i(t)| << |v_c(t)|$, and consequently v may be quasi-continuous; however, the switch-drive d is never quasi-continuous.

3.3 Models for the Buck and Buck-Boost Power Stages

The boost power stage exemplified in Sec. 3.2 the development of an approximate averaged model which is suitable for meaningful analytic manipulations. The method used for deriving the model is quite general and can readily be extended to other circuit configurations. The corresponding models for the buck and buck-boost power stages are presented in this section.

Because the details in the development of these averaged models so closely follow the example in Sec. 3.2, only the final power-stage models will be presented here. For generality, the parasitic components R_ℓ and R_c are included as before.

The approximate averaged model of the buck power stage with parasitic resistances is shown in Fig. 3.8. As usual, the quasi-static restriction in the averaging procedure limits the frequencies associated with the model to those less than the switching frequency $\frac{1}{T}$; in addition, the source voltage must be quasi-continuous:

$$\left| \frac{v_s(t) - \langle v_s \rangle(t)}{v_s(t)} \right| << 1 \quad . \tag{3.33}$$

The dependent generators in the model of Fig. 3.8 can be eliminated by the equivalent rearrangement as shown in Fig. 3.9. Interpretation of

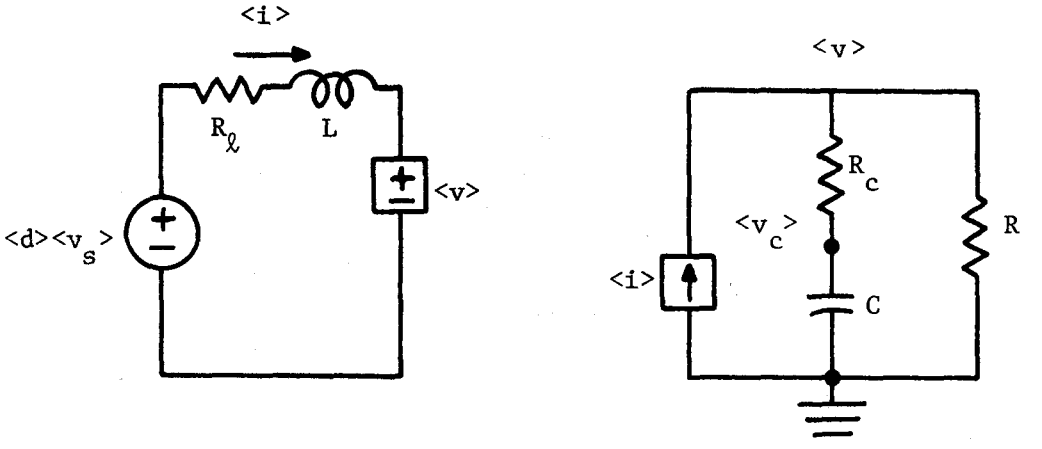

Fig. 3.8 Averaged model of the buck power stage.

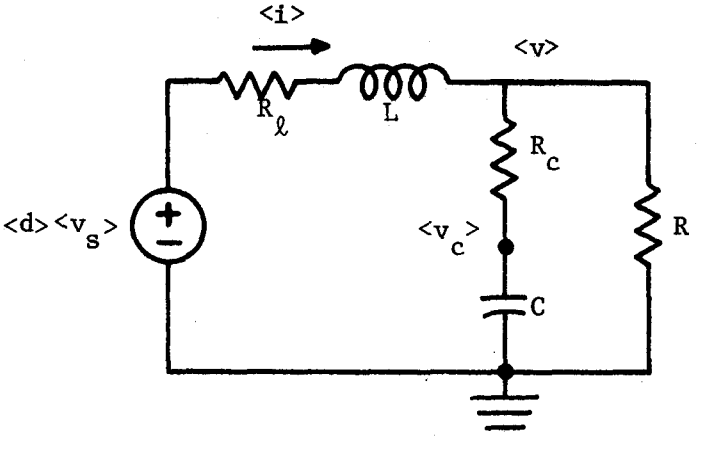

Fig. 3.9 Equivalent averaged model of the buck power stage.

the model in Fig. 3.9 is gratifyingly simple; the average output voltage is related to the product of the switch-drive and source averages by a linear transfer function. This result was anticipated in Chap. 1, and occurs because the circuit components in the buck power stage can be identified as a separate linear filter. As an alternative procedure, one could have applied the averaging method directly to Fig. 2.1 to arrive at Fig. 3.9 and thus bypassed the intermediate stage of Fig. 3.8; however, equivalent circuits similar to Fig. 3.2 are necessary in the formulation of boost and buck-boost average models.

Figure 3.10 shows the approximate averaged model of the buck-boost power stage with parasitic resistances. The model is valid only for frequencies less than the switching frequency, and the quantities v_s, v, and i must be quasi-continuous.

One should compare Figs. 3.5, 3.8, and 3.10 to appreciate the similarity of the averaged models for all types of switching power stages. The resultant equivalent circuits are not only developed from a unified averaging technique, but are also believed to be the first useful models of boost or buck-boost power stages from which frequency characteristics can be easily derived. The following chapter investigates the models derived here to determine such quantities as source step response, control step response, source-input describing function, and control-input describing function.

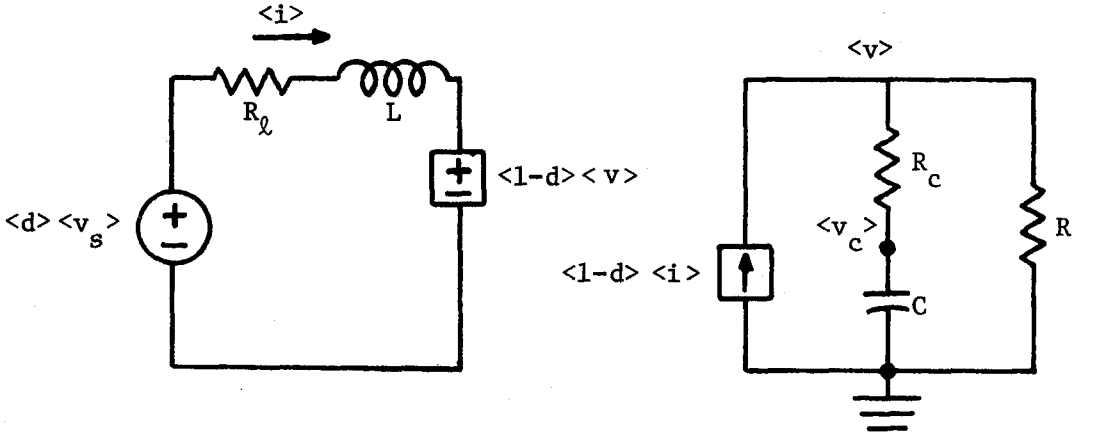

Fig. 3.10 Averaged model of the buck-boost power stage.

Chapter 4

ANALYTICAL RESULTS

4.1 Introduction

The analysis and design, in the time or frequency domain, of switching converters has long been neglected because the appropriate power-stage models have been nonexistent. Even the relatively simple theory of describing functions has not been directly applicable to other than buck power stages. In an attempt to alleviate pre-existing analytical deficiencies, averaged power-stage models have been developed in Chap. 3.

Behavior of both linear and nonlinear circuits is typically characterized by two types of responses: the transient response relates step changes of input to the corresponding time response of the output, whereas the frequency response links a sinusoidal input component to a corresponding output sinusoid. Furthermore, two separate inputs have been identified in switching power stages: source voltage and switch control. Since the mere existence of continuous power-stage models is not an end in itself, another contribution of this work with potential impact is the extraction, demonstrated in this chapter, of original analytical expressions for transient and frequency response from the averaged power-stage models.

Section 4.2 deals with the situation when the source voltage is variable and the switch drive is static; the converse possibility is treated in Sec. 4.3. A small-amplitude restriction on the time-variable

component of d is necessary in order to obtain the control-input frequency response. One of the salient results in these sections is the emergence of effective filter components whose values depend on the switch duty ratio. Results are summarized in Sec. 4.4.

Section 4.5 compares the analytical transfer functions of the averaged power-stage models with the corresponding transfer functions, if tractable, of the actual switched power stages. Since the precipitating factor in this study was the absence of such analytical transfer functions for most power-stage types, this section is, of necessity, brief. Finally, critical gains are computed in Sec. 4.6 for the various types of switching converters in a closed-loop configuration.

4.2 Source Variations

In this section, an investigation is conducted into the relationships between variations of the source voltage and the resultant changes in output voltage for various power stages. A static switch drive is assumed whose average value is a constant D. As repeatedly emphasized, the buck power stage is more amenable to analysis than the boost or buck-boost types; thus, analysis shall begin with the buck power stage.

Figure 3.9 shows the simplified equivalent circuit for the averaged buck power stage, and has been redrawn in Fig. 4.1(a) to show explicitly the assumption

$$\langle d \rangle (t) = D = \text{constant} \tag{4.1}$$

which is appropriate for the study of source variations. Several

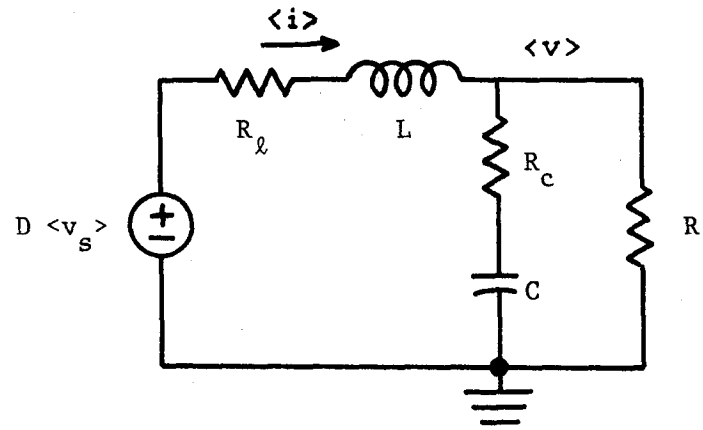

(a)

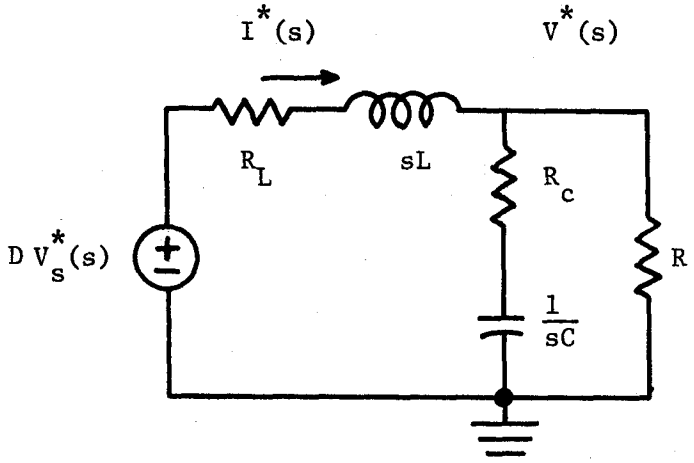

(b)

Fig. 4.1 Equivalent circuit for source variations in the averaged buck power stage, <d>(t) = D; (a) time domain, (b) Laplace transformed equivalent.

conclusions are immediately obvious upon inspection of Fig. 4.1(a). The effective values of the circuit components are constants independent of any source or switch-control variations. While this observation may seem trivial, it will shortly assume importance as a comparative distinction between buck and other power stages. The second observation concerns the linearity of the equivalent circuit; thus, an impressive array of techniques is available to resolve in detail the various desired responses.

The output of a linear system can be expressed as a superposition of the responses due to the input and the initial conditions; however, the steady-state frequency response must be independent of initial conditions, and initial conditions can be readily introduced at any time into transient analysis, so initial conditions will henceforth be neglected (assumed zero) for the sake of simplicity. The frequency and transient responses of linear systems can conveniently be described by the system transfer function, which is defined as the ratio in the Laplace transform domain of output to input with zero initial conditions. Cumbersome analytical expressions obtained for the transient response by the inversion of Laplace transforms will be omitted in favor of the appropriate (possibly transformed) equivalent circuits.

Figure 4.1(b) shows the Laplace transformed version of the averaged buck power stage in Fig. 4.1(a), where

$$V^*(s) \equiv \text{Laplace transform of } \langle v \rangle(t) \tag{4.2}$$

and

$$V_s^*(s) \equiv \text{Laplace transform of } \langle v_s \rangle(t) \quad . \tag{4.3}$$

Throughout this chapter, the superscript asterisk is used to associate quantities with the averaged power-stage models. The subscript "s" refers to the source voltage as the variable input: "c" will be used for inputs from the duty-ratio controller. The describing function of a linear system

$$DF_s^* \equiv \text{source-input describing function of averaged power stage} \quad , \tag{4.4}$$

is given simply by the system transfer function

$$\begin{aligned} G_s^*(s) &\equiv \text{source-to-output transfer function} \\ &= V^*(s)/V_s^*(s)\Big|_{\text{zero initial conditions}} \end{aligned} \quad , \tag{4.5}$$

evaluated at $s = j\omega$. Inspection of Fig. 4.1(b) shows that the source-to-output transfer function for the averaged buck power stage is given by

$$G_s^*(s) = A_{so}\, G_f(s) \quad , \tag{4.6}$$

where A_{so} is an effective amplifier gain

$$A_{so} = D \quad , \text{ buck} \quad , \tag{4.7}$$

and $G_f(s)$ is the filter transfer function previously encountered in Eq. (2.5). The filter transfer function can be expressed in a normalized form as

$$G_f(s) = \frac{R}{R + R_\ell} \frac{1 + sCR_c}{1 + s\left[CR_c + \frac{CRR_\ell + L}{R_\ell + R}\right] + s^2 LC\left(\frac{R + R_c}{R + R_\ell}\right)}$$

$$= G_{fo} \frac{1 + \frac{s}{\omega_z}}{1 + \frac{s}{(Q\omega_o)} + \left(\frac{s}{\omega_o}\right)^2} \quad , \tag{4.8}$$

where

$$\left.\begin{aligned} G_{fo} &= \frac{R}{R + R_\ell} \\ \omega_z &= \frac{1}{CR_c} \\ \omega_o &= \sqrt{\frac{R + R_\ell}{LC(R + R_c)}} \\ \frac{1}{Q} &= \omega_o \left[CR_c + \frac{CRR_\ell + L}{R_\ell + R}\right] \end{aligned}\right\} \quad \text{buck} \tag{4.9}$$

The frequency ω_o is commonly referred to as the natural frequency and the parameter Q is a quality factor.

Since the transfer function of the averaged buck power stage is given by Eq. (4.6), one can now seek the corresponding expression for the averaged boost model illustrated in Fig. 3.5. Given Eq. (4.1) and the definition

$$D' \equiv 1 - D = \text{constant} \quad , \tag{4.10}$$

one finds that the dependent generator gains in the model are constants

$$\langle 1 - d \rangle(t) = 1 - \langle d \rangle(t) = 1 - D = D' \quad , \qquad (4.11)$$

as shown explicitly in Fig. 4.2(a). The gains of the dependent generators have been normalized to unity in the equivalent circuit model of Fig. 4.2(b). Notice that the 2-port network enclosed by the dotted line is equivalent to a pair of wires internally connecting the two ports; thus, the model can be further simplified to that in Fig. 4.2(c).

Since the equivalent circuit of the averaged boost model is linear for static switch drive, the comments made in conjunction with the buck power stage apply here as well. The transfer function from source to output is again sufficient to characterize both frequency and transient response; however, in contrast with the buck model, the effective source voltage and circuit components of the boost model are modified by the factor D'. Considering the analogy between Fig. 4.2(c) and 4.1(a), one can obtain the source-input transfer function of the boost model by inspection

$$G_s^*(s) = A_{so}\, G_f(s) \quad ; \qquad (4.12)$$

where the effective filter transfer function has the same form as for the buck power stage

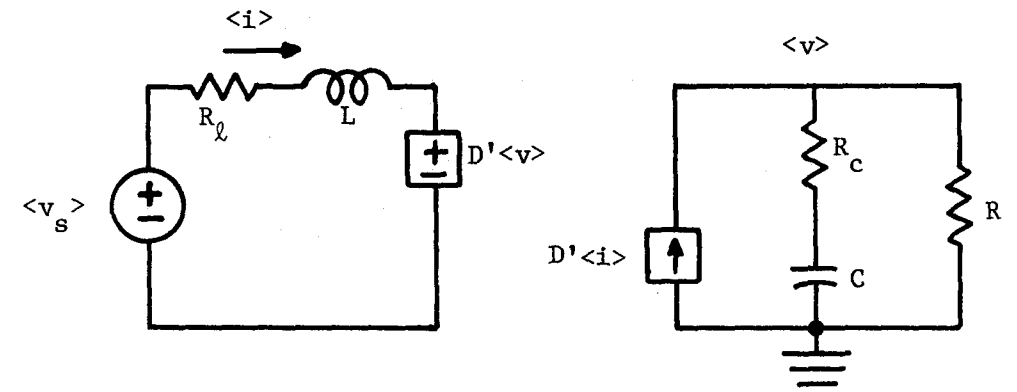

(a)

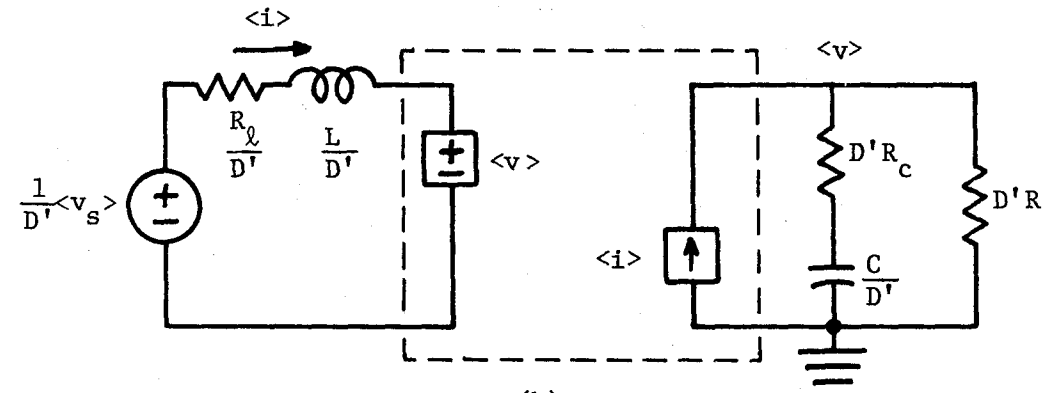

(b)

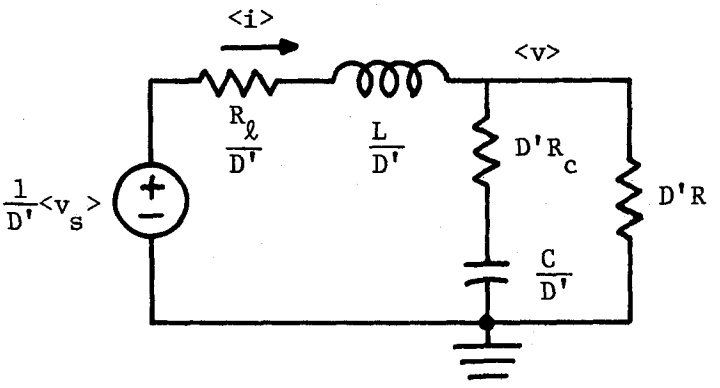

(c)

Fig. 4.2 Reduction of the averaged boost power stage to an equivalent circuit for source variations, where <d>(t) = D = 1 - D'.

$$G_f(s) = G_{fo} \frac{1 + \frac{s}{\omega_z}}{1 + \frac{s}{(Q\omega_o)} + \left(\frac{s}{\omega_o}\right)^2} \quad , \qquad (4.13)$$

but the parameters are now expressed as

$$A_{so} = \frac{1}{D'} \quad , \text{ boost} \quad , \qquad (4.14)$$

and

$$\left.\begin{aligned} G_{fo} &= \frac{(D')^2 R}{(D')^2 R + R_\ell} \\ \omega_z &= \frac{1}{C R_c} \\ \omega_o &= \frac{1}{\sqrt{LC}} \sqrt{\frac{R_\ell + (D')^2 R}{R_c + R}} \\ \frac{1}{Q} &= \omega_o \left[CR_c + \frac{CRR_\ell + L}{R_\ell + (D')^2 R}\right] \end{aligned}\right\} \text{ boost} \quad . \qquad (4.15)$$

The transfer function of the remaining (buck-boost) power stage can be obtained by a simple extension of the boost result. Comparing Figs. 3.5 and 3.10, one observes that the averaged boost equivalent circuit is identical with the averaged buck-boost model if, in the boost model, one replaces $\langle v_s \rangle$ by $\langle d \rangle \langle v_s \rangle$. The indicated replacement in the boost model of Fig. 4.2(c) leads directly to the simplified

equivalent circuit, shown in Fig. 4.3, for the averaged buck-boost power stage. The appropriate transfer function can again be expressed by Eqs. (4.12) and (4.13), where now

$$A_{so} = \frac{D}{D'} \quad \text{, buck boost,} \tag{4.16}$$

and

$$\left.\begin{aligned} G_{fo} &= \frac{(D')^2 R}{(D')^2 R + R_\ell} \\ \omega_z &= \frac{1}{C R_c} \\ \omega_o &= \frac{1}{\sqrt{LC}} \sqrt{\frac{R_\ell + (D')^2 R}{R_c + R}} \\ \frac{1}{Q} &= \omega_o \left[CR_c + \frac{CRR_\ell + L}{R_\ell + (D')^2 R}\right] \end{aligned}\right\} \text{buck-boost .} \tag{4.17}$$

Equivalent circuits and analytic transfer functions which describe the behavior of power stages with a static control input have been derived here from the averaged power-stage models. Interpretation of these results is postponed until Sec. 4.4 to facilitate comparisons there with similar results which are obtained in Sec. 4.3 for variations

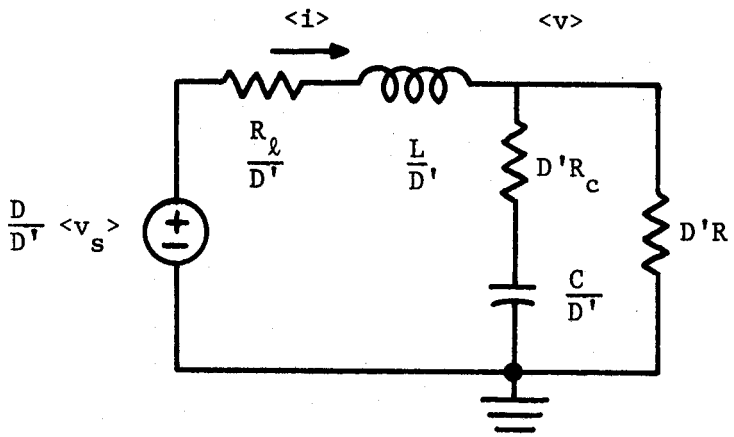

Fig. 4.3 Equivalent circuit for source variations in the averaged buck-boost power stage, where <d>(t) = D = 1 - D'.

of control input when the source voltage is constant.

4.3 Control Variations

The manner in which output voltage changes in response to switch-drive variations will be examined in this section. One assumes here that the averaged source voltage is a constant for the various power-stage models

$$\langle v_s \rangle(t) = V_s = \text{constant} \tag{4.18}$$

and investigates the control-input transfer function:

$$\begin{aligned} G_c^*(s) &\equiv \text{control-to-output transfer function} \\ &= V^*(s)/D^*(s)\Big|_{\text{zero initial conditions}} , \end{aligned} \tag{4.19}$$

where

$$D^*(s) \equiv \text{Laplace transform of } \langle d \rangle(t) , \tag{4.20}$$

and $V^*(s)$ was previously defined in Eq. (4.2). The control-input describing function is given by

$$\begin{aligned} DF_c^* &\equiv \text{control-input describing function of averaged power} \\ &\quad \text{stage} \end{aligned} \tag{4.21}$$

One can begin the analysis by considering the buck model shown in

Fig. 3.9. By virtue of Eq. 4.18, that circuit can be redrawn as in Fig. 4.4. Precisely the same interpretative comments concerning model linearity and invariance of effective component values with respect to input signals, drawn in Sec. 4.2 regarding source variations, apply here for control variations. Since the equivalent circuit in Fig. 4.4 is linear for arbitrary excursions of $\langle d \rangle$, a single transfer function is characteristic of both transient and frequency response. By comparing Fig. 4.4 with Fig. 4.1(a), one can easily evaluate the control-input transfer function as

$$G_c^*(s) = A_{co}\, G_f(s) \quad , \tag{4.22}$$

where G_f is given by Eqs. (4.8) and (4.9), and where

$$A_{co} = V_s \quad , \text{ buck} \quad . \tag{4.23}$$

The analysis of control variations has thus far closely paralleled that of source variations in Sec. 4.2; however, an apparent dilemma appears as one approaches analysis of the boost and buck-boost models. The derivation of linear equivalent circuits for the boost and buck-boost models in Sec. 4.2 was based upon the constant value of the dependent generator gains; for time variations in $\langle d \rangle$, a linear model no longer occurs. Since the form of the reduced equivalent circuits depends on the nature of the control variation, two specific control variations, which correspond to transient and frequency response, will be separately

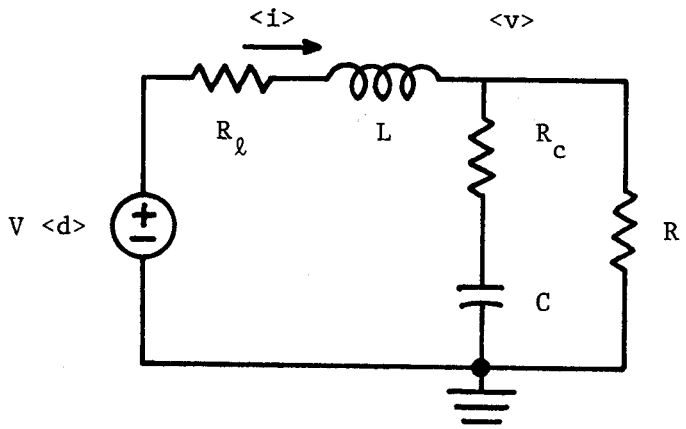

Fig. 4.4 Equivalent circuit for control variations in the averaged buck power stage, where $\langle v_s \rangle(t) = V_s$.

examined.

Consider first the transient initiated at time t_o by a sudden change in control from one static value to another static value D:

$$\langle d \rangle(t) = D, \quad t > t_o \qquad . \qquad (4.24)$$

The control value preceding t_o can be accounted for by choosing the appropriate initial conditions. Equation (4.24) was just the condition used to simplify the averaged boost and buck-boost models to the linear equivalent circuits shown in Fig. 4.2(c) and 4.3; therefore, by simply invoking Eq. (4.18) in these models, the equivalent circuits appropriate for control transient response emerge as seen in Figs. 4.5 and 4.6. Comparing Figs. 4.2(c) and 4.3 with Figs. 4.5 and 4.6, respectively, one reaches the unexpected conclusion that the averaged equivalent circuits are identical, except for possible differences in the corresponding initial conditions, for either source or control transients.

Since the transient response is now characterized, one can shift attention to the frequency response of the boost and buck-boost averaged models. Assume for the moment that the averaged power-stage control input can be expressed in the form

$$\langle d \rangle(t) = D + \hat{d}(t) \qquad , \qquad (4.25)$$

where $\hat{d}$ is a control variation or disturbance and D is a constant

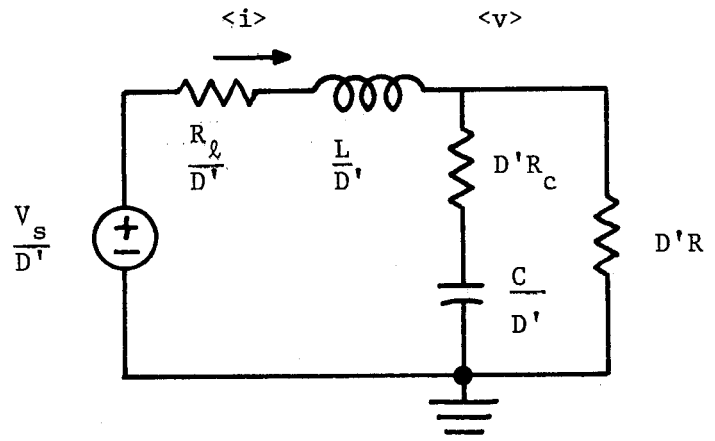

Fig. 4.5 Equivalent circuit for transient response from step control variations in the averaged boost power stage, where $\langle v_s \rangle(t) = V_s$.

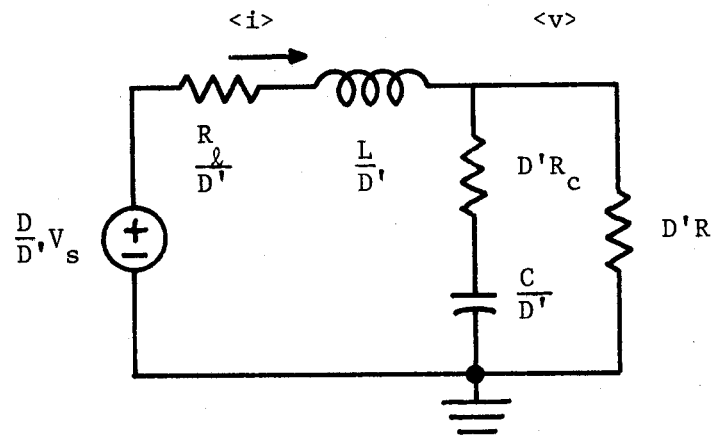

Fig. 4.6 Equivalent circuit for transient response from step control variations in the averaged buck-boost power stage, where $\langle v_s \rangle(t) = V_s$.

steady-state control. The instantaneous values of <d> should be limited between zero and unity to be physically meaningful, so $\hat{d}$ is consequently restricted in amplitude. Equation (4.25), together with Eq. (4.10), shows that

$$\langle 1 - d \rangle(t) = 1 - \langle d \rangle(t) = D' - \hat{d}(t) \quad . \tag{4.26}$$

The control variation causes related variations in each state variable

$$\langle i \rangle(t) = I + \hat{i}(t) \tag{4.27}$$

$$\langle v \rangle(t) = V + \hat{v}(t) \quad , \tag{4.28}$$

where I and V are steady-state values, and $\hat{i}$ and $\hat{v}$ are perturbations. To obtain the frequency response, one must relate $\hat{v}$ to $\hat{d}$ when the control disturbance is sinusoidal.

Consider the averaged boost power-stage model shown in Fig. 3.5. Substitution of Eq. (4.18) and Eqs. (4.26) to (4.28) for the appropriate quantities in Fig. 3.5 produces the model displayed in Fig. 4.7(a). The dependent generators have both dc and perturbation components which, in turn, support dc and perturbation components, respectively, of the inductor current and output voltage. These dc and perturbation signals are separately determined by the equivalent circuits shown in Figs. 4.7(b) and 4.7(c), respectively. The presence of second-order variations in the dependent generators makes the perturbation equivalent circuit nonlinear,

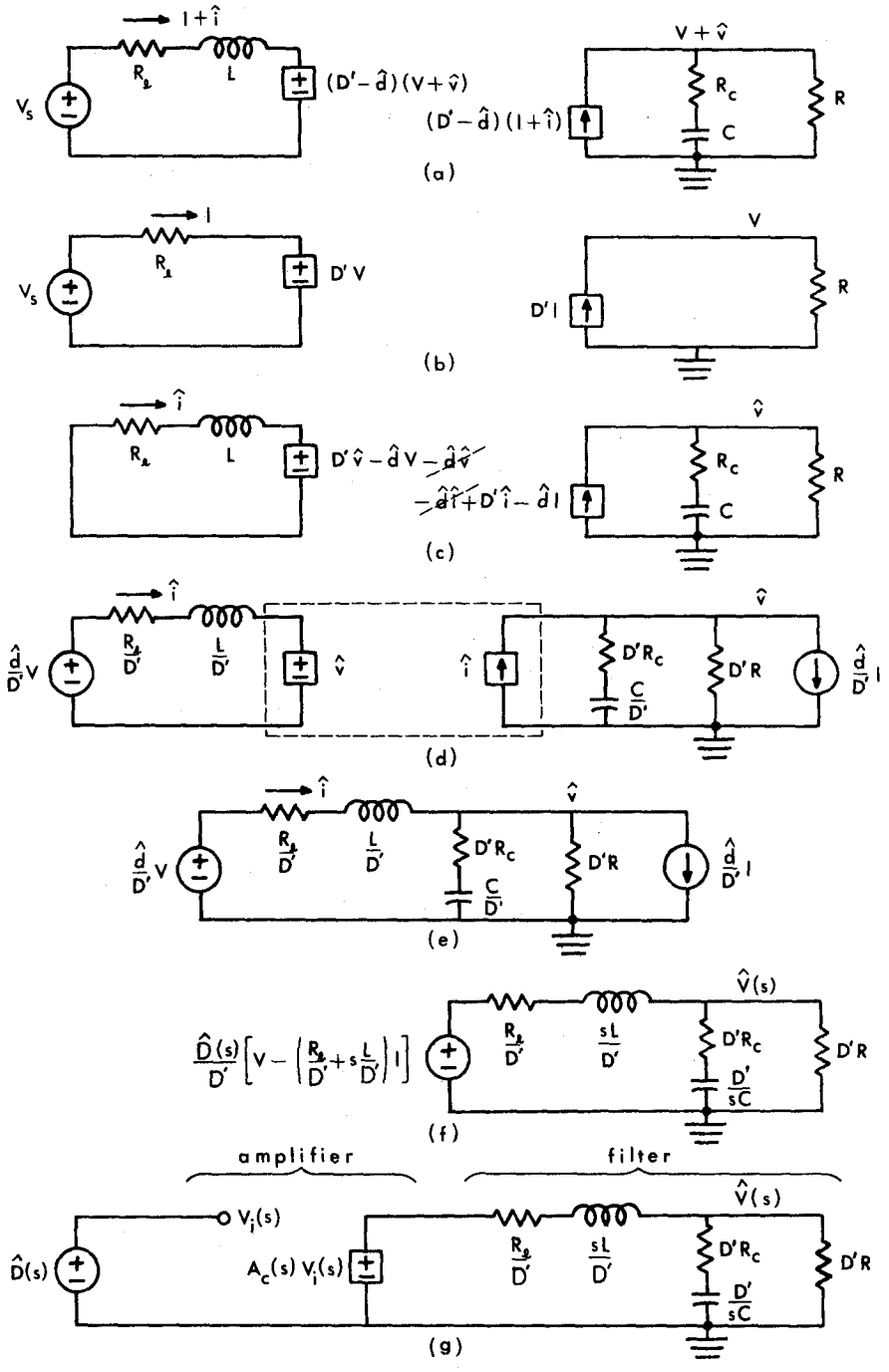

Fig. 4.7 Reduction of the averaged boost power stage to a linearized equivalent circuit for control variations; $\langle v_s \rangle(t) = V_s$, $\langle d \rangle(t) = D + \hat{d}(t)$.

so if $\hat{d}$ were a sinusoid with frequency ω, the output perturbation $\hat{v}$ would contain components with frequencies at all harmonics of ω. Even analysis of the describing function would be difficult for such a situation; however, by restricting the amplitude of $\hat{d}$ small enough to assure that second-order terms in the generator driving functions are negligible with respect to the remaining first-order terms, the perturbation circuit can be linearized. Subsequent manipulations of the linearized perturbation equivalent circuit are equally valid in the time or frequency domain and no longer depend on the assumed form of the control variation.

After one imposes the linearizing restriction

$$\left.\begin{array}{l} \hat{v} \ll V \\ \\ \hat{i} \ll I \end{array}\right\} \quad \text{for small-amplitude } \hat{d}\,, \tag{4.29}$$

the voltage generator is composed of two terms: $D'\hat{v}$ is proportional to a circuit-dependent perturbation, whereas $\hat{d}V$ varies directly with the independent control perturbation. Since similar comments apply to the current generator, the dependent and independent generator terms are explicitly separated, as shown in Fig. 4.7(d), in the hope of eliminating the dependent generators. The factors D' which modify the effective values of circuit components result from normalization to unity of the dependent generator gains, a technique first encountered in Fig. 4.2(b). Once again, the section of Fig. 4.7(d) which is enclosed by dotted lines is equivalent to a pair of wires connecting the two ports, as shown in Fig. 4.7(e).

Since Fig. 4.7(e) is a linear equivalent circuit, one is now in a position to find $\hat{v}$ in terms of $\hat{d}$; however, the presence of $\hat{d}$ in two separate generators obscures the relationship between $\hat{d}$ and $\hat{v}$. After the Laplace transform is applied to Fig. 4.7(e), Norton and Thevenin equivalents are used to combine the two independent generators into the one shown in Fig. 4.7(f), where

$$\hat{V}(s) \equiv \text{Laplace transform of } \hat{v}(t) \quad , \tag{4.30}$$

and

$$\hat{D}(s) \equiv \text{Laplace transform of } \hat{d}(t) \quad . \tag{4.31}$$

The linearized control-input transfer function

$$\hat{G}_c(s) \equiv \text{linearized control-input transfer function}$$

$$= \hat{V}(s)/\hat{D}(s)\Big|_{\text{zero initial conditions}} \quad , \tag{4.32}$$

of the averaged boost power stage can be evaluated from Fig. 4.7(f) and expressed in the form

$$\hat{G}_c(s) = A_c(s)\, G_f(s) \quad , \tag{4.33}$$

where $A_c(s)$ is the transfer function of the equivalent amplifier shown

in Fig. 4.7(g)

$$\left.\begin{aligned} A_c(s) &= \frac{1}{D'}\left[V - \frac{R_\ell + sL}{D'}\, I\right] \\ &= \frac{V_s/(D')^2}{R_\ell + (D')^2 R}\left[(D')^2 R - R_\ell - sL\right] \end{aligned}\right\} \text{boost} , \tag{4.34}$$

and where $G_f(s)$ is the same function encountered in Eqs. (4.13) and (4.15). The values of I and V in Eq. (4.34) are obtained from the dc model in Fig. 4.7(b). Notice that the effective amplifier transfer function can be written as

$$A_c(s) = A_{co}\left(1 - \frac{s}{\omega_a}\right) , \tag{4.35}$$

where

$$\left.\begin{aligned} A_{co} &= \frac{V_s}{(D')^2}\,\frac{(D')^2 R - R_\ell}{(D')^2 R + R_\ell} \\ \omega_a &= \frac{(D')^2 R - R_\ell}{L} \end{aligned}\right\} , \text{ boost.} \tag{4.36}$$

Since the averaged boost model is nonlinear, it is important to bear in mind the fact that $\hat{G}_c$ is the <u>linearized</u> transfer function and relates only the small-amplitude perturbations of control and output. The

describing function provides the long-sought frequency response and is given by

$$DF_c^* = \hat{G}_c(j\omega) \tag{4.37}$$

Frequency analysis of the averaged buck-boost power stage follows precisely the procedure just demonstrated for the boost model; hence, only the results will be discussed here. The initial buck-boost equivalent circuit is shown in Fig. 4.8(a). Figure 4.8(b) is used to evaluate the dc components I and V. The perturbation circuit is again linearized by assuming that $\hat{d}$ is small in amplitude. Laplace transformation of the approximate perturbation circuit, followed by rearrangement to combine the independent sources, leads to Fig. 4.8(c). An equivalent amplifier can again be associated with the transfer function

$$\left.\begin{aligned} A_c(s) &= \frac{1}{D'}\left[V + V_s - \frac{R_\ell + sL}{D'}\ I\right] \\ &= \frac{V_s/(D')^2}{R_\ell + (D')^2 R}\left[(D')^2 R - (D - D')R_\ell - sDL\right] \end{aligned}\right\} \text{buck-boost,} \tag{4.38}$$

as shown in Fig. 4.8(d). If $A_c(s)$ is expressed in the form of Eq. (4.35), its parameters are:

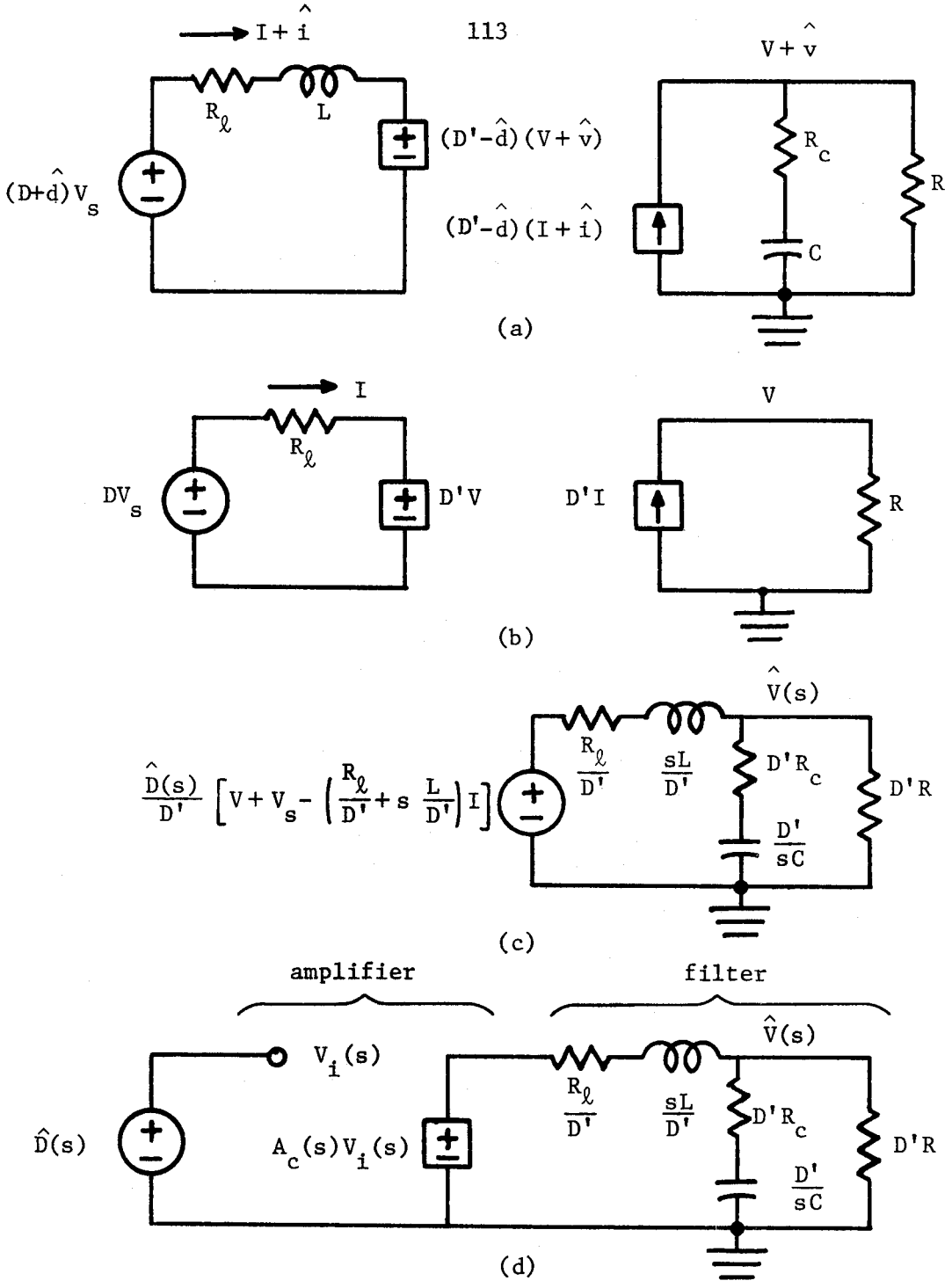

Fig. 4.8 Linearized equivalent circuit for control variations in the averaged buck-boost power stage; $\langle v_s \rangle(t) = V_s$, $\langle d \rangle(t) = D + \hat{d}(t)$.

$$\left.\begin{aligned} A_{co} &= \frac{V_s}{(D')^2}\,\frac{(D')^2 R - (D - D')\,R_\ell}{(D')^2 R + R_\ell} \\ \omega_a &= \frac{(D')^2 R - (D - D')\,R_\ell}{D\,L} \end{aligned}\right\} \text{ buck-boost .} \qquad (4.39)$$

The linearized transfer function is evaluated from Fig. 4.8(d) as

$$\hat{G}_c(s) = A_c(s)\; G_f(s) \quad , \qquad (4.40)$$

where $A_c(s)$ is given above and $G_f(s)$ is the same filter transfer function characterized by Eqs. (4.13) and (4.17).

The results expressed in this section are interpreted in Sec. 4.4.

4.4 Summary and Interpretations

Based on averaged models, linearized equivalent circuits and transfer functions were derived in Secs. 4.2 and 4.3 for the transient and frequency response of all basic switched power stages. These results are summarized, interpreted, and compared in this section.

In summary of Sec. 4.2, if the averaged power-stage models are subjected to source variations while simultaneously the averaged switch control is a constant D, the equivalent circuits for all power-stage types are linear and topologically identical. Source-input transfer functions were derived for all the various power stages from their corresponding equivalent circuits and are represented by the common block diagram shown in Fig. 4.9(a); the transfer function is identified

$$G_f(s) = G_{fo} \frac{1 + \frac{s}{\omega_z}}{1 + \frac{1}{Q}\frac{s}{\omega_o} + \left(\frac{s}{\omega_o}\right)^2}$$

$$A_s(s) = A_{so}$$

$$A_c(s) = A_{co}\left(1 - \frac{s}{\omega_a}\right)$$

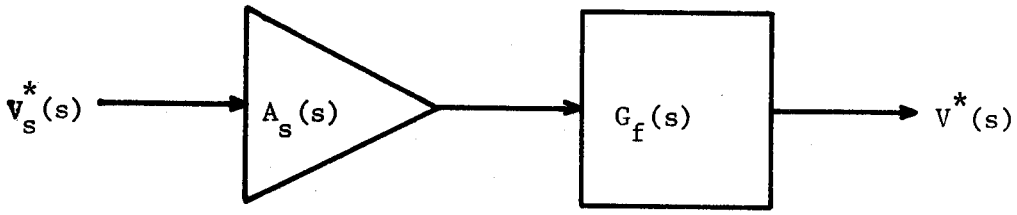

(a)

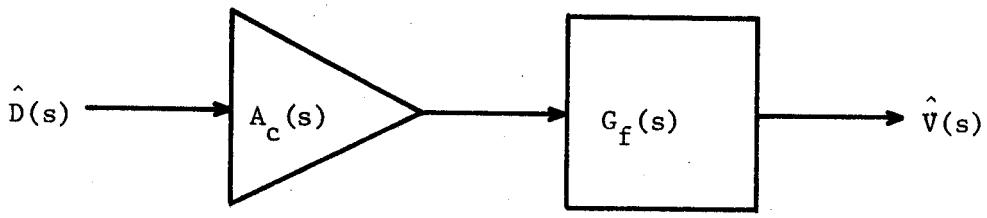

(b)

Fig. 4.9 Generalized block diagram of (a) the source-input transfer function, and (b) the linearized control-input transfer function.

as that of an amplifier in cascade with a filter. Analytic expressions for the various filter and amplifier parameters are presented for convenient reference in Table 4.1.

It is shown in Sec. 4.3 that the equivalent circuits for all types of averaged power stages with control variations and a constant source voltage V_s can be linearized by restricting the amplitude of control variations. The block diagram of the linearized control-input transfer function derived for each power-stage type is shown in Fig. 4.9(b) and can again be identified as an amplifier in series with a filter. Refer to Table 4.1 for the appropriate analytical parameters in the amplifier and filter expressions.

One may observe from Fig. 4.9 and Table 4.1 that each type of power stage has the same filter for either source or control variations. Whereas the buck filter is completely independent of the static duty ratio D, the effective filter component values, and hence the natural frequency ω_o and quality factor Q associated with the denominator quadratic of the transfer function, in the boost and buck-boost power stages are modified by the complementary duty-ratio factor $D' = 1 - D$. The effect of D on the shape of the filter frequency response is investigated in Chap. 5.

Figure 4.9 and Table 4.1 show that in contrast with the effective amplifier factor of the source-input transfer function, which is independent of frequency and varies only with D, the effective amplifier for control variations is novel in a number of ways. Not only is the effective control-input amplifier a function of frequency, but the

Table 4.1

Summary of analytic parameters in power-stage transfer functions.

	Buck	Boost	Buck-Boost
A_{so}	D	$1/D'$	D/D'
A_{co}	V_s	$\frac{(D')^2R - R_\ell}{(D')^2R + R_\ell} \frac{V_s}{(D')^2}$	$\frac{(D')^2R - (D-D')R_\ell}{(D')^2R + R_\ell} \frac{V_s}{(D')^2}$
G_{fo}	$\frac{R}{R + R_\ell}$	$\frac{R}{R+R_\ell/(D')^2}$	$\frac{R}{R+R_\ell/(D')^2}$
ω_o	$\frac{1}{\sqrt{LC}}\sqrt{\frac{R + R_\ell}{R + R_c}}$	$\frac{1}{\sqrt{LC}}\sqrt{\frac{(D')^2R + R_\ell}{R+R_c}}$	$\frac{1}{\sqrt{LC}}\sqrt{\frac{(D')^2R + R_\ell}{R + R_c}}$
Q	$\frac{1}{\omega_o}\left[CR_c + \frac{CRR_\ell + L}{R+R_\ell}\right]^{-1}$	$\frac{1}{\omega_o}\left[CR_c + \frac{CRR_\ell + L}{(D')^2 R + R_\ell}\right]^{-1}$	$\frac{1}{\omega_o}\left[CR_c + \frac{CRR_\ell + L}{(D')^2R+R_\ell}\right]^{-1}$
ω_z	$\frac{1}{CR_c}$	$\frac{1}{CR_c}$	$\frac{1}{CR_c}$
ω_a	∞	$\frac{(D')^2R - R_\ell}{L}$	$\frac{(D')^2R - (D-D')R_\ell}{DL}$

"corner" frequency and scale factor of the amplifier transfer function vary with D for the boost and buck-boost power stages; however, the principal uniqueness concerns the nature of the frequency response. The control-input amplifier transfer function has a single real zero, which is positive for $D' > D'_o$, where

$$D'_o \equiv \begin{cases} \sqrt{\frac{R_\ell}{R}} & \text{, boost} \\ \sqrt{(1 + \frac{R_\ell}{R}) \frac{R_\ell}{R}} - \sqrt{\frac{R_\ell}{R}} & \text{, buck-boost} \end{cases} \quad . \tag{4.41}$$

Since $\frac{R_\ell}{R}$, and consequently D'_o, is normally very small, the zero in $A_c(s)$ is usually positive, so for high frequencies the phase of $A_c(j\omega)$ is asymptotic to minus $\frac{\pi}{2}$, even though the amplitude of $A_c(j\omega)$ increases with frequency.

The analytical results summarized in this section are unique in their own right; furthermore, their utility is enhanced by the resultant capability for critical comparisons between various types of power stages. For example, one can predict that the phase lag of the effective amplifier $A_c(s)$ makes boost and buck-boost power stages less stable in a control feedback configuration than is the buck; Sec. 4.6 investigates this premise after the correlations between known switched responses and the corresponding predictions of averaged models are compared in Sec. 4.5.

4.5 Analytical Verification

Rather startling analytical results have been derived from the averaged power-stage models. In order to establish a measure of confidence in the averaged models and their associated responses, one should

investigate the switched power stages for special situations which have known solutions. Admittedly, exact analysis of switched power stages is limited; to the author's knowledge, no analysis of transient or frequency response has appeared in the literature for boost or buck-boost power stages. However, Kossov[1] has performed an exact static analysis of the source-to-output gain for the three basic power stages, so for comparison the corresponding gains will be derived from the averaged power-stage models.

For static conditions

$$\left.\begin{aligned} \langle d\rangle(t) &= D = 1 - D' \\ \langle v_s\rangle(t) &= V_s \\ \langle v\rangle(t) &= V \end{aligned}\right\} \quad , \tag{4.42}$$

the averaged power-stage models are particularly simple since there is no capacitor current or inductor voltage in the steady state. Figure 4.10 shows for various power-stage configurations the simplified equivalent circuits, from which the static source-to-output gains are easily obtained as:

$$\frac{V}{V_s} = \frac{D\,R}{R_\ell + R} \quad , \text{ buck} \tag{4.43}$$

$$\frac{V}{V_s} = \frac{D'\,R}{R_\ell + (D')^2\,R} \quad , \text{ boost} \tag{4.44}$$

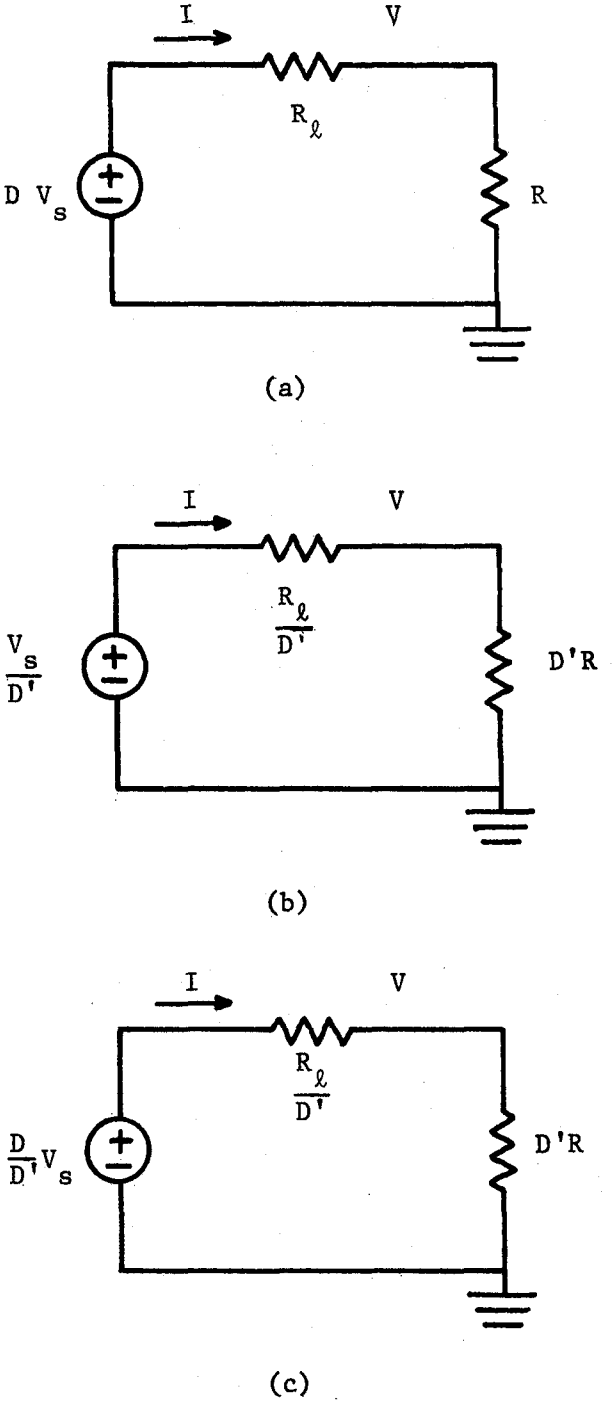

Fig. 4.10 Equivalent circuit for static conditions in each power stage: (a) buck, (b) boost, and (c) buck-boost.

$$\frac{V}{V_s} = \frac{D\,D'\,R}{R_\ell + (D')^2\,R} \quad , \quad \text{buck-boost} \quad . \qquad (4.45)$$

It is indeed comforting to observe that with corresponding notation Eqs. (4.43) to (4.45) agree precisely with Kossov's Eqs. (6a), (6b), and (6c). Notice how the presence of R_ℓ has dramatically altered, with respect to the ideal static characteristics in Eqs. (1.5) to (1.7), the nature of the static gain as D' approaches zero.

The exact analysis in Chap. 2 is possible because the buck power stage is linear. The equivalent circuit of the averaged buck model shown in Fig. 3.9 is not only linear; it is also identical to the filter circuit of the switched buck power stage. Thus, it is not surprising to find that the transfer functions of the switched and averaged buck power stages are identical; however, the absence of theoretical transfer functions for switched boost and buck-boost power stages make further analytical comparisons impossible.

Though not analytically founded, a hypothesis was postulated by Wells et al.[8] which states that the lowest corner frequency in the open-loop boost control-input describing function varies proportionally with D'. Wells' hypothesis was reportedly supported by experimental observations of a particular boost configuration with additional input and output filtering. The averaged model of the boost power stage under consideration here has a quadratic pole with a break frequency

$$\omega_o = \frac{1}{\sqrt{LC}} \sqrt{\frac{R_\ell + (D')^2\,R}{R_c + R}} \quad , \quad \text{boost} \quad , \qquad (4.46)$$

which does, in fact, vary approximately with D' for typical circuit values and operating conditions:

$$\omega_o \doteq \frac{D'}{\sqrt{LC}} \sqrt{\frac{R}{R_c + R}} \quad \text{for } D' >> \sqrt{\frac{R_\ell}{R}} \text{ , boost.} \qquad (4.47)$$

To the extent that the effective source impedance (source impedance, input filter, and boosting inductor) is inductive and the effective load impedance (output filter plus load) is capacitive, Wells' hypothesis may be a general result. While Eq. (4.47) neither proves nor disproves Wells' hypothesis, it does show that appropriate analysis of the averaged model correlates well with published empirical observations.

The conclusion to be drawn from this section is that analysis of the averaged power-stage models agrees with exact or observed behavior of switched power stages for the few special situations which have "exact" solutions.

4.6 Closed-loop Stability

Since the ultimate goal of frequency analysis is to deduce information concerning closed-loop stability, the "loop gain", or "return ratio", $r(\omega)$ will be computed here for various power-stage models in a typical negative-feedback configuration. The closed-loop system may[3] be unstable if $|r(\omega_c)| \geq 1$, where the crossover frequency ω_c is defined by $\angle r(\omega_c) = -\pi$; thus, the gain magnitude at ω_c is indicative of relative

[3] Systems exist that are conditionally stable even though $|r(\omega_c)| > 1$.

system stability. The computation in this section of crossover frequency and gain magnitude from averaged models permits one to assess the validity of averaging techniques by comparison with simple experimental measurements of switched converters in Chap. 5; however, one must first digress to establish some typical component values for use in quantitative stability predictions.

4.6.1 Numerical Component Values

Two restrictions on the circuit component values were previously noted in Eq. (3.15); namely, the time constants τ_i and τ_v defined in Eqs. (3.8) and (3.9) must both be large with respect to the period T. A third restriction arises from the requirement that $i(t) > 0$ in order to force the diode, which is interchangeable with switch S', to behave like a switch. For each switched power stage, the steady-state deviation Δi of the inductor current which occurs during a switching cycle can be computed by assuming the output voltage is well filtered by the capacitor; the averaged (dc) inductor current $\langle i \rangle$ is also computed for the same duty ratio. The requirement $i(t) > 0$ is equivalent to the restriction $\langle i \rangle - \frac{\Delta i}{2} > 0$, which is satisfied for all power stages if

$$\frac{2L}{R} > T \quad . \tag{4.48}$$

Henceforth, the following component values

$$\left.\begin{aligned} T &= 10^{-4} \text{ seconds} \\ R &= 60 \text{ ohms} \\ L &= 6 \cdot 10^{-3} \text{ henry} = 6 \text{ mh} \\ C &= 1/24 \cdot 10^{-3} \text{ farad} = 41.7 \ \mu\text{f} \\ R_{\ell} &= 3 \text{ ohms} \\ R_{c} &= 1 \text{ ohm} \\ V_{s} &= 60 \text{ volts} \end{aligned}\right\} , \qquad (4.49)$$

will be used for numerical computations. The above numbers not only represent typical design figures, but also satisfy Eqs. (3.15) and (4.48) by moderate safety factors. The same components will be used for all power-stage types to extract meaningful comparisons.

4.6.2 Computations

The feedback configuration used for subsequent analysis is shown in Fig. 4.11 and provides two notable characteristics: when K = 0 (no feedback), the static PWM output D, and thus the averaged power-stage model, is determined solely by the dc controller input U; and, if V_r is chosen as the static output voltage V which results for K = 0, then the dc output voltage remains approximately constant as K increases. The feedback configuration was designed to make the dc controller output D independent of the value of K.

The return ratio can be written in terms of describing functions as

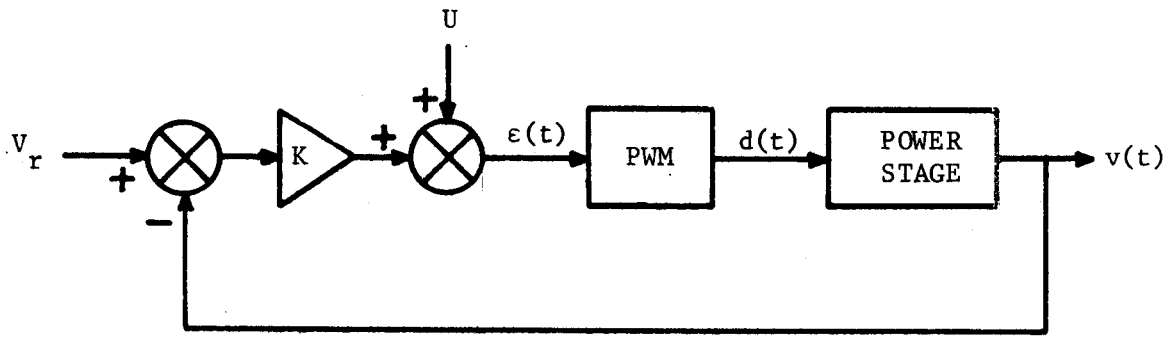

Fig. 4.11 Closed-loop configuration of a switching converter.

$$r = K \cdot \left(\begin{matrix}\text{describing function} \\ \text{of PWM}\end{matrix}\right) \cdot \left(\begin{matrix}\text{control-input} \\ \text{describing function} \\ \text{of power stage}\end{matrix}\right)$$

$$= K\, DF_m\, DF_c^* \qquad . \qquad (4.50)$$

Since DF_m is a function of the modulator sinusoidal input amplitude u, the loop gain also varies with u. This vicious cycle can be broken for analysis by using the linearized PWM describing function DF_{mo} defined in Eq. (2.26) and evaluated for $\frac{\omega}{\omega_s} < \frac{1}{2}$ by Eq. (2.52). Equation (2.48) shows that the dc component of the modulated PWM output equals U so, to simplify the number of independent parameters, replace U by D in DF_{mo}

$$DF_m \simeq DF_{mo} = e^{-j\omega DT}, \quad \frac{\omega}{\omega_s} < \frac{1}{2} \qquad . \qquad (4.51)$$

One can combine Eq. (4.51) with the relevant equations in Secs. 4.2 and 4.3 to express Eq. (4.50) in the form:

$$\frac{r(\omega)}{K} = DF_{mo}(\omega)\, DF_c^*(\omega)$$

$$= A_{co}\, G_{fo}\, \frac{(1 + j\omega/\omega_z)\,(1 - j\omega/\omega_a)}{1 - (\omega/\omega_o)^2 + j\omega/(Q\omega_o)}\, e^{-j\omega DT}, \qquad (4.52)$$

where the parameters are given analytically in Table 4.1. Equation (4.52) relates the frequency response of the loop gain to circuit components and the static duty ratio D, thus forming a powerful tool for the design and analysis of switched converters.

To proceed with an analytic measure of stability, one must find the frequency at which the phase of r is minus π. Given D and the component values, one can compute the constants (A_{co}, G_{fo}, ω_o, Q, ω_z, ω_a) in Eq. (4.52) from Table 4.1: numerical values are shown in Table 4.2. The phase crossover frequency is then determined by graphical means or by digital computer techniques (the method used here) from the transcendental equation:

$$\underline{/r(\omega_c)} = -\pi \quad , \tag{4.53}$$

where

$$\underline{/r(\omega)} = -\omega DT - \tan^{-1}\left[\frac{\frac{\omega}{Q\omega_o}}{1-\left(\frac{\omega}{\omega_o}\right)^2}\right] + \tan^{-1}\frac{\omega}{\omega_z} - \tan^{-1}\frac{\omega}{\omega_a} \quad . \tag{4.54}$$

Having found ω_c, one knows that the system stability is just marginal if the magnitude of the return ratio is unity at ω_c, so a critical amplifier gain K_c can be determined from

$$1 = K_c \left| DF_{mo}(\omega_c)\ DF_c^*(\omega_c) \right| \quad . \tag{4.55}$$

Thus, the closed-loop feedback system will be unstable for $K > K_c$, where

Table 4.2

Numerical Values for Transfer-Function Parameters

Parameter	Buck			Boost			Buck-Boost		
D	0.25	0.50	0.75	0.25	0.50	0.75	0.25	0.50	0.75
A_{so}	0.25	0.50	0.75	1.33	2.00	4.00	0.33	1.00	3.00
A_{co}	60.00	60.00	60.00	89.25	160.00	106.67	102.31	200.00	320.00
G_{fo}	0.95	0.95	0.95	0.92	0.83	0.56	0.92	0.83	0.56
$\omega_o[10^3$ rad/sec]	2.03	2.03	2.03	1.55	1.09	0.66	1.55	1.09	0.66
Q	1.92	1.92	1.92	1.57	1.16	0.74	1.57	1.16	0.74
$\omega_z[10^3$ rad/sec]	24.00	24.00	24.00	24.00	24.00	24.00	24.00	24.00	24.00
$\omega_a[10^3$ rad/sec]	∞	∞	∞	5.12	2.00	0.12	23.50	5.00	0.50
$\omega_c[10^3$ rad/sec]	43.72	10.18	5.89	2.84	1.73	0.73	6.34	2.37	0.93
K_c	3.89	0.39	0.13	0.028	0.012	0.004	0.158	0.023	0.006

$$K_c = \left| DF_{mo}(\omega_c)\ DF_c^*(\omega_c) \right|^{-1}$$

$$= \frac{1}{A_{co}\ G_{fo}} \sqrt{\frac{(1 - \omega_c^2/\omega_o^2)^2 + (\omega_c/Q\omega_o)^2}{(1 + \omega_c^2/\omega_a^2)(1 + \omega_c^2/\omega_z^2)}}$$

$$= \text{critical amplifier gain} \quad . \qquad (4.56)$$

The value of K_c expressed in decibels is appropriately referred to as "gain margin".

Figure 4.12 shows pictorially the role of ω_c and K_c in the Bode plot of a typical[4] converter open-loop frequency response. Values of ω_c and K_c, as computed by Eqs. (4.53) and (4.56), are given in Table 4.2 for various power stages and duty ratios, and offer objective measures of relative converter stability; for example, if two competitive systems are potentially capable of meeting all design specifications and have identical crossover frequencies, then one should choose the system with the largest gain margin.

Some important qualitative conclusions can be drawn from Tables 4.1 and 4.2. Since A_{co} is directly proportional to V_s for all basic power stages, then systems which must be designed for a range of V_s will be least stable when V_s has its maximum value. Notice that for all power stages both ω_c and K_c decrease as D increases. Graphical

[4] Specifically, Fig. 4.12 was computed from Eq. (4.52) for an averaged boost power stage with D = 0.5.

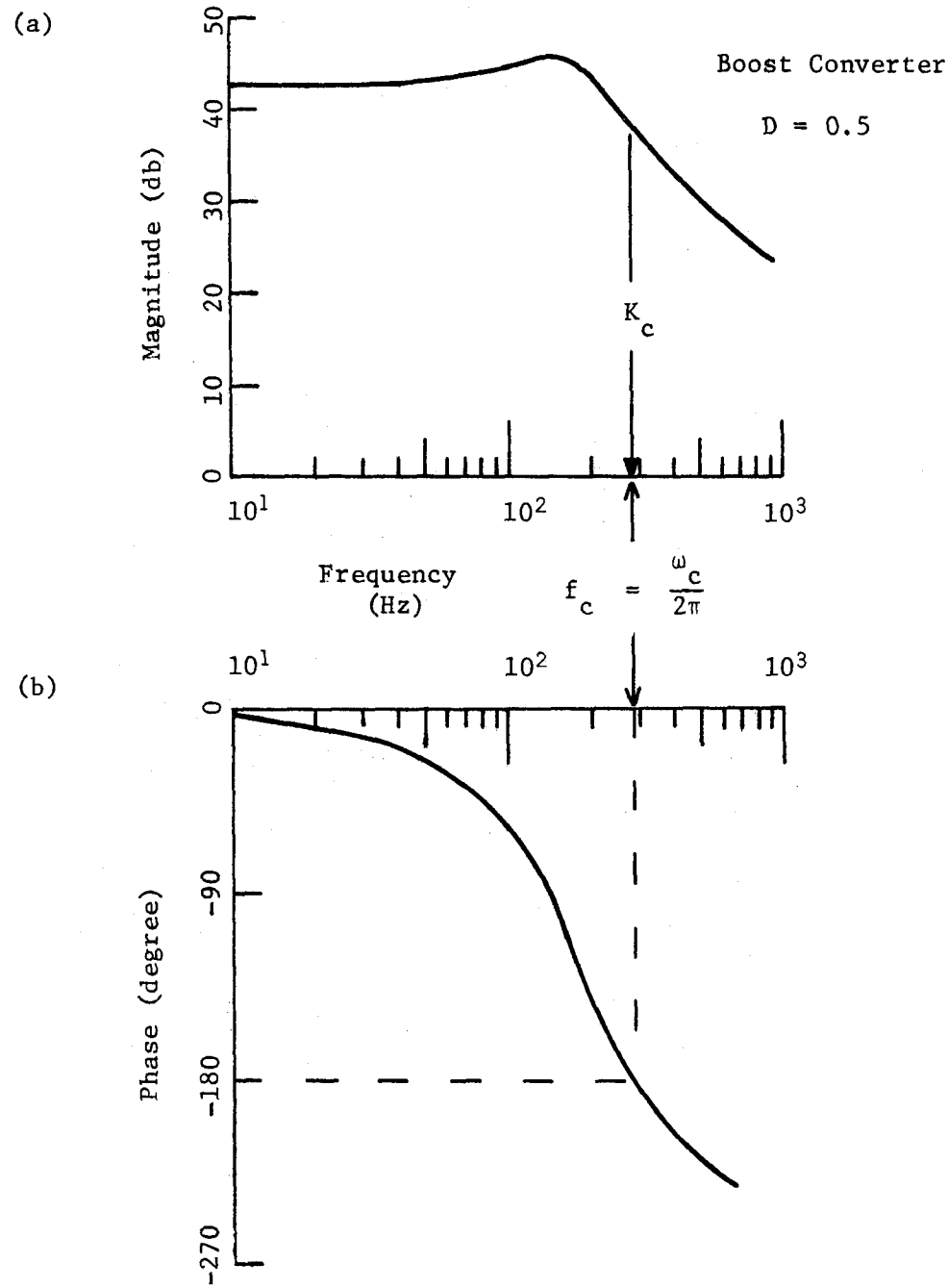

Fig. 4.12 Bode plot of frequency response for t
with D = 0.5 to illustrate the meanir
(a) magnitude, (b) phase.

presentation of frequency response characteristics for each power stage is deferred until Chap. 5 in order to make convenient comparisons there between experimental and theoretical results.

Chapter 5

EXPERIMENTAL VERIFICATION

5.1 Introduction

The purpose of this chapter is to verify the analytical expressions derived in Chap. 4 and, consequently, to provide confidence in the use of averaging techniques and resulting power-stage models. Substantiation is necessary for two reasons: the averaged model and associated analytical results are original, and the control-input frequency response of power stages capable of boosting the output voltage higher than the source voltage is given by unusual transfer functions with a real positive zero.

Consider the alternative methods one could conceivably employ to examine converter behavior. Theoretical confirmation is not possible because comparable analytical foundations have been lacking, so one immediately contemplates an experimental verification of results. Direct physical implementation of the switched converters investigated herein is an attractive possibility that permits measurement of transient and frequency response using ordinary laboratory instruments (i.e., oscilloscope, wave-analyzer); however, this technique was not used because unavoidable parasitics in the circuit components not only contaminate measured data in an unpredictable manner, but also jeopardize the experimental repeatability.

On the other hand, digital computers can perform a numerical analysis of equations which describe arbitrarily complex component models.

The modulation-frequency component of the output is necessary for frequency analysis of switched converters; however, the nature of the analysis used to evaluate that component depends on whether the modulation and switching frequencies are commensurable or incommensurable, as discussed in Chap. 2. This difference in technique of analysis is undesirable.

The analog computer is yet another possibility. Electronic analog computers can in a straightforward fashion simulate both transient and frequency responses of either the switched or averaged circuit model; however, they lack the inherent accuracy of digital computers. Still, analog accuracy should be sufficient for the comparative purposes of this chapter, and provided he has access to an analog computer, any investigator can readily duplicate the systems studied here.

After consideration of the goals of this chapter and the relative merits of the various procedural alternatives, the analog computer was chosen as the basic experimental tool. Details of the simulation appear in Appendix B, while the results are contained in the present chapter. Both switched and averaged models of the buck, boost, and buck-boost power stages, shown in Fig. 2.1, 3.8, 3.1, 3.5, 1.8[5], and 3.10, will be simulated; in addition, the pulse-width-modulator (PWM) described in Chap. 2 is simulated to control the switch operation of the switched power stages. The block diagrams of the switched and averaged configurations are shown in Fig. 5.1(a) and 5.1(b), respectively.

Section 5.2 deals with transient response. Since the theory in Chap. 4 predicts a dependence of the effective circuit components

---

[5]Parasitic resistances R_ℓ and R_c are included in each model.

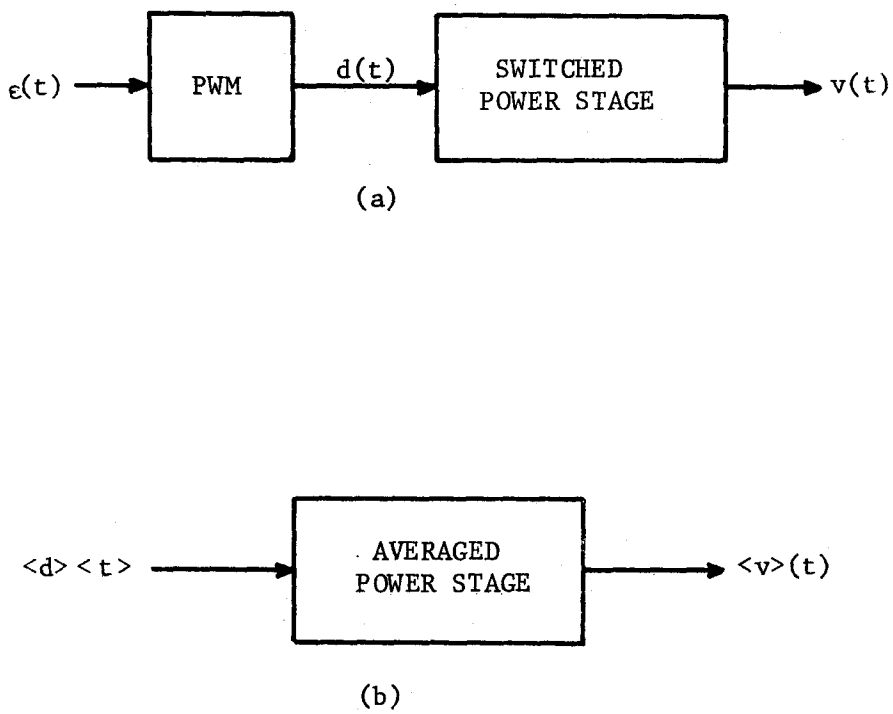

Fig. 5.1 Configurations simulated with the analog computer: (a) switched power stage and controller, (b) averaged power stage.

upon the dc-average of the switch drive, control transients promise to be more interesting than corresponding source transients; consequently, the transient response caused by step variations in the switch control only are studied in Sec. 5.2.

The frequency response for each type of converter is investigated in Sec. 5.3. There the experimental data for switched and averaged models are compared with the theoretical expressions derived in Chap. 4. It is shown that the presence of the real positive zero in the control-input transfer function of the boost and buck-boost power stages is essential to produce good agreement between theory and experiment.

In Sec. 5.4, the gain margin and critical oscillation frequency, which characterize closed-loop stability, are determined experimentally for the switched power stages and compared with nominal values computed from the averaged models. The practical utility of averaged models depends on how easily and accurately closed-loop behavior of switched power stages can be predicted; thus, this section provides results for the acid test of usefulness.

5.2 Transient Response

It is convenient to record on a strip chart the transient reponse of switched and averaged converter models as simulated on the analog computer; thus, comparisons are primarily qualitative in nature. In this section the expected transient behavior for each type of power stage, as determined in Chap. 4, will be summarized and then followed by interpretation of experimental observations.

Figure 5.2 shows the control transitions experimentally investigated;

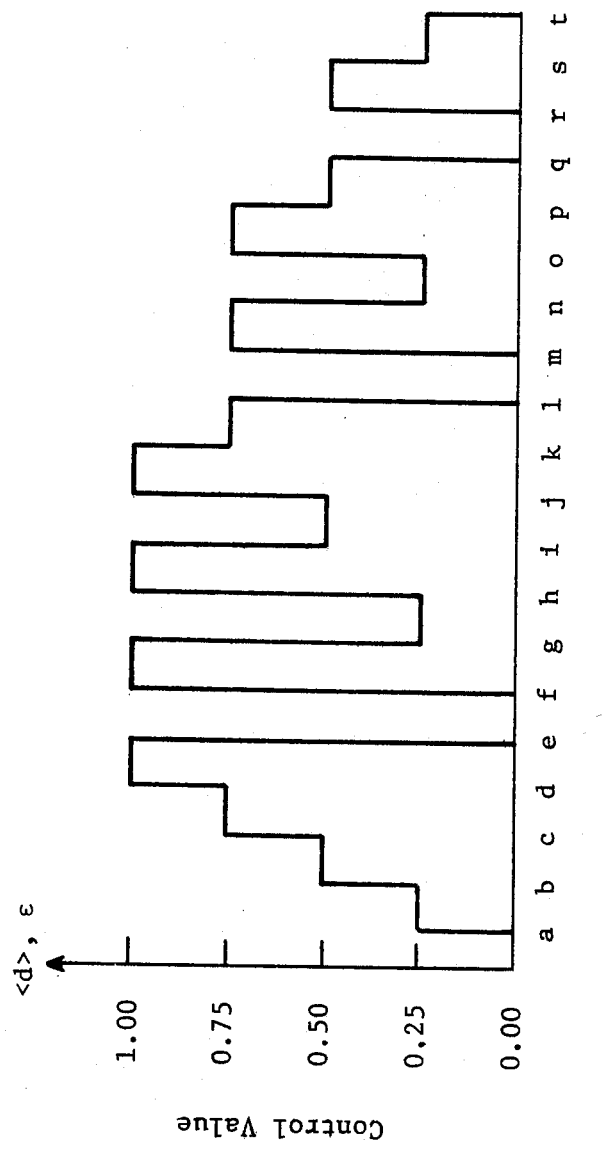

Fig. 5.2 Representative control transitions experimentally considered.

certain transitions will be singled out to illustrate various features. In practice, the PWM could not be simulated well for either very large or very small duty ratios without affecting the nature of the switching action, so the PWM input was limited to transitions between the levels 0.25, 0.50, and 0.75.

Since the effective filter component values in the averaged buck power-stage model are independent of the switch-control, a given percentage step change in control signal should cause an output transient with a characteristic shape and amplitude regardless of the final value of the control; furthermore, the transient caused by a negative control step should be the mirror image of the transient associated with a positive control step.

The control-input transient response of switched and averaged buck power stages is shown in Fig. 5.3; notice the close correlation between the corresponding switched and averaged responses. The responses in Figs. 5.3(a) and 5.3(c) are identical and are the mirror image of the transient in Fig. 5.3(b), which verifies the predictions stated in the preceding paragraph. The control step of Fig. 5.3(d) is twice the amplitude of the step size represented by Figs. 5.3(a) to 5.3(c); the characteristic shape of the corresponding transient is unchanged and its magnitude is doubled with respect to Fig. 5.3(c). Fundamental transient properties, natural frequency and damping factor, are thus independent of the initial value, magnitude, and final value of the control step for the buck power stage.

In contrast to the buck type, the averaged boost and buck-boost power-stage models have effective component values which are modified

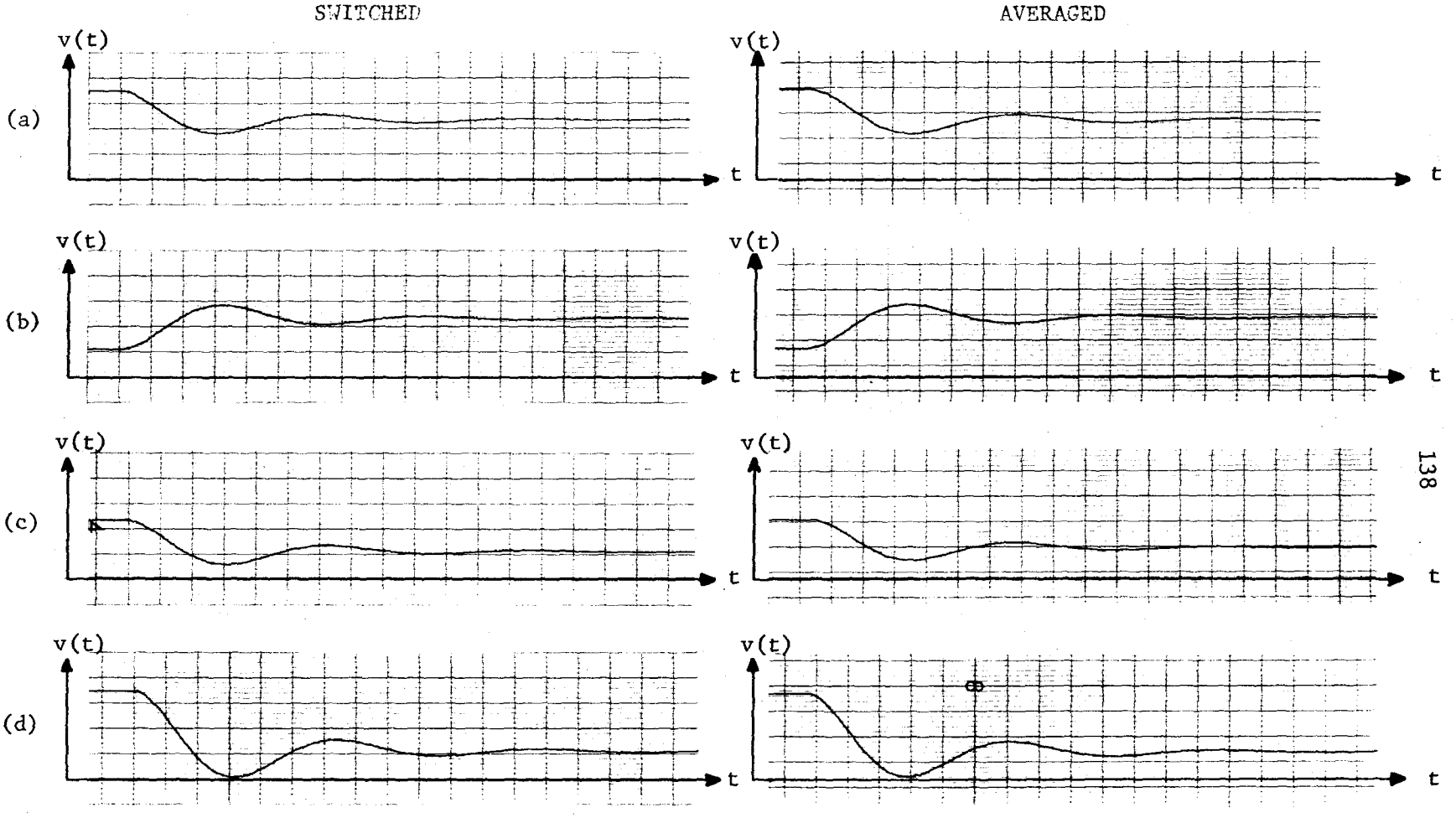

Fig. 5.3 Experimental transient responses of switched and averaged **buck** power stages: control transitions are (a) 0.75 → 0.50, (b) 0.25 → 0.50, (c) 0.50 → 0.25, (d) 0.75 → 0.25; [scale factors: 12 v/Div vertical, 0.5 msec/Div horizontal].

by the switch control; hence, the transient characteristics should vary with the final value of the control step. In fact, any control step which terminates at a certain level produces the same kind of transient response, the only differences being in the initial conditions which correspond to the pre-existing control value.

Figures 5.4 and 5.5 show the switched and averaged transient responses of the boost and buck-boost power stages. Once again, the fact that switched and averaged data agrees closely in all essential aspects indicates that averaged models are valid representations of the switched power stages. The transient characteristics, natural frequency and damping factor, in the Figs. 5.4(a), 5.4(b), 5.5(a), and 5.5(b) are identical, whereas Figs. 5.4(c), 5.4(d), 5.5(c), and 5.5(d) show different, but common, transient characteristics. Together these figures verify the dependence of transient characteristics upon the final value of the control step as predicted.

One can deduce a considerable amount of quantitative information from Figs. 5.3 to 5.5; for example, when the natural frequencies and damping ratios of the simulated systems are estimated from the strip chart traces, the values are approximately those computed in Table 4.2.

In summary, the transient responses of the averaged power-stage models correlate very well in all respects with those of switched power stages. Notice how the dominant response times are always much greater than the switching period; this condition, which is usually observed in switched converters by design, is necessary for proper application of the averaging technique.

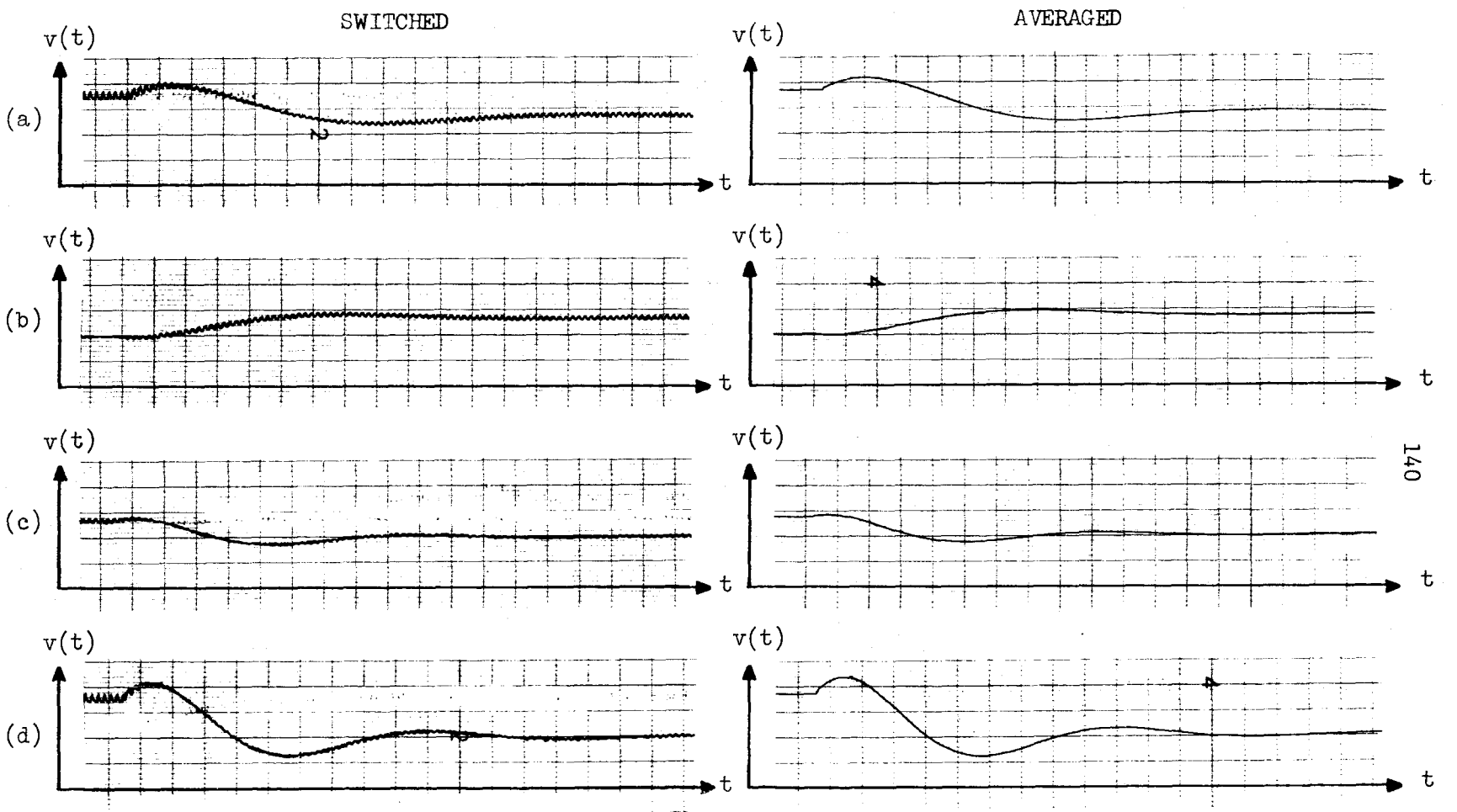

Fig. 5.4 Experimental transient responses of switched and averaged boost power stages: control transitions are (a) 0.75 → 0.50, (b) 0.25 → 0.50, (c) 0.50 → 0.25, (d) 0.75 → 0.25; [scale factors: 36 v/Div vertical, 0.5 msec/Div horizontal].

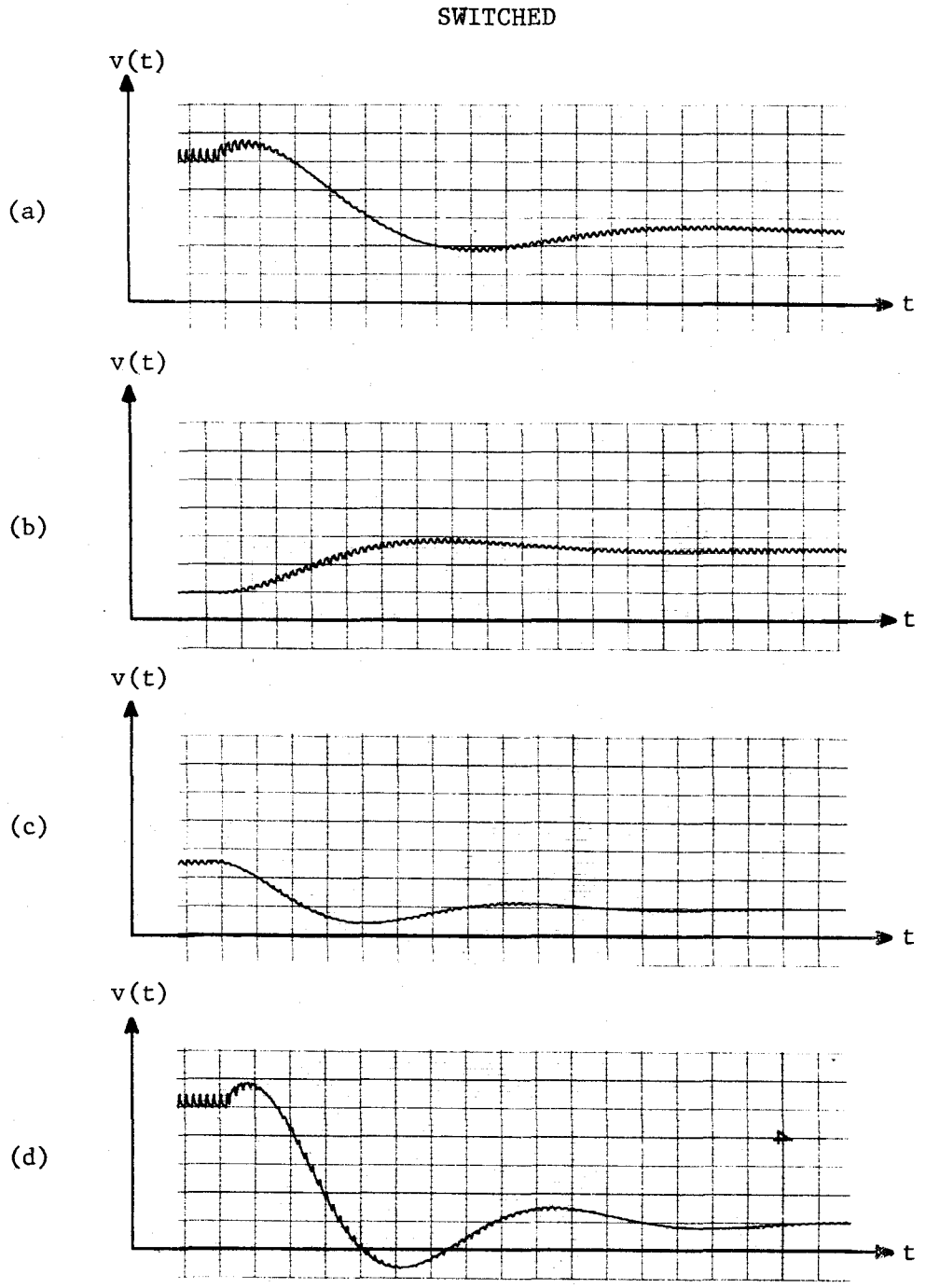

Fig. 5-5 Experimental transient responses of switched and averaged buck-boost power stages: control transitions are (a) 0.75 → 0.50, (b) 0.25 → 0.50, (c) 0.50 → 0.25, (d) 0.75 → 0.25; [scale factors: 19.2 v/Div vertical, 0.5 msec/Div horizontal].

AVERAGED

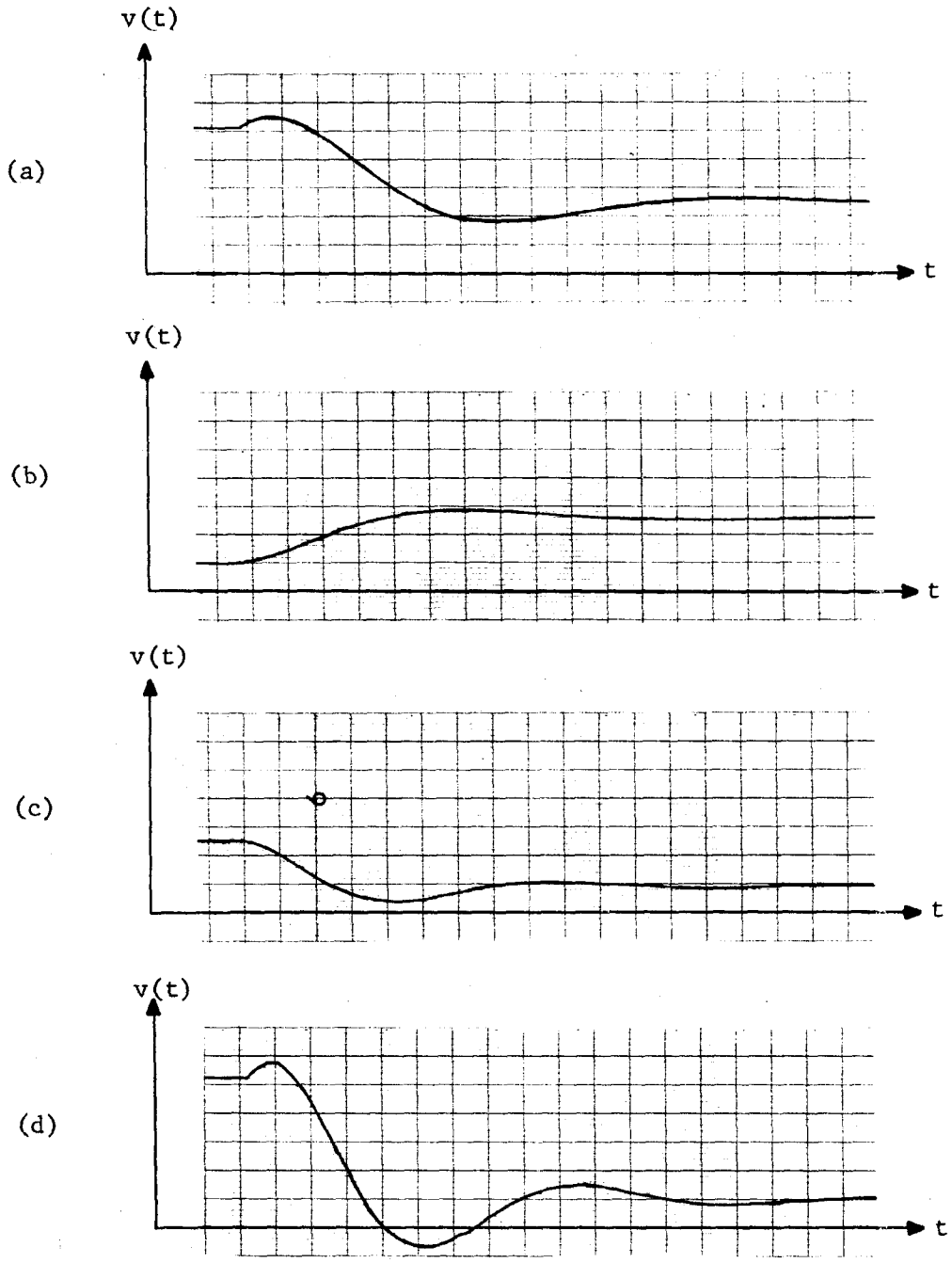

Fig. 5-5 CONTINUED

5.3 Frequency Response

For this series of measurements, a sinusoidal signal is injected in series with a dc control input D for the configurations shown in Fig. 5.1. At any given modulation frequency ω, the control input and power-stage output are simultaneously recorded on a strip chart, from which the amplitude and phase of the output component at the modulation frequency can be measured with respect to the modulation amplitude and phase. The magnitude and phase of the effective transfer function are:

$$\text{magnitude} = \frac{\left(\begin{array}{c}\text{amplitude of modulation-}\\ \text{frequency output component}\end{array}\right)}{\text{modulation amplitude}} \qquad (5.1)$$

$$\text{phase} = \begin{array}{l}\text{relative phase of modulation-}\\ \text{frequency output component}\\ \text{with respect to modulation}\end{array} \qquad (5.2)$$

and can be conveniently presented in a Bode plot. An additional phase term, $-\omega DT$, is added to experimental phase data from the averaged simulations to account for phase delay associated with the PWM in Eq. (4.51) since a linear time-delay device is not available in analog computers.

Figure 5.6(a) shows a typical trace of switched output for a modulation whose frequency is moderately low when compared to the switching frequency. The upper limit on useful modulation frequency for describing-function purposes was determined in Chap. 2 to be one-half the switching frequency, but in practice, the switching frequency masks the modulation component of the output at even lower frequencies as shown in Fig. 5.6(b);

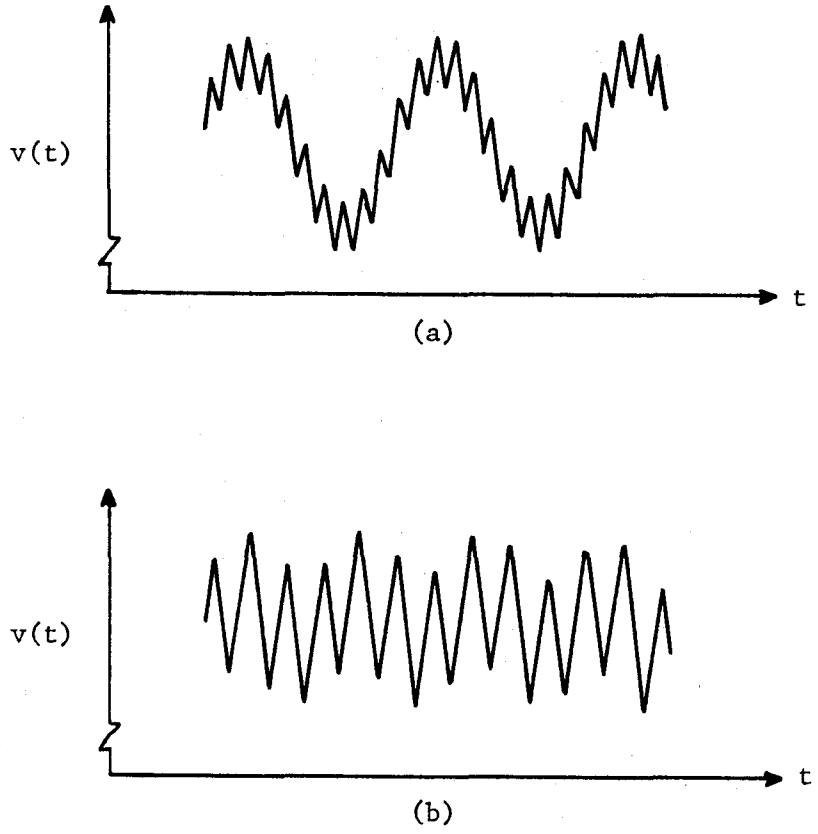

Fig. 5.6 Typical frequency-response traces of switched output voltage: (a) $\omega/\omega_s = 0.100$, (b) $\omega/\omega_s = 0.316$.

consequently, problems in interpretation of the switched data make experimental values of the transfer-function magnitude and phase relatively inaccurate at the higher modulation frequencies.

A Bode plot of the theoretical control-input transfer function derived in Sec. 4.3 (see also Eq. (4.22) and Table 4.1) for the averaged buck power stage and PWM is shown as the solid line in Figs. 5.7 to 5.9 for different values of the parameter D; superimposed on these figures are the experimental data from the switched and from the averaged models. Since the transfer function of the switched buck power stage is known a priori to be independent of switch-control parameters, the principal purpose in illustrating the performance of the buck power stage is to demonstrate the calibration of the experimental procedure. Figure 5.10 shows how the theoretical Bode plots of the averaged buck power stage vary as a function of the switch duty ratio D: the magnitude is unaffected by D, but the phase varies with D as a consequence of the PWM phase factor.

Two qualitative conclusions can be drawn from a study of Figs. 5.7 to 5.9. First, there is virtually no difference between the experimental measurements of the averaged power stage and the theoretical predictions which were derived from the averaged power stage, and second, although the switched data tends to scatter somewhat when the modulation frequency approaches the switching frequency as previously explained, the switched data does correlate very well with the averaged data at lower frequencies. Both conclusions are fundamentally gratifying and justify for the buck configuration the representation of switched

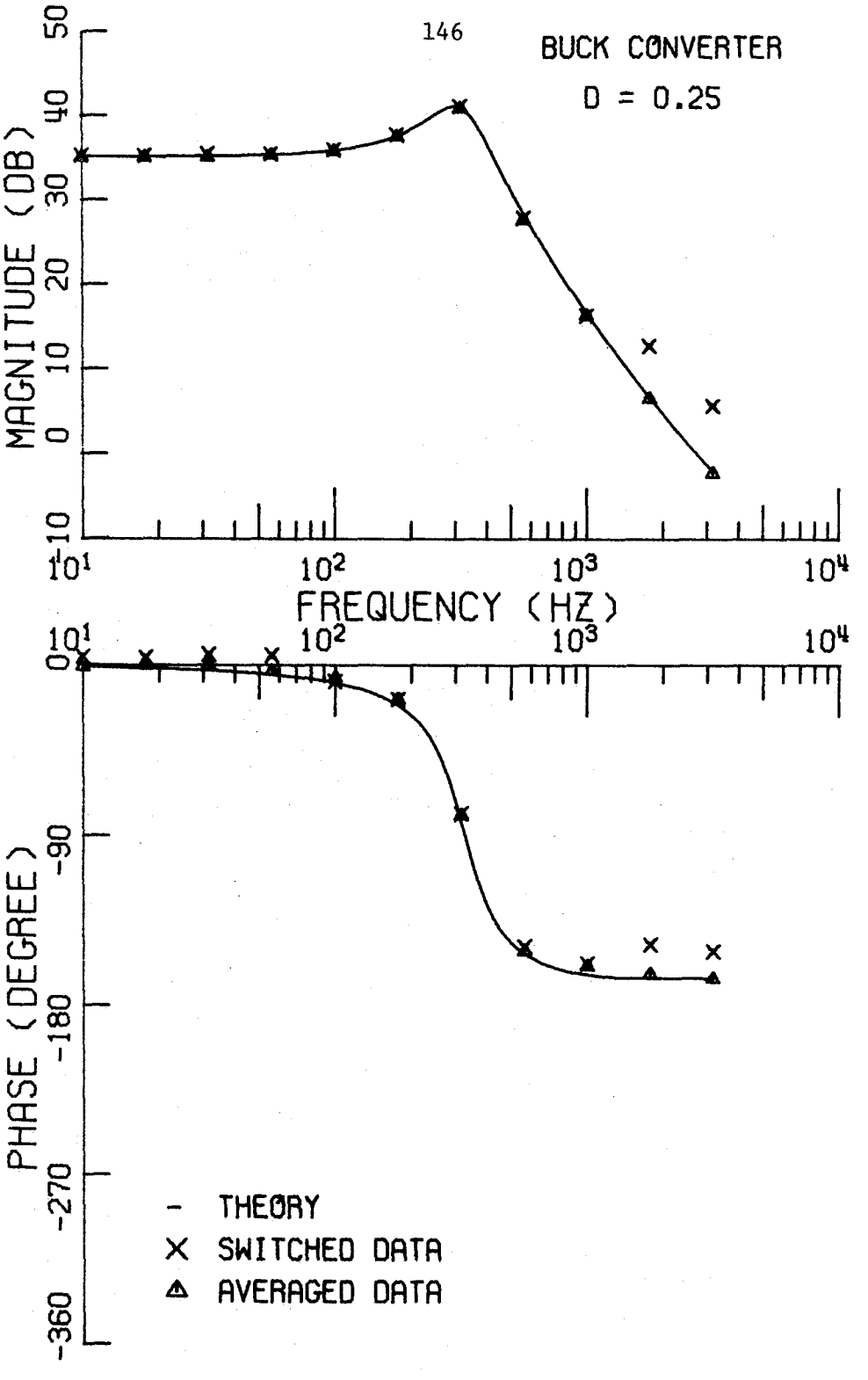

Fig. 5.7 Control-input frequency response of the buck converter for D = 0.25.

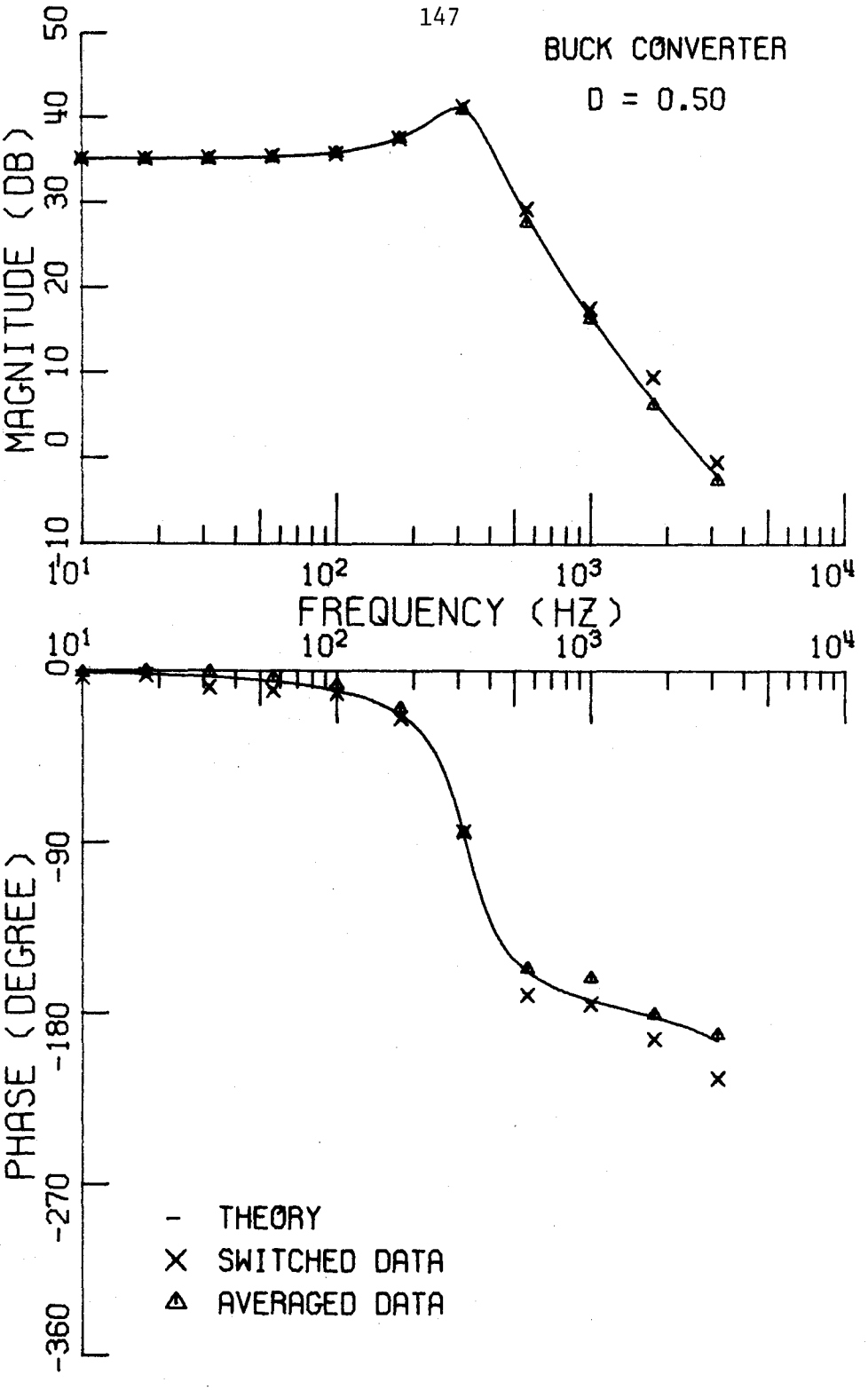

Fig. 5.8 Control-input frequency response of the buck converter for D = 0.50.

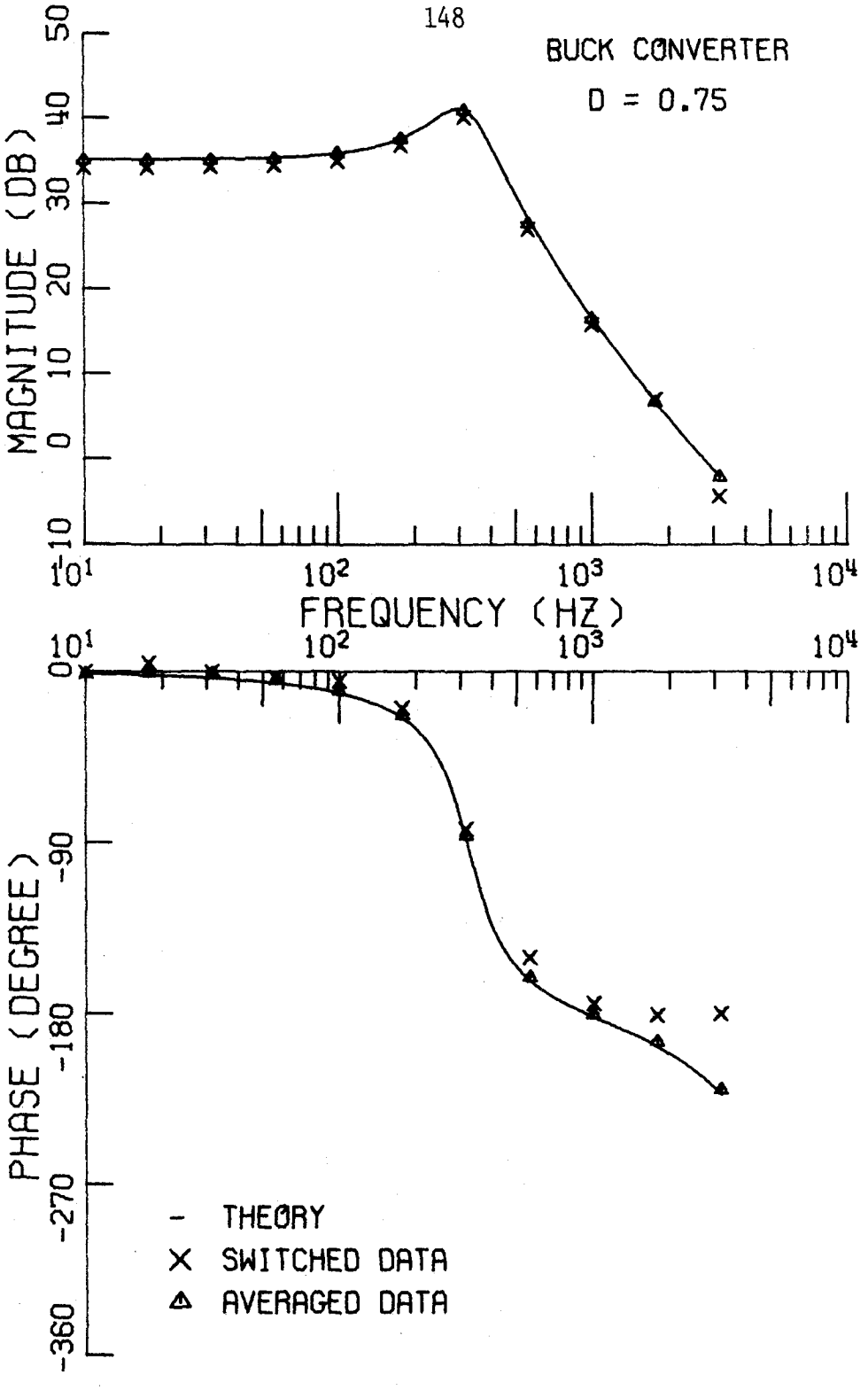

Fig. 5.9 Control-input frequency response of the buck converter for D = 0.75.

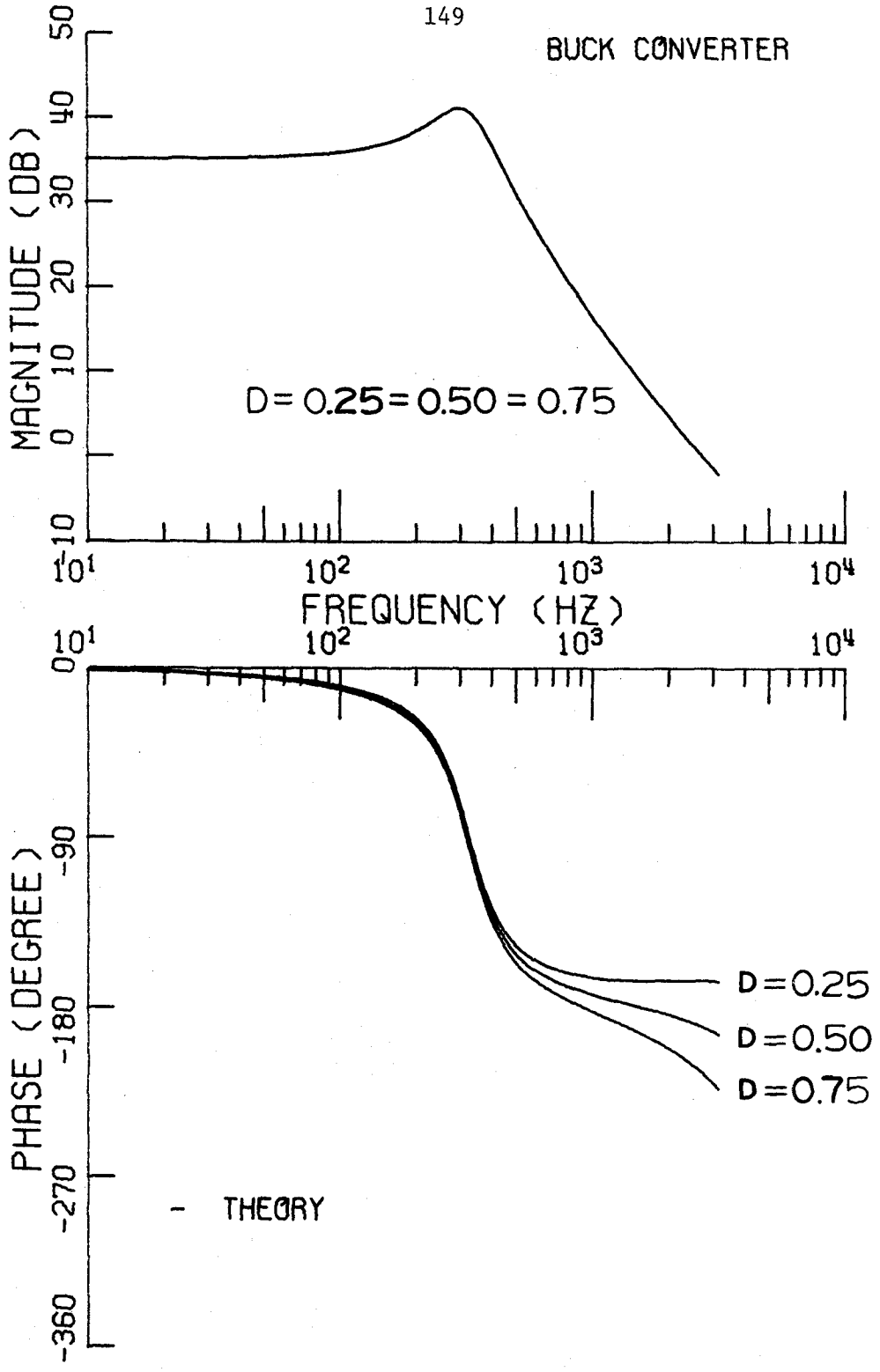

Fig. 5.10 Theoretical control-input frequency response of the buck converter.

power stages by averaged power-stage models; still, it is essential to investigate experimentally the frequency response of the boost and buck-boost power-stage configurations and the correspondence between the actual switched power stages and the averaged power-stage models, not only because the appropriate circuit models and analytic expressions are original, but also because the frequency responses predicted for these power-stage types in Chap. 4 are unusual.

Experimental data from the switched and averaged boost power-stage models is shown superimposed on the theoretical Bode plots in Figs. 5.11 to 5.13. Once again, the correlation between averaged and theoretical datum points is nearly perfect and, in turn, the switched data agrees well with averaged data at lower frequencies, but the inaccuracy of switched data at higher frequencies leaves a lingering uncertainty concerning the role of various theoretical factors in determining the overall frequency response.

To study this question, one can decompose the theoretical transfer function into distinct factors[6] which represent the effective amplifier, filter, and switch controller of the averaged boost power stage. These component factors, together with the composite response, are plotted as a function of frequency in Figs. 5.14 to 5.16 for three values of duty ratio and reveal useful conclusions. It is unmistakably clear that, even though there is some experimental uncertainty at higher frequencies, the data correlation with the computer curve would be much

[6]For convenient amplitude normalization, the scale factor V_s is divided from the amplifier factor and multiplied with the filter factor.

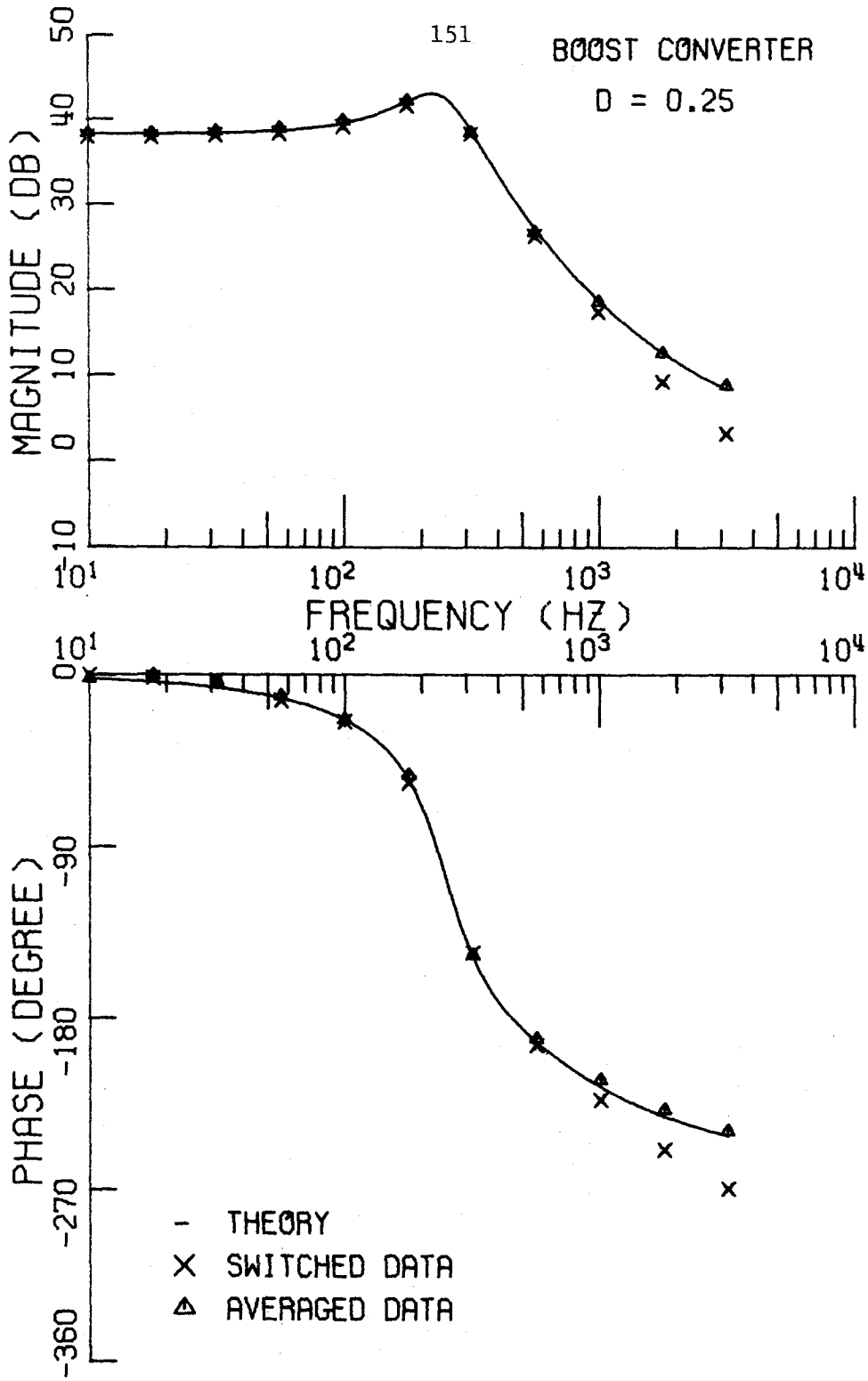

Fig. 5.11 Control-input frequency response of the boost converter for D = 0.25.

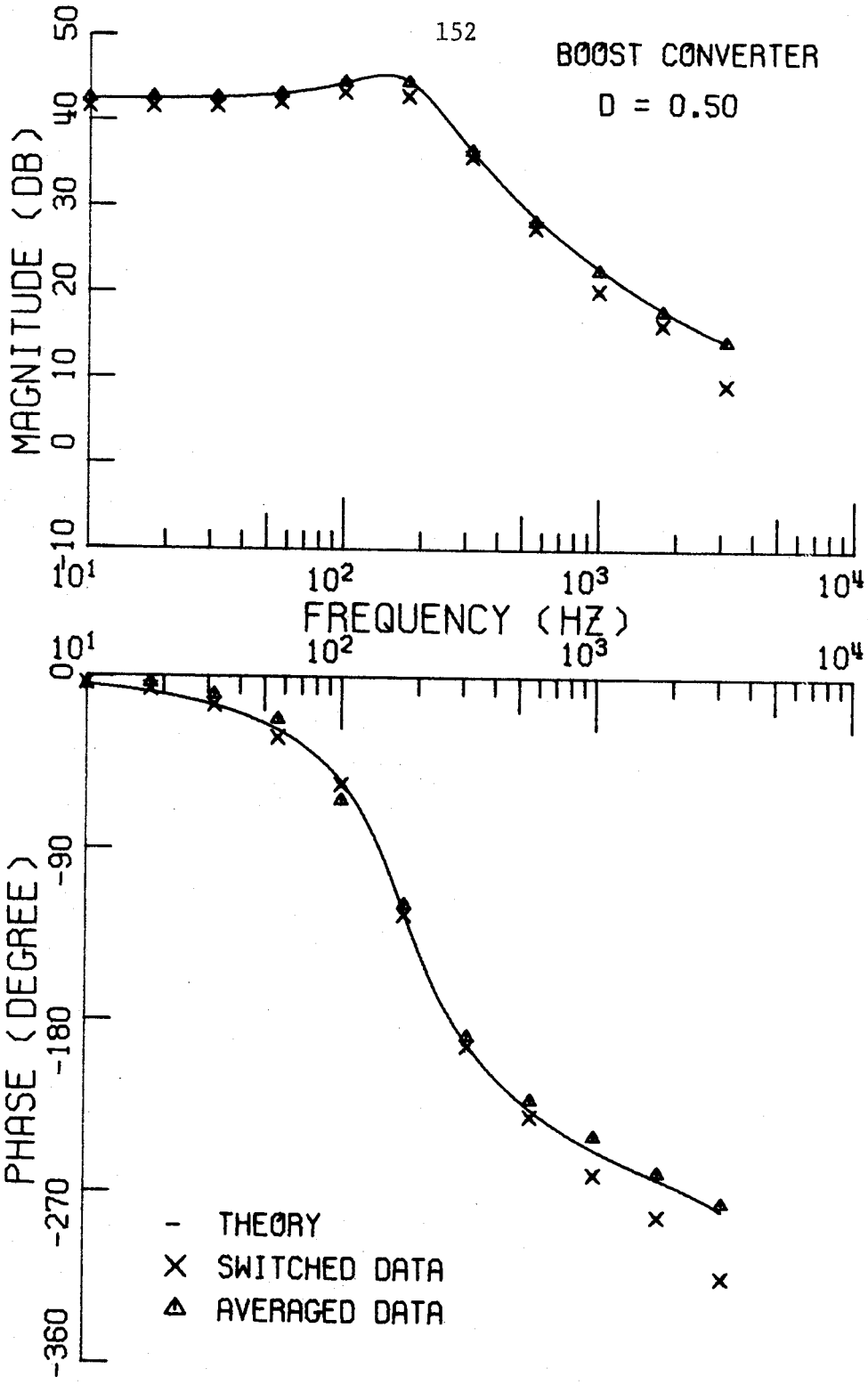

Fig. 5.12 Control-input frequency response of the boost converter for D = 0.50.

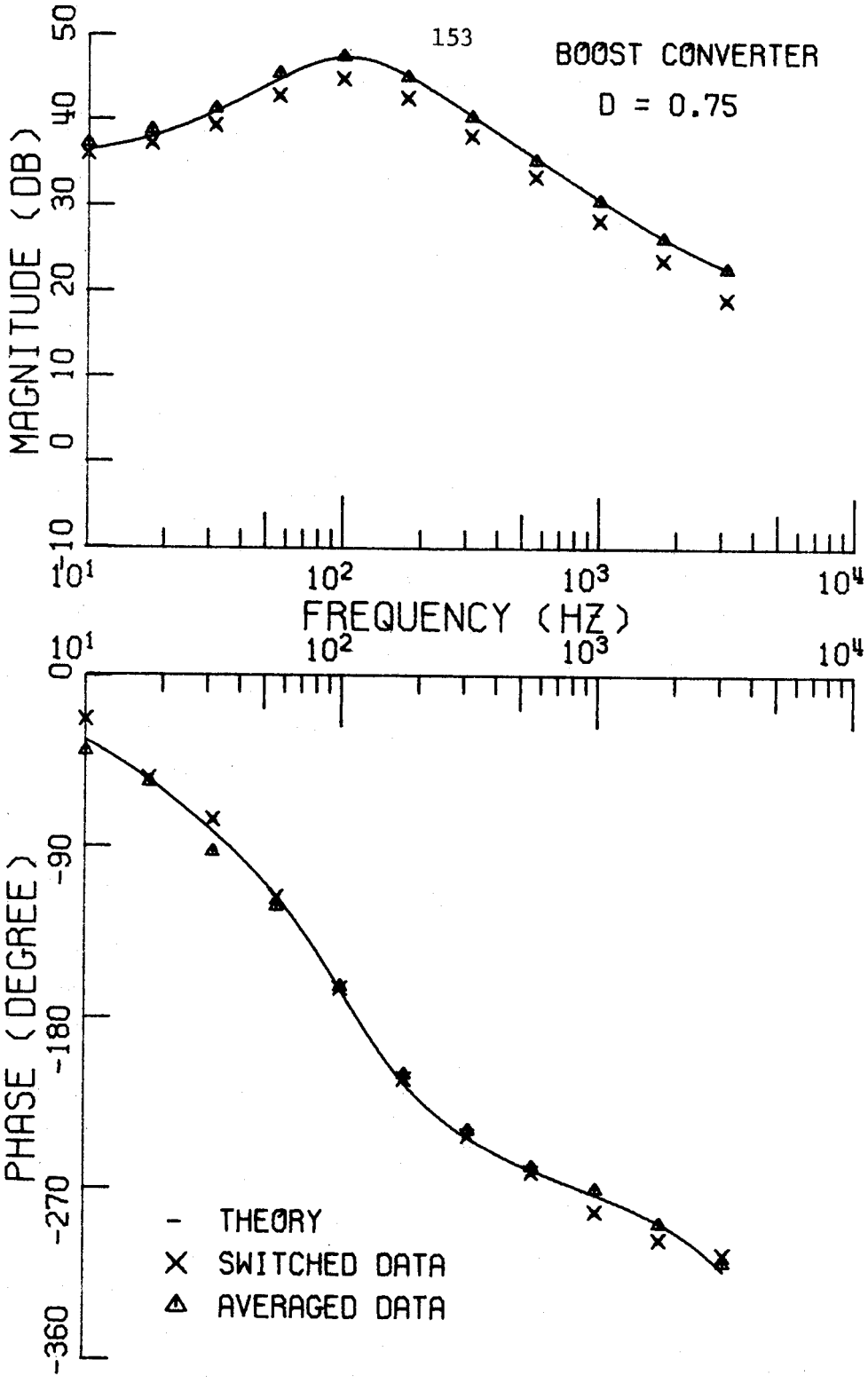

Fig. 5.13 Control-input frequency response of the boost converter for D = 0.75.

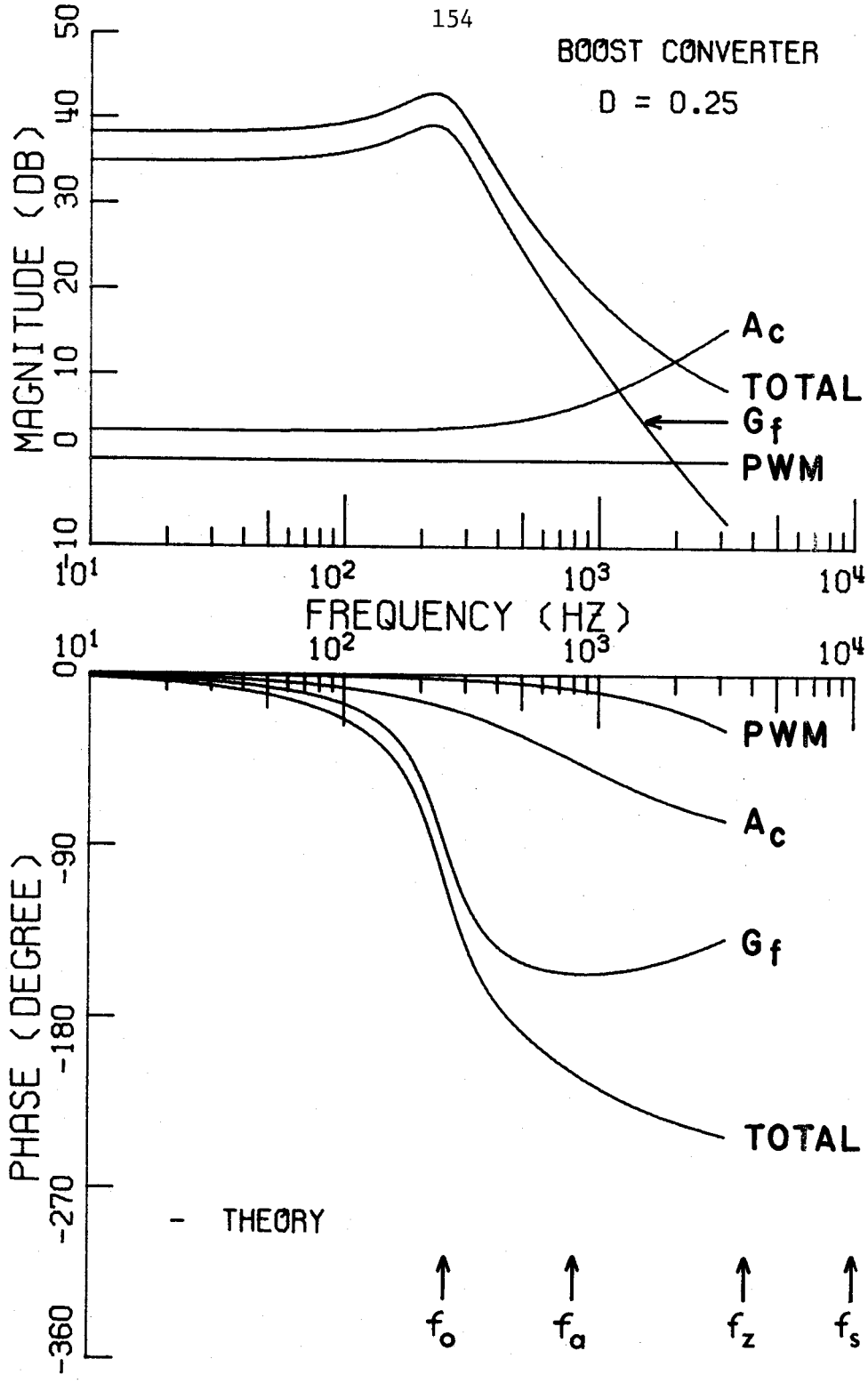

Fig. 5.14 Components of the theoretical control-input frequency response of the boost converter for D = 0.25.

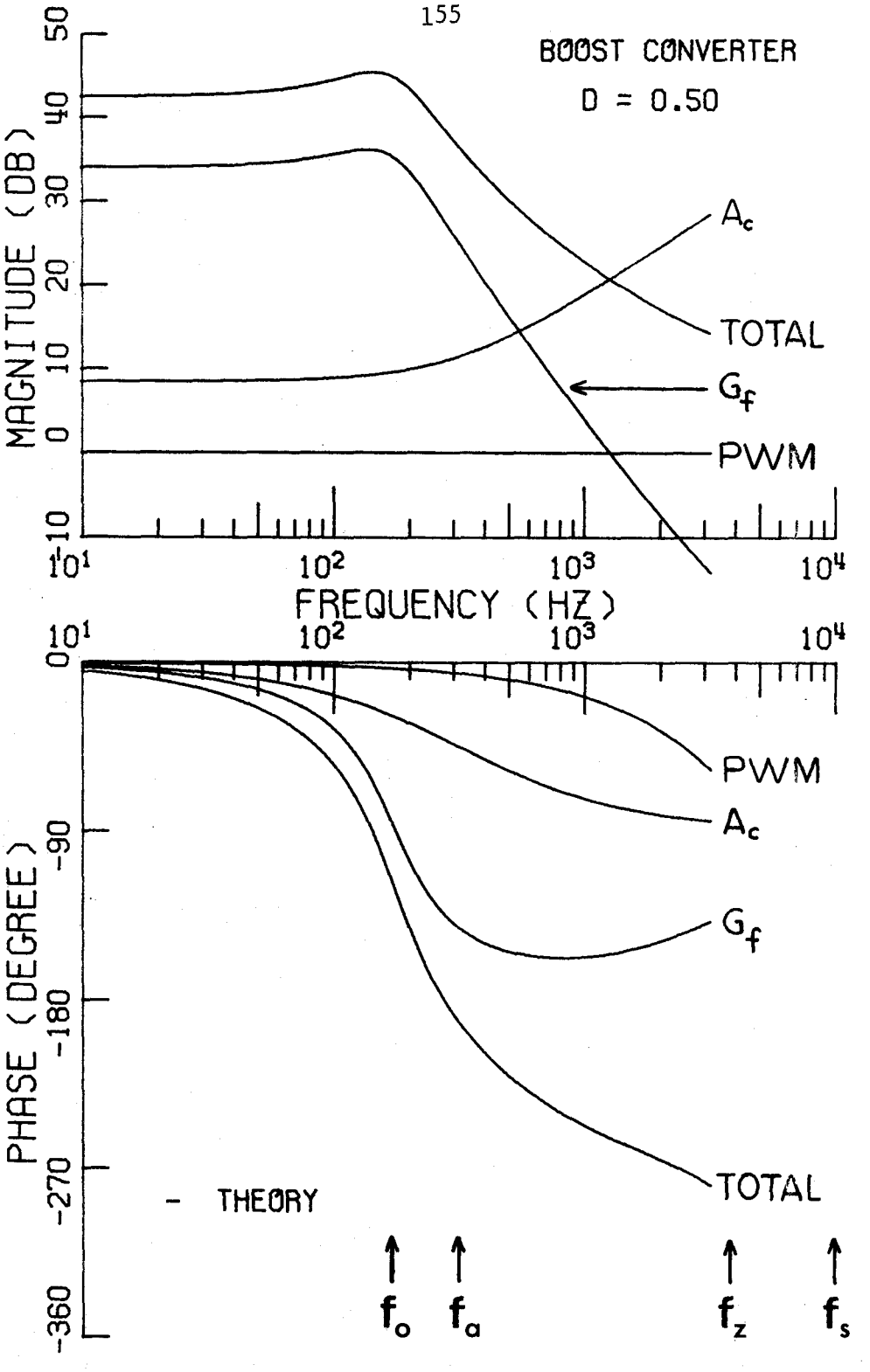

Fig. 5.15 Components of the theoretical control-input frequency response of the boost converter for D = 0.50.

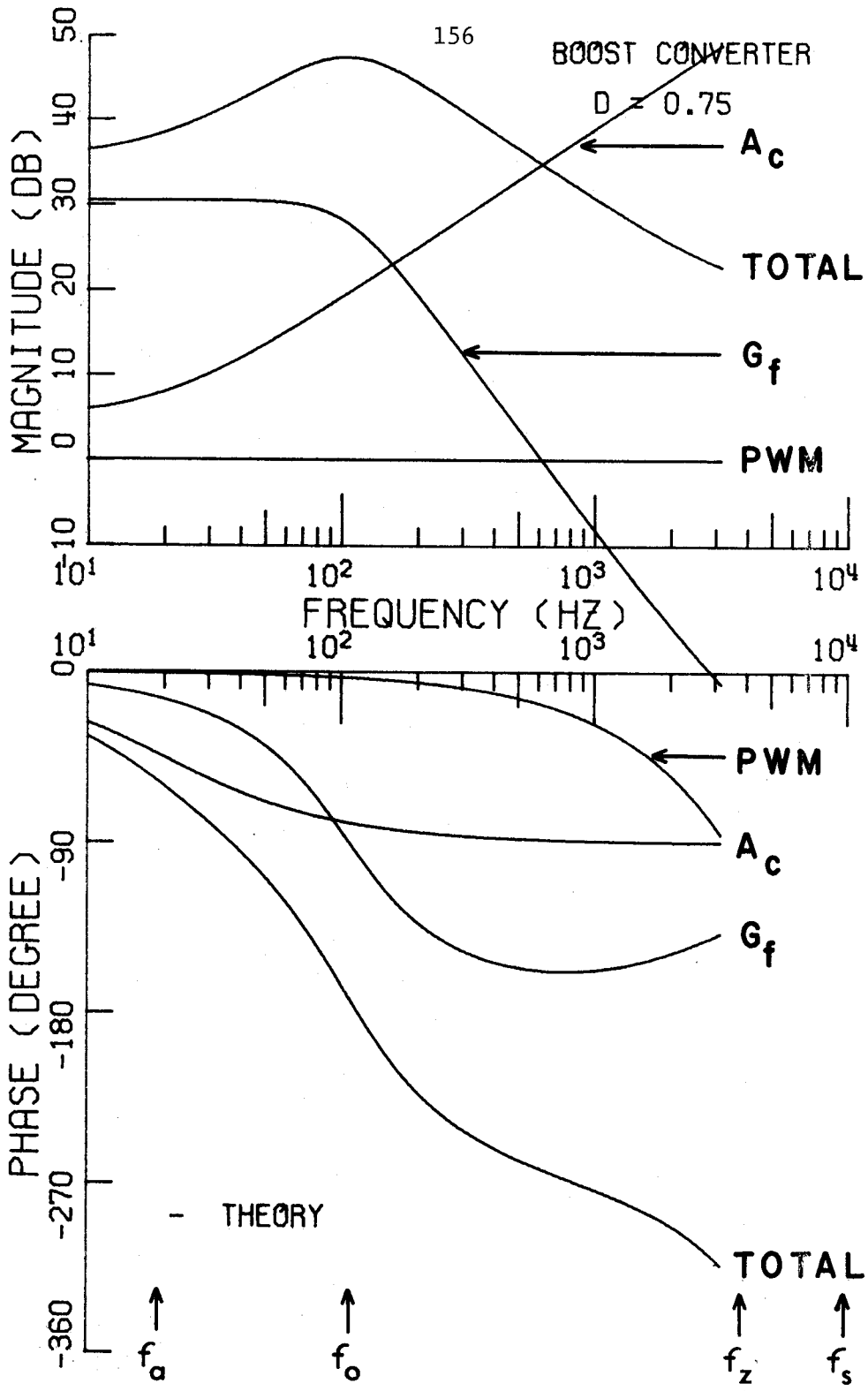

Fig. 5.16 Components of the theoretical control-input frequency response of the boost converter for D = 0.75.

worse if any single theoretical factor were missing; thus, each factor of the overall transfer function is necessary to correctly describe the behavior of switching power stages. In particular, the effective amplifier term, novel because of its real positive zero, is essential for good correlation of the results for D=0.75, even at relatively low frequencies where the switched data is fairly accurate.

Another observation concerns the variation of component factors with switch duty ratio. Viewed on the basis of logarithmic frequency, the PWM factor assumes importance only at the higher frequencies, but its influence on the phase cannot be neglected there, especially for large values of D since the PWM phase lag is proportional to D. The quadratic corner frequency in the effective filter term which arises from modified circuit components varies about one-third of a decade when D changes from 0.25 to 0.75, but far more sensitive is the corner frequency of the effective amplifier because it shifts over one and one-half decades for the same change in D; thus, the effective amplifier term which emerged from approximate describing-function analysis of the averaged boost model plays an undeniable role in determining the power-stage response to frequency and duty-ratio variations. For comparative purposes, the theoretical Bode plot of the boost power stage and modulator is shown in Fig. 5.17 for various values of D; insight into the nature of the differences is best obtained from the component plots in Figs. 5.14 to 5.16.

Armed with new confidence that the accuracy of experimental data is sufficient for verification of the averaged model, one can now

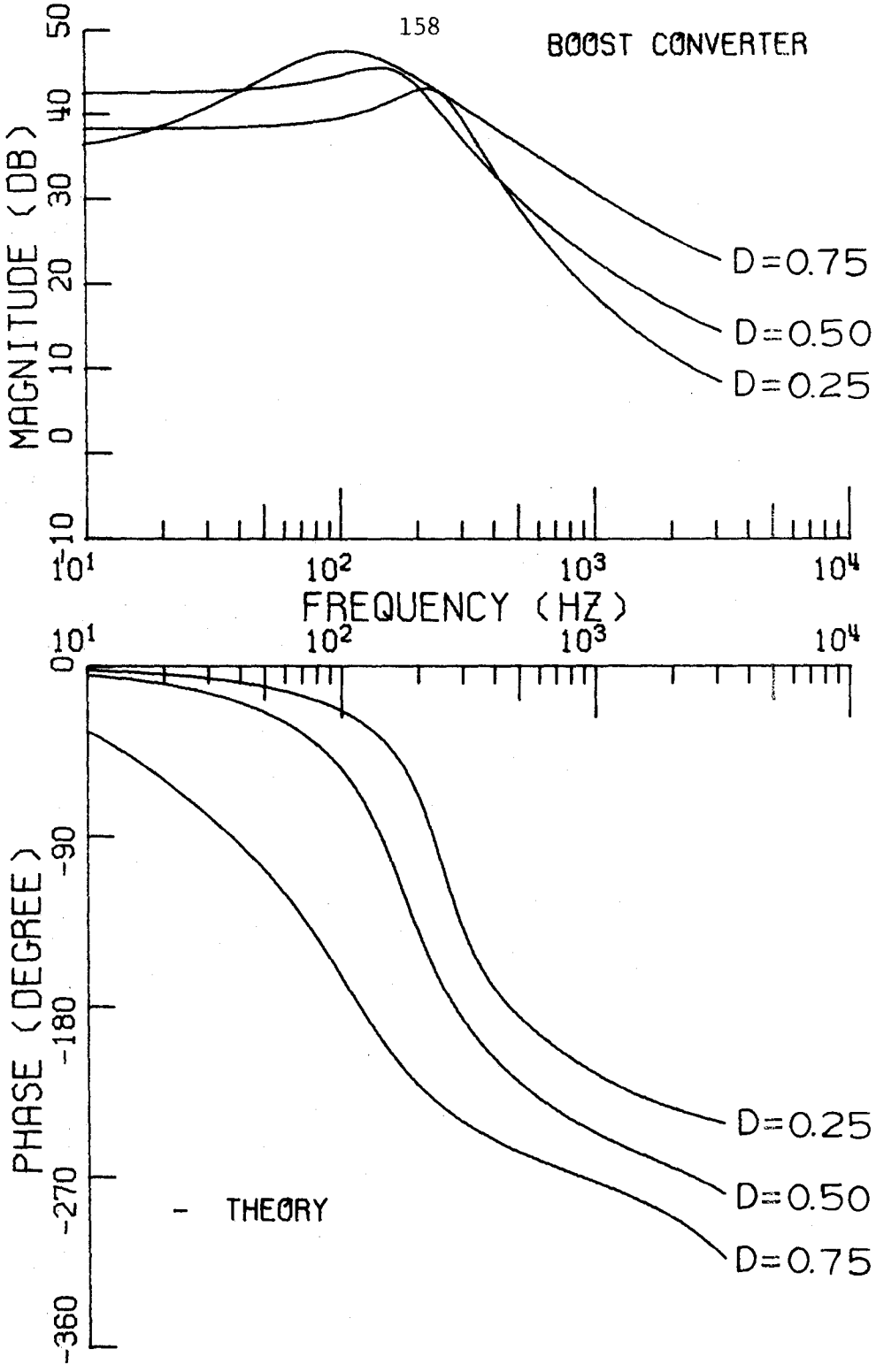

Fig. 5.17 Theoretical control-input frequency response of the boost converter.

investigate the remaining power-stage type. Figs. 5.18 to 5.20 show the experimental data from the switched and averaged buck-boost power-stage models superimposed on the theoretical Bode plot for various duty ratios. It is clear that measurements and theory from the averaged model correlate very well with data from the switched model. The analytical expressions for the frequency response of the averaged power stage and controller are plotted in Fig. 5.21 to show the comparative effects of duty ratio; the qualitative variations are similar to those of the boost power stage, but are less extreme.

In conclusion, it is established in this section that for each type of power stage the averaged model gives essentially the same experimental frequency response as the switched model; therefore, the averaged model is a valid representation of the switched power stage. Furthermore, the analytical expressions derived from the averaged model in Chap. 4 are verified here by excellent correlation of experimental data with computed frequency response. Analysis of the component factors associated with the effective amplifier, filter, and switch controller shows that each distinct factor produces a significant contribution to the overall frequency response.

5.4 Closed-Loop Stability

Given that the open-loop frequency response of switched power stages is approximated by that of the averaged model, the inherent nonlinearity of the PWM and switched power stage leaves one uncertain at this point how well the closed-loop behavior of the switched system can be predicted by the averaged system; however, for clocked switch

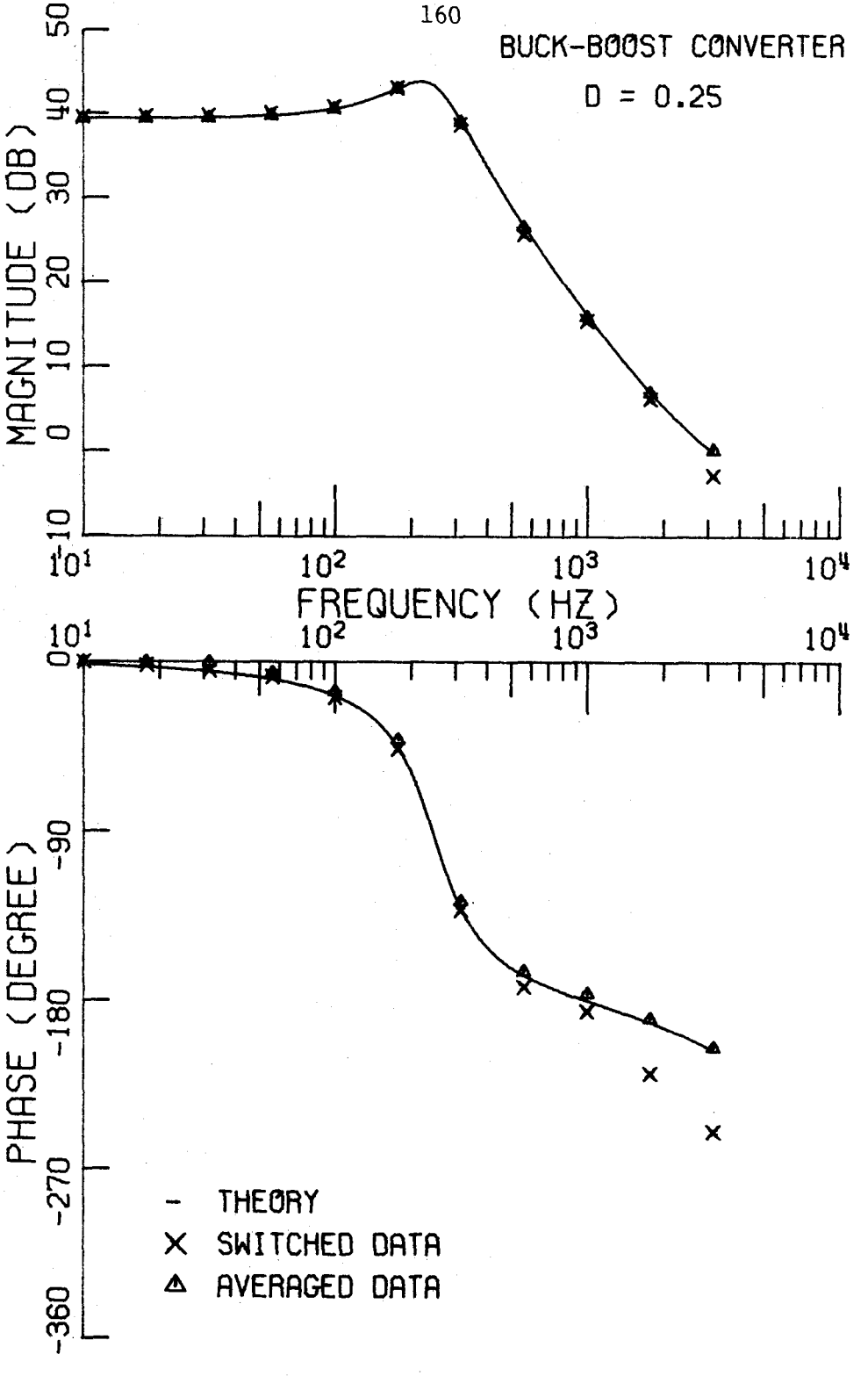

Fig. 5.18 Control-input frequency response of the buck-boost converter for D = 0.25.

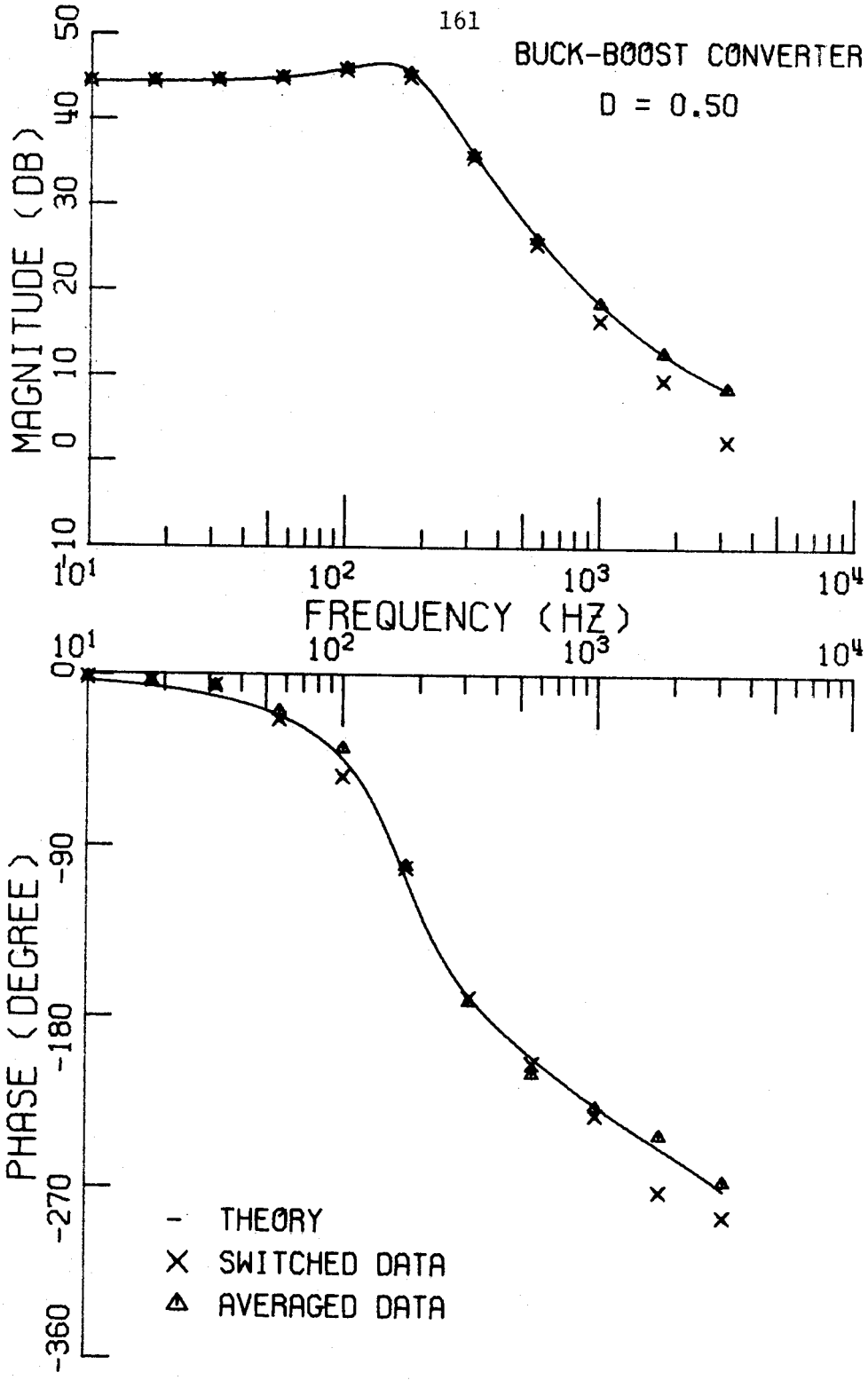

Fig. 5.19 Control-input frequency response of the buck-boost converter for D = 0.50.

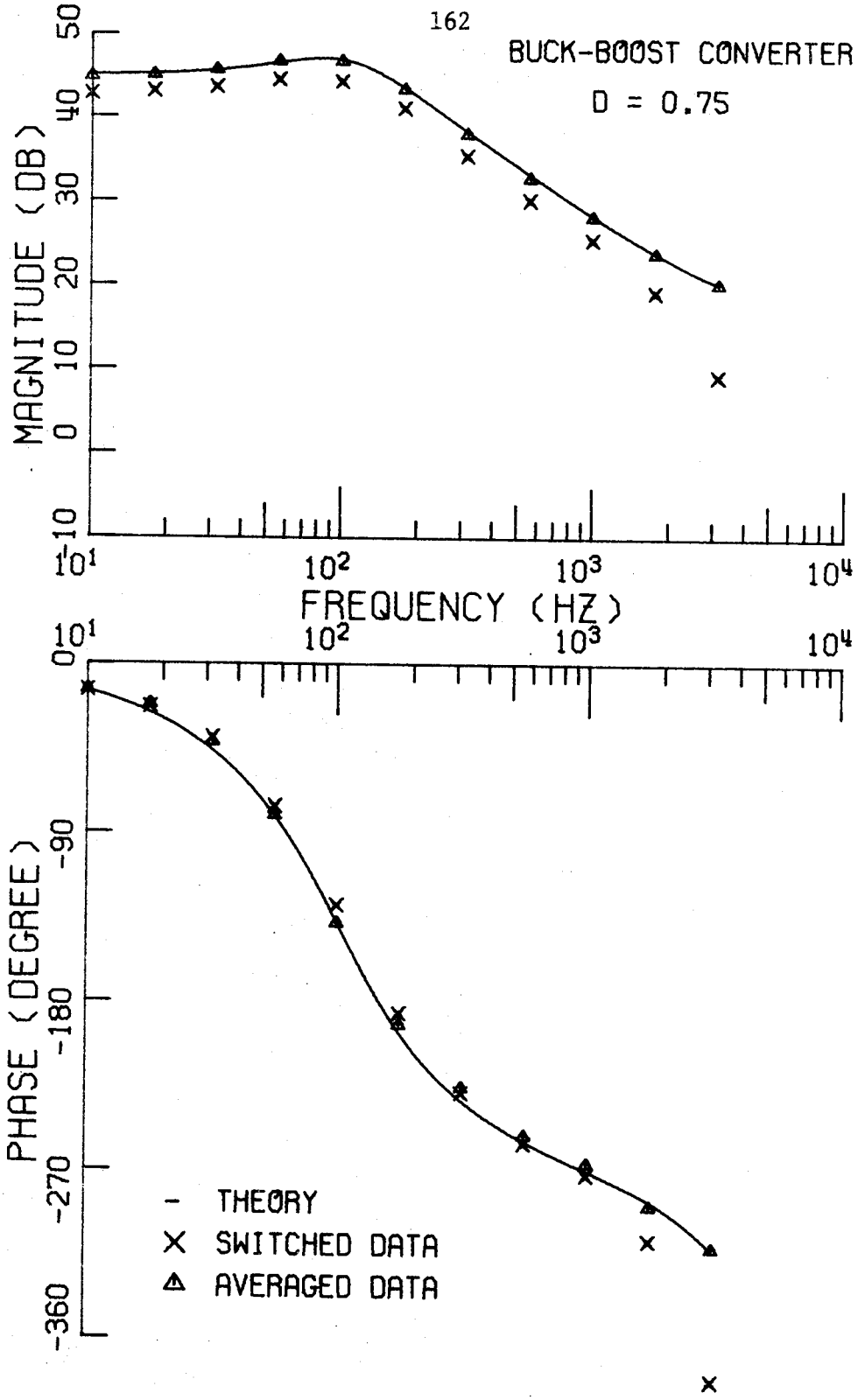

Fig. 5.20 Control-input frequency response of the buck-boost converter for D = 0.75.

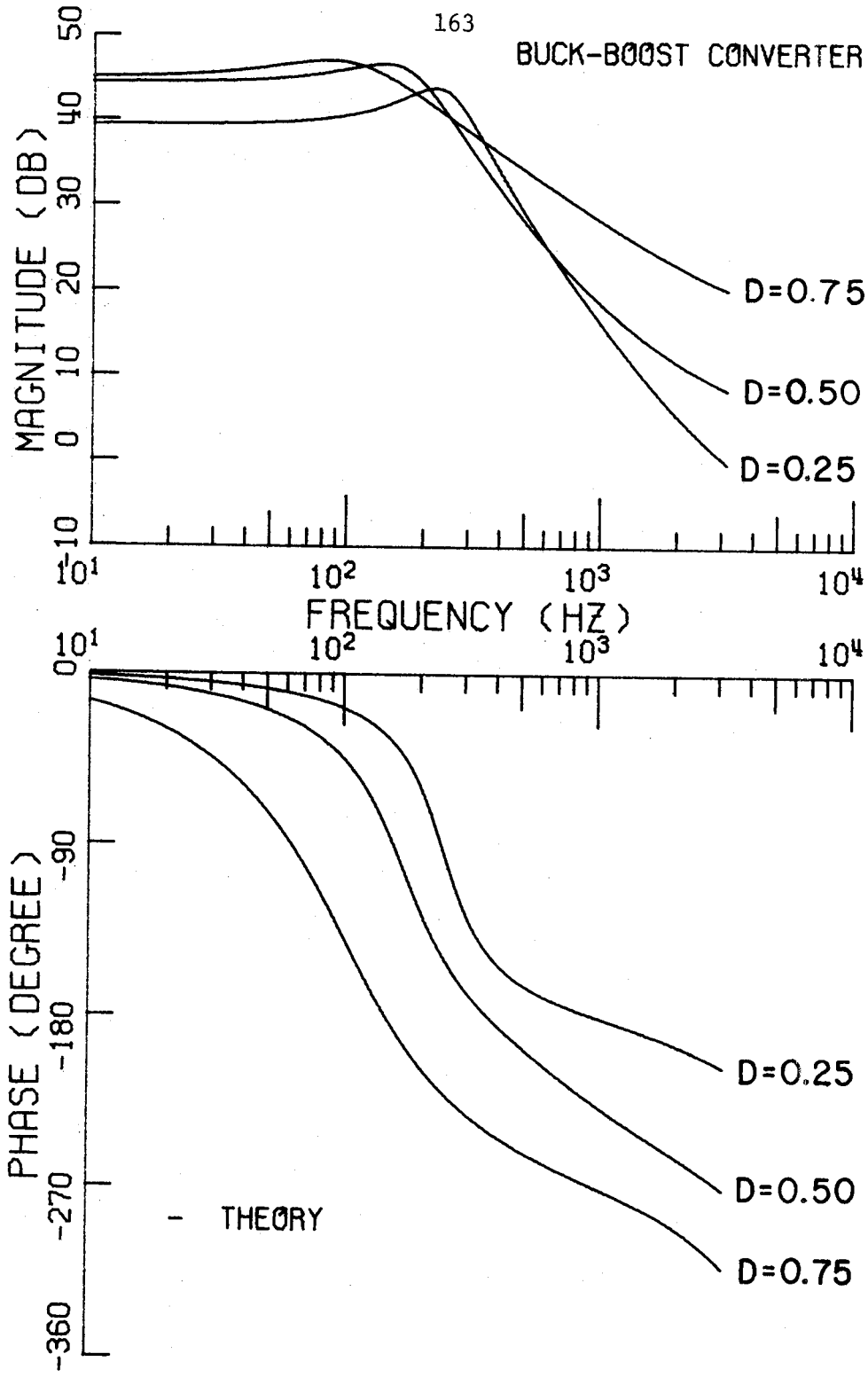

Fig. 5.21 Theoretical control-input frequency response of the buck-boost converter.

controllers such as the PWM, one intuitively expects the fundamental component of the feedback signal to be more significant in determining closed-loop behavior than the shape of the feedback waveform, so there may be a reasonable correlation between switched and averaged system stability. The behavior of the switched system cannot be predicted from the averaged model for frequencies higher than one-half the switching frequency because the describing-function requirements are not satisfied then for the PWM; therefore, any derived stability conditions will be merely necessary, but not sufficient, for stability. The objective of this section is to provide an experimental basis for the comparison of closed-loop stability associated with switched systems and averaged systems.

Refer to Fig. 4.11 for the closed-loop configuration of the switching converter. Local stability can be experimentally examined by gradually increasing the value of the gain factor K until a small disturbance in the steady-state limit cycle no longer decays with time but grows in amplitude. The critical value of K which separates the two modes of behavior is denoted K_c, and the corresponding oscillation occurs at frequency ω_c. In practice, the perturbation is originated by changing U for a few switching cycles and then returning U to its steady-state value; the effect is to initiate non-steady-state initial conditions in the state variables of the system.

Theoretical values for K_c and ω_c were computed from the averaged models in Sec. 4.6.2 by observing the frequency ω_c where the phase lag is π and then choosing a gain factor K_c which makes the magnitude

of the open-loop-gain equal to unity; values are summarized in Table 4.2.

Experimental values of K_c and ω_c are compared in Table 5.1 with predicted analytical values. Considering the possibility that experimental values for ω_c and K_c may lie in a semi-infinite interval, one must conclude that the empirical data correlates well with values derived analytically from the averaged models. Experimental values could not be obtained in the buck-boost simulation for D=0.25 because, as K increases, the discontinuities in output voltage, which are a consequence of switched current through the parasitic resistance of the imperfect filter capacitor, drive the switch controller into a saturated condition before the system becomes unstable. The same problem plagues the simulation of the buck converter to an even greater extent since the critical gains expected there are larger; although it could be a real operational characteristic, the problem in the simulation was traced to amplifier loading.

The essential agreement between experimental and theoretical closed-loop behavior indicates that even closed-loop response of switched dc-dc converters can be well predicted by averaged models; hence, the averaging technique should be a useful tool for the design and analysis of switching converters.

Table 5.1

Critical stability factors of the closed-loop regulator configuration.

	D	K_c		$\omega_c[10^3$ rad/sec]	
		Theory	Measured	Theory	Measured
Boost	0.25	0.028	0.034	2.84	2.87
	0.50	0.012	0.015	1.73	1.65
	0.75	0.004	0.007	0.73	0.82
Buck-Boost	0.25	0.158	-	6.34	-
	0.50	0.023	0.037	2.37	1.89
	0.75	0.006	0.010	0.93	1.13

Chapter 6

CONCLUSIONS

Techniques have been developed in this work for the representation of switched voltage converters by averaged models. These models were subsequently used to derive analytical expressions for the characteristic transient and frequency responses of switched power stages. The averaging method avoids a dependence on transcendental equations and thus applies for high-order systems without a commensurate increase in complexity; however, it portrays only those responses[7] whose characteristic times are large compared to the switching period. One of the general results which emerge from analysis is the dependence of effective component values upon the switch duty ratio.

Chapter 1 introduces several switched circuits (buck, boost, and buck-boost) which are often used for conversion of dc voltages from one level to another when efficiency is a fundamental concern. There the nonlinear nature of switched converters is exposed. Conventional methods of nonlinear analysis are discussed and found to be not only lacking in design interpretation, but also difficult or impossible to apply. The practical design implications of transient response and frequency response lead to a problem formulation in search of (at least) these quantities.

---

[7] This limitation is not a serious one since practical switched converters invariably satisfy the slow-response criterion.

Of the two functional blocks with which switched converters are composed, the switch controller is well defined, so the power stage is chosen for further study. Chapter 2 deals with the buck power stage, which is a simple linear circuit because the filter components are not separated by switches. For this case the problem reduces to a knowledge of the controller characteristics, so for illustrative purposes a pulse width modulator (PWM) is chosen as controller and the output spectrum corresponding to a monofrequency input modulation is Fourier analyzed to determine the conditions for which a simple describing function is representative of the PWM.

The difficulty previously encountered in nonlinear analysis of switched power stages is successfully surmounted in Chap. 3 by the semiheuristic development of a continuous power-stage model. The model is derived by a technique which averages discontinuous state variables over a time interval that is comparable with the switching period and hence is limited to response times greater than the averaging interval.

Equivalent circuits and analytic expressions for the transient and frequency responses of each power-stage type are derived in Chap. 4 from the averaged models. A linearized control-input transfer function is obtained for small amplitude variations of the averaged control and is then identified as that of an effective amplifier and filter in cascade. Analytic expressions for the amplifier and filter transfer functions which correspond to variations of either the source or control input are summarized in Sec. 4.4. Consequential observations in Chap. 4 include the modification of effective component values, and hence filter

characteristics, by the control input, and the presence of a factor in the control-input amplifier transfer function which has a real positive zero. After it was verified that present analysis is compatible with existent published results, Chap. 4 is concluded by computing critical gain factors and oscillation frequencies for marginal stability of a given feedback configuration. Analysis of a particular feedback configuration indicates that closed-loop stability of each power stage decreases as either the duty ratio or the source voltage increases.

The ultimate destiny of any model is its portrayal of the essential characteristics of reality; thus, the appropriate responses of both switched power stages and averaged power-stage models are experimentally determined in Chap. 5 with the aid of an analog computer and found to be in excellent correlation. Each component of the theoretical control-input transfer function is found to be necessary for correct prediction of the experimental frequency response; consequently, the theoretical and experimental frequency responses agree very well. Finally, it is determined experimentally that critical gain factors and oscillation frequencies for marginal closed-loop stability of switched power stages in a feedback configuration can be adequately predicted by theoretical analysis of the corresponding averaged power stages.

It has been shown here that the averaging technique is a powerful analytical tool for exposing tractable characteristics of switched circuits. With such a general tool, one can now consider research extensions into several areas of practical and theoretical interest

such as:

(a) A study of the effects of nonresistive loads and their variations,

(b) Evaluation of line (source) rejection and output impedance for a given feedback configuration,

(c) A study of comparative power-stage merits,

(d) Analysis of other feedback configurations,

(e) Feedback optimization for given performance criteria.

Appendix A

EVALUATION OF THE PWM SPECTRUM

The output d of the PWM defined in Eq. (2.20) can be expressed[8] as a superposition of unit steps:

$$d(t) = \sum_{k=-\infty}^{\infty} [h(t - kT) - h(t - kT - T\,\varepsilon(kT))], \qquad (A.1)$$

where

$$h(t) = \begin{cases} 0; & t < o \\ 1; & t > o \end{cases} . \qquad (A.2)$$

The problem is to evaluate the frequency components of d when the PWM input ε is given by

$$\varepsilon(t) = U + u \sin(\omega t - \phi) . \qquad (A.3)$$

To attain a solution, one must determine the coefficients in the Fourier series which represents d.

One intuitively expects the interaction of two independent frequencies, ω and $\omega_s = \frac{2\pi}{T}$, in the PWM output, so consider the two-dimensional

---

[8] Equation (A.1) assumes that the PWM input does not exceed saturation limits: $0 \leq \varepsilon(kT) \leq 1$.

method demonstrated by Rowe[6] to evaluate a double Fourier series. Although the method can be applied to find the spectrum of d directly, the derivation is considerably shortened if one uses some of Rowe's results to determine the spectrum of the time derivative of d.

Differentiate the expression in Eq. (A.1) to get the time derivative of d:

$$d'(t) = \sum_{k=-\infty}^{\infty} [\delta(t - kT) - \delta(t - kT - T\,\varepsilon(kT))]$$

$$= \sum\nolimits_1(t) - \sum\nolimits_2(t) \quad , \tag{A.4}$$

where

$$\sum\nolimits_1(t) \equiv \sum_{k=-\infty}^{\infty} \delta(t - kT) \tag{A.5}$$

$$\sum\nolimits_2(t) \equiv \sum_{k=-\infty}^{\infty} \delta(t - kT - T\,\varepsilon(kT))$$

$$= \sum_{k=-\infty}^{\infty} \delta(t - kT - TU - Tu \sin(\omega kT - \phi)) \quad , \tag{A.6}$$

and where $\delta(t)$ is the Dirac delta function. Since $\sum_1(t + pT) = \sum_1(t)$ for any interger p, the summation in Eq. (A.5) can be easily expanded in a Fourier series:

$$\sum\nolimits_1(t) = \sum_{m=-\infty}^{\infty} a_m e^{jm\omega_s t} \quad , \tag{A.7}$$

where

$$a_m = \frac{1}{T} \int_{-T/2}^{T/2} \sum\nolimits_1 (t)\ e^{-jm\omega_s t}\ dt$$

$$= \frac{1}{T} \qquad . \qquad \text{(A.8)}$$

Substitute Eq. (A.8) into Eq. (A.7) to get the frequency spectrum of $\sum_1$:

$$\sum\nolimits_1 (t) = \frac{1}{T} \sum_{m=-\infty}^{\infty} e^{jm\omega_s t} \qquad . \qquad \text{(A.9)}$$

Consider now the spectrum of $\sum_2$. Rowe used the two-dimensional method to derive the following identity:

$$\sum_{k=-\infty}^{\infty} \delta[y - kT - uT\cos(\omega kT)] \equiv \frac{1}{T} \sum_{m=-\infty}^{\infty} \sum_{n=-\infty}^{\infty} (-j)^n\ J_n[uT(m\omega_s + n\omega)]\ e^{j(m\omega_s + n\omega)y} \qquad \text{(A.10)}$$

where $J_n[z]$ is the Bessel function of the first kind with argument z and order n. The summation over k in Eq. (A.10) is similar to that in Eq. (A.6), but the absence of a phase term in the cosine makes direct analogy impossible; however, an appropriate phase term can be carried through Rowe's derivation to show that

$$\sum_{k=-\infty}^{\infty} \delta[y - kT - uT \sin(\omega kT - \phi)]$$

$$= \frac{1}{T} \sum_{m=-\infty}^{\infty} \sum_{n=-\infty}^{\infty} e^{-jn(\phi + \pi)} J_n[uT(m\omega_s + n\omega)] e^{j(m\omega_s + n\omega)y} . \quad (A.11)$$

Replace y by t - UT in Eq. (A.11) to get the frequency spectrum of $\sum_2$:

$$\sum_2(t) = \frac{1}{T} \sum_{m=-\infty}^{\infty} \sum_{n=-\infty}^{\infty} e^{-jn(\phi + \pi)} J_n[uT\Omega] e^{j\Omega(t - UT)} , \quad (A.12)$$

where

$$\Omega \equiv m\omega_s + n\omega . \quad (A.13)$$

Substitute Eqs. (A.9) and (A.12) into Eq. (A.4) to obtain the frequency spectrum of d':

$$d'(t) = \frac{1}{T} \sum_{m=-\infty}^{\infty} e^{jm\omega_s t} - \frac{1}{T} \sum_{\substack{m=-\infty \\ m \neq 0}}^{\infty} \sum_{\substack{n=-\infty \\ \Omega = m\omega_s + n\omega \neq 0}}^{\infty} e^{-jn(\phi + \pi)} J_n[uT\Omega] e^{j\Omega(t - UT)} . \quad (A.14)$$

The m = 0 term in $\sum_1$ cancels with the m = n = 0 term in $\sum_2$ so d' has no dc component. The indices m and n which conceivably make Ω zero do not contribute components to d' since $J_n(0) = 0$ for $n \neq 0$. Equation (A.14) can now be integrated to get the frequency spectrum of d:

$$d(t) = C_i + \sum_{\substack{m=-\infty \\ m \neq 0}}^{\infty} \frac{1}{jm\omega_s T} e^{jm\omega_s t} - \sum_{m=-\infty}^{\infty} \sum_{\substack{n=-\infty \\ \Omega = m\omega_s + n\omega \neq 0}}^{\infty} e^{-jn(\phi + \pi)} \frac{J_n[u\Omega T]}{j\Omega T} e^{j\Omega(t - UT)} . \quad (A.15)$$

The integration constant C_i can be evaluated for a special case of the PWM input; for example, if u = 0 in Eq. (A.3), then d has a single periodicity T in Eq. (A.1), and the spectrum of d is contained in Eq. (A.15). In particular, C_i is the dc component of d given by the expression:

$$\begin{aligned} C_i &= \frac{1}{T} \int_0^T d(t) \Big|_{u = 0} \, dt \\ &= \frac{1}{T} \int_0^T [h(t) - h(t - UT)] \, dt \\ &= U \end{aligned} \quad . \quad (A.16)$$

Appendix B

ANALOG COMPUTER SIMULATION

Experimental data was obtained from simulations on a Beckman 2132 analog computer of the switched and averaged models for each power-stage type. The simulation procedure is demonstrated here in detail for the boost power stage, but since the procedures are similar, only the final computer diagrams are given for the other types.

To make the actual system compatible with computer capabilities, amplitude and time must be scaled. Amplitude scale factors are chosen in such a way that the normalized amplitudes are always less than unity The actual switching frequency of 10 kHz is scaled down by a factor of 10^3 so simulated responses can be adequately computed and recorded. In the following discussions, the prefixes A, P, C, and M, respectively, refer to identification numbers for amplifiers, potentiometers, comparators, and multipliers.

B.1 Switched Boost Power Stage

The problem variables in Eq. (3.1) to (3.5), which characterize the switched boost power stage, are multiplied by the scale factors h to create normalized simulation variables X:

$$\left.\begin{aligned} X_i &= h_i\, i \\ X_v &= h_v\, v \\ \tau &= h_t\, t \\ X_{vs} &= h_{vs}\, v_s \\ X_{in} &= h_i\, i_n \\ X_{vn} &= h_v\, v_v \end{aligned}\right\} \qquad \text{(B.1)}$$

Notice that i_n and i have the same peak amplitude, so their scale factors are identical; likewise, for v_n and v. To illustrate the use of scale factors, the normalized version of Eq. (3.1) is given as

$$L \frac{h_t}{h_i} \frac{dX_i}{d\tau} = \frac{X_{vs}}{h_{vs}} - \frac{X_{vn}}{h_v} - \frac{R_\ell\, X_i}{h_i} \quad . \qquad \text{(B.2)}$$

For a constant source voltage V_s and with the scale factors given by

$$\left.\begin{aligned} h_t &= 10^3 \\ h_{vs} &= V_s^{-1} = 1/60 \\ h_i &= 1/10 \\ h_v &= h_{vs}/3 \end{aligned}\right\} \quad , \qquad \text{(B.3)}$$

the simulation equations are:

$$\frac{dX_i}{d\tau} = 1 - 0.500\, X_i - 3\, X_{vn} \qquad \text{(B.4)}$$

$$\frac{dX_{vc}}{d\tau} = 1.312\, X_{in} - 0.3935\, X_{vc} \qquad \text{(B.5)}$$

$$X_v = 0.9836\, X_{vc} + 0.0546\, X_{in} \tag{B.6}$$

$$X_{vn} = \begin{cases} 0 \text{ ; switch state "on"} \\ X_v \text{; switch state "off"} \end{cases} \tag{B.7}$$

$$X_{in} = \begin{cases} 0 \text{ ; switch state "on"} \\ X_i \text{; switch state "off"} \end{cases} . \tag{B.8}$$

The computer diagram to solve Eqs. (B.4) to (B.8) is shown in Fig. B.1. The two double-throw switches are relay contacts which simulate the actual switches S and S' and are further discussed in the following section.

B.2 PWM Switch Controller

The pulse-width-modulator described in Sec. 2.3 is simulated to operate the power-stage switches. Because the PWM describing function used in the analysis assumes that the dimensionless input is restricted between zero and unity, only the linear portion of the PWM characteristic shown in Fig. 2.3 must be simulated.

Without belaboring the synthesis, the computer diagram to simulate the linear PWM characteristic is shown in Fig. B.2. Each comparator C_a, C_b, and C_c operates a double-pole double-throw relay switch in such a way that a positive comparator input causes switch connections to be made as shown: the opposite switch connections correspond to a negative comparator input. Operation of the simulated PWM is explained with the aid of typical waveforms shown in Fig. B.3. A periodic timing waveform

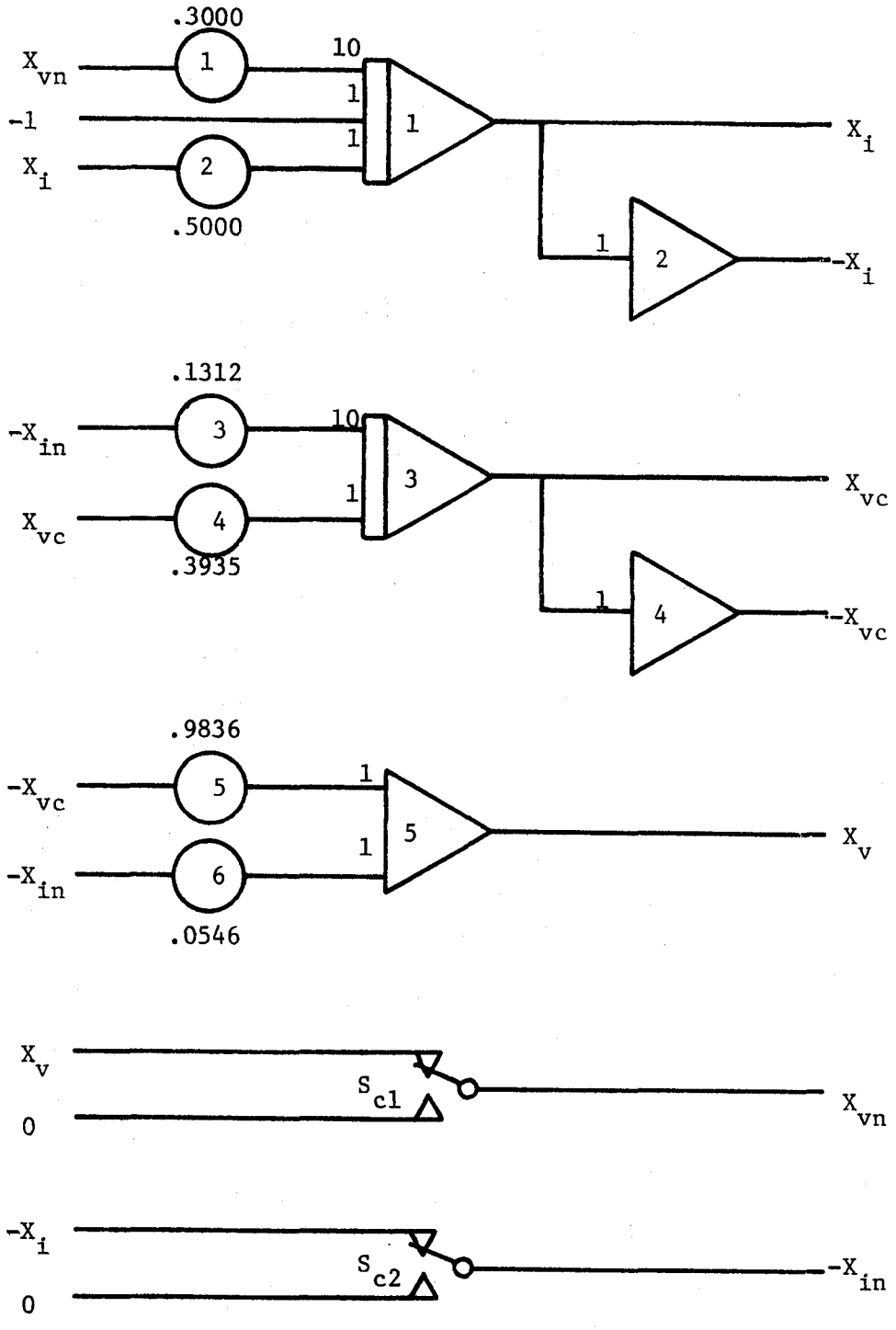

Fig. B.1 Computer diagram of switched boost power stage.

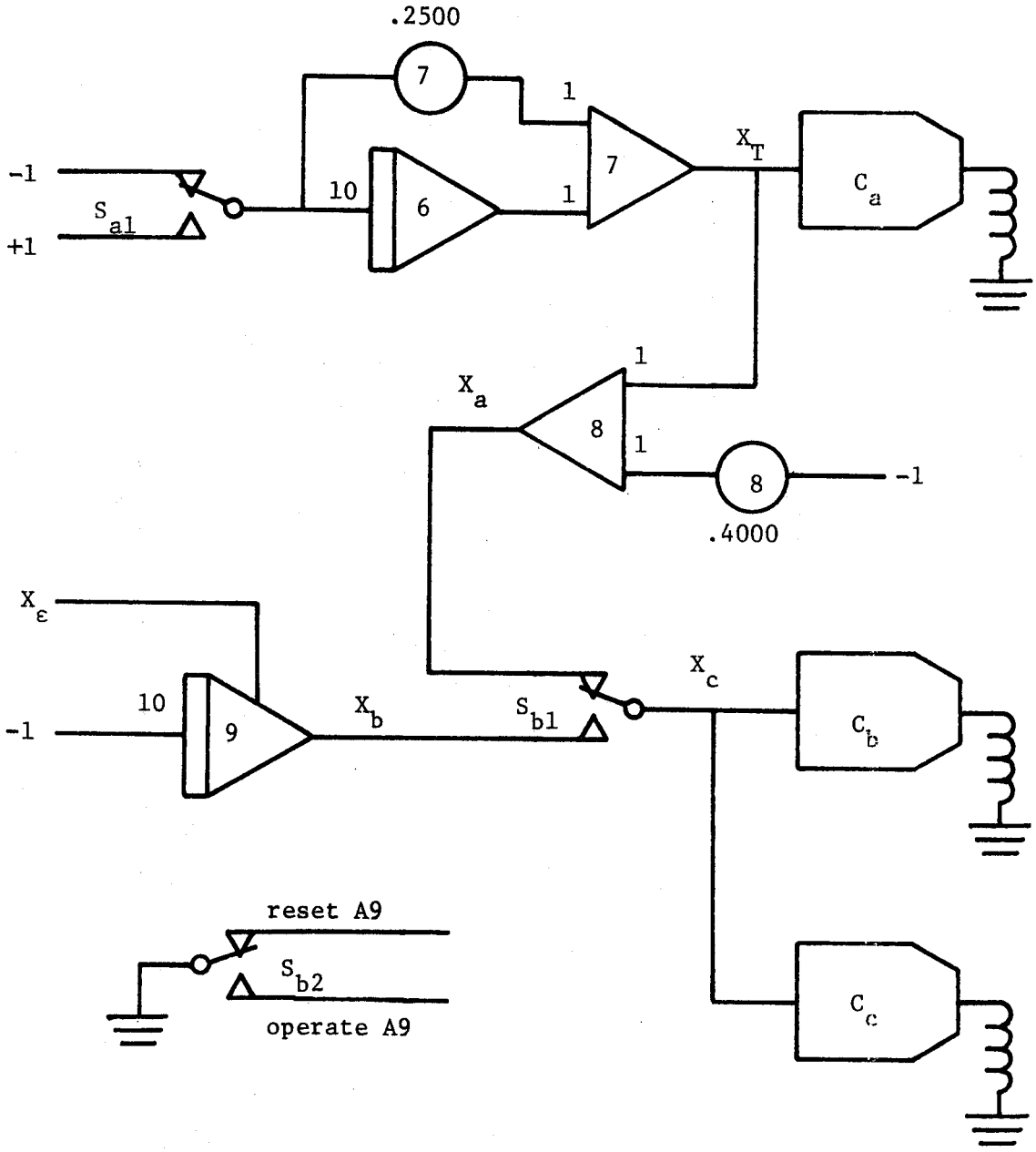

Fig. B.2 Computer diagram of PWM.

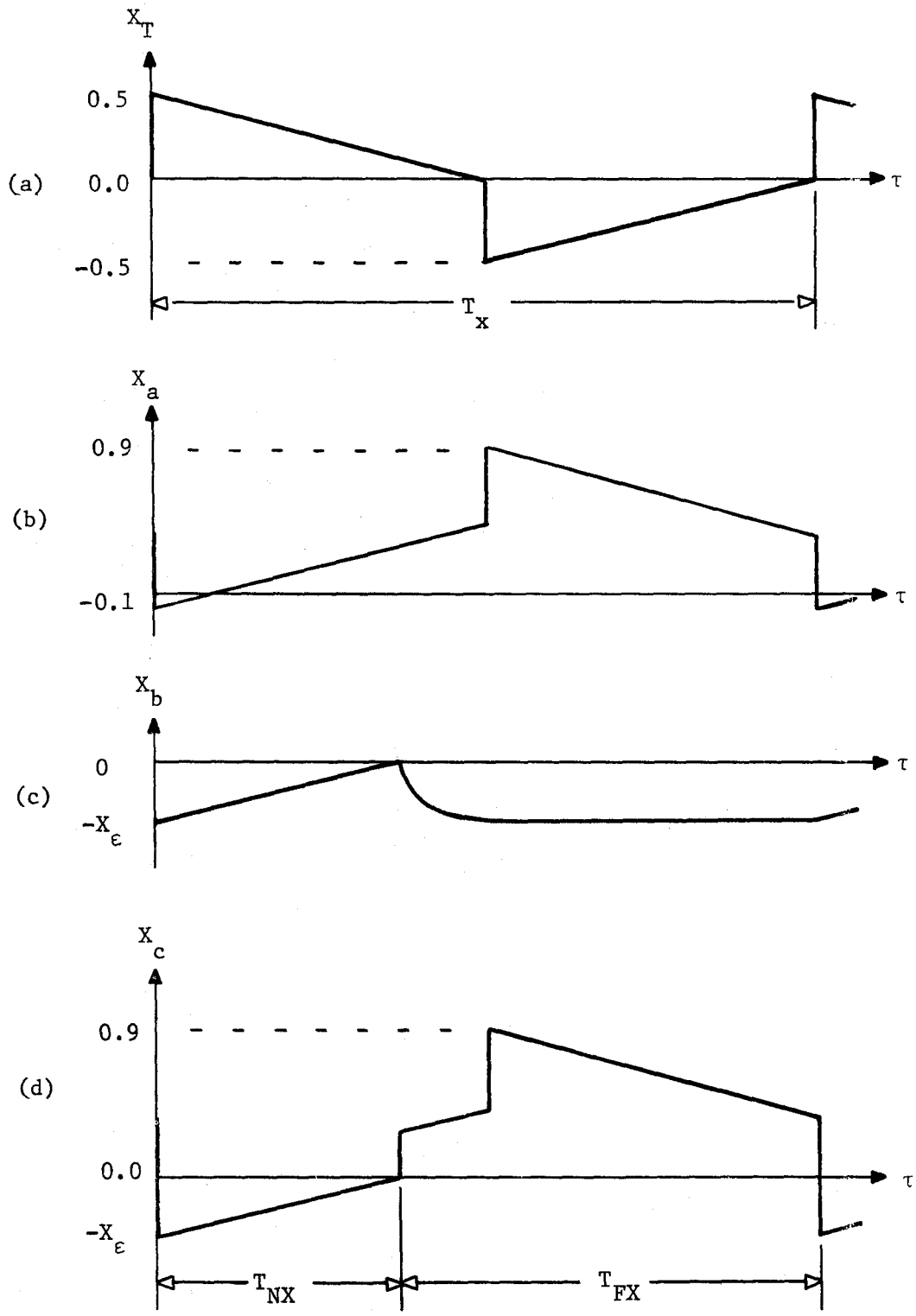

Fig. B.3 Computer waveforms in PWM simulation.

with period T_x is generated in the upper portion of the computer diagram and is shown in Fig. B.3(a); by adjusting P7, one can set $T_x = 0.1$ sec as specified by the time scale factor in Eq. (B.3). If the input X_c of comparator C_b is positive, then the position of switches S_{b1} and S_{b2} will remain as shown until the quantity X_a illustrated in Fig. B.3(b) becomes negative. During this time interval the integrator A9 is reset to the value of X_ε, which is the dimensionless PWM input (notice that the scale factor which relates ε to X_ε is unity since in its definition the actual PWM input is properly scaled for simulation). When X_c is negative, then A9 operates to increase X_b at a linear rate as shown in Fig. B.3(c) until X_b becomes positive, at which time the comparator C_b again changes state. The resultant waveform of X_c shown in Fig. B.3(d) drives an additional comparator C_c which operates the contacts S_{c1} and S_{c2} used in Sec. B.1 to simulate the switched power stage. The computer configuration described above successfully divides a uniform timing period T_x into two subintervals as required to simulate the PWM: the duration of the first subinterval is proportional to the value of the input sampled at the initiation of T_x.

B.3 Averaged Boost Power Stage

Some of the normalized equations -- namely, Eqs. (B.4) to (B.6) -- which describe the switched boost power stage also apply for the corresponding averaged model shown in Fig. 3.5; however, the driving functions X_{vn} and X_{in} are no longer switched, but continuous. If the analog variable X_d represents the slowly-varying (averaged) components of the digital switch-drive signal, then the driving functions suitable for simulation

of the averaged boost power-stage model are

$$X_{vn} = (1 - X_d)\, X_v \qquad (B.9)$$

$$X_{in} = (1 - X_d)\, X_i \qquad (B.10)$$

The computer diagram to simulate the averaged boost stage is shown in Fig. B.4. Equations (B.9) and (B.10) are implemented with analog multipliers M1 and M2.

Step changes and sinusoidal modulations are readily programmed for the analog inputs X_ε and X_d to investigate the various responses of the switched power stage and its averaged model.

B.4 Buck and Buck-Boost Power Stages

The computer diagrams used to simulate the switched and averaged models of the buck and buck-boost power stages are presented for reference in Figs. B.5 to B.8. The scale factors which normalize the problem variables are listed below.

Scale factor	Buck	Buck-boost
h_t	10^3	10^3
h_{vs}	1/60	1/60
h_i	2/5	1/20
h_v	1/60	1/240

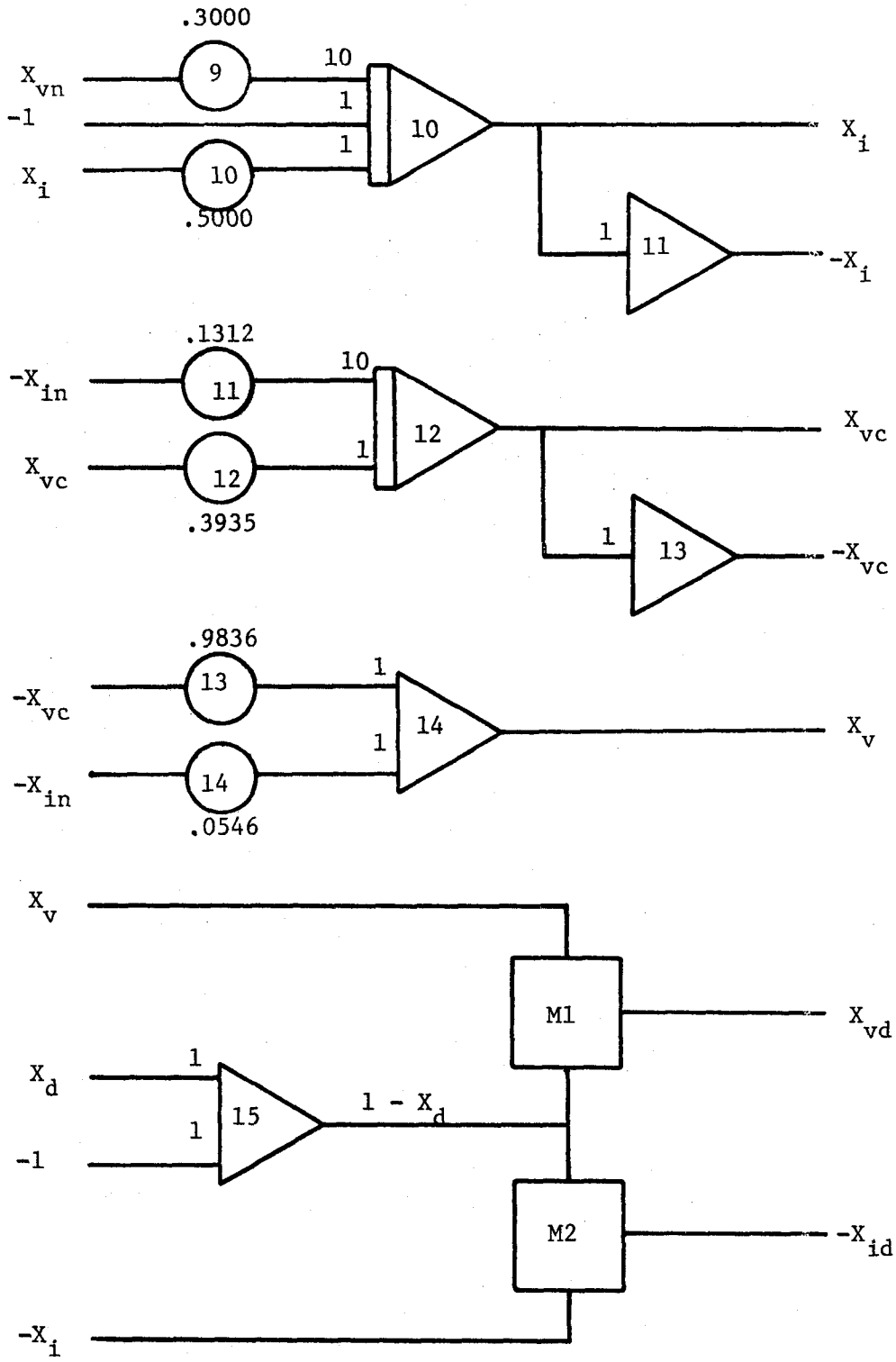

Fig. B.4 Computer diagram of averaged boost power stage.

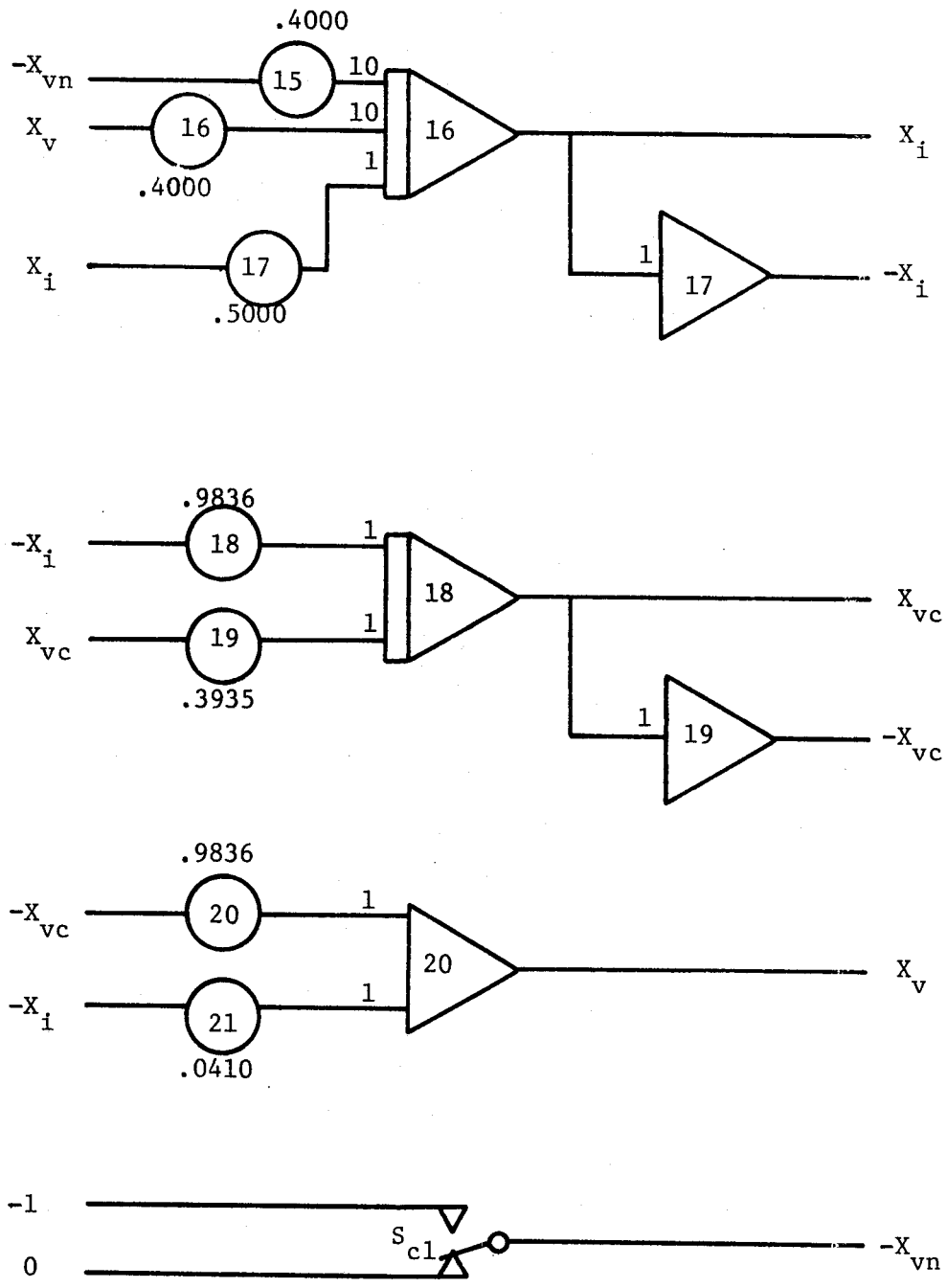

Fig. B.5 Computer diagram of switched buck power stage.

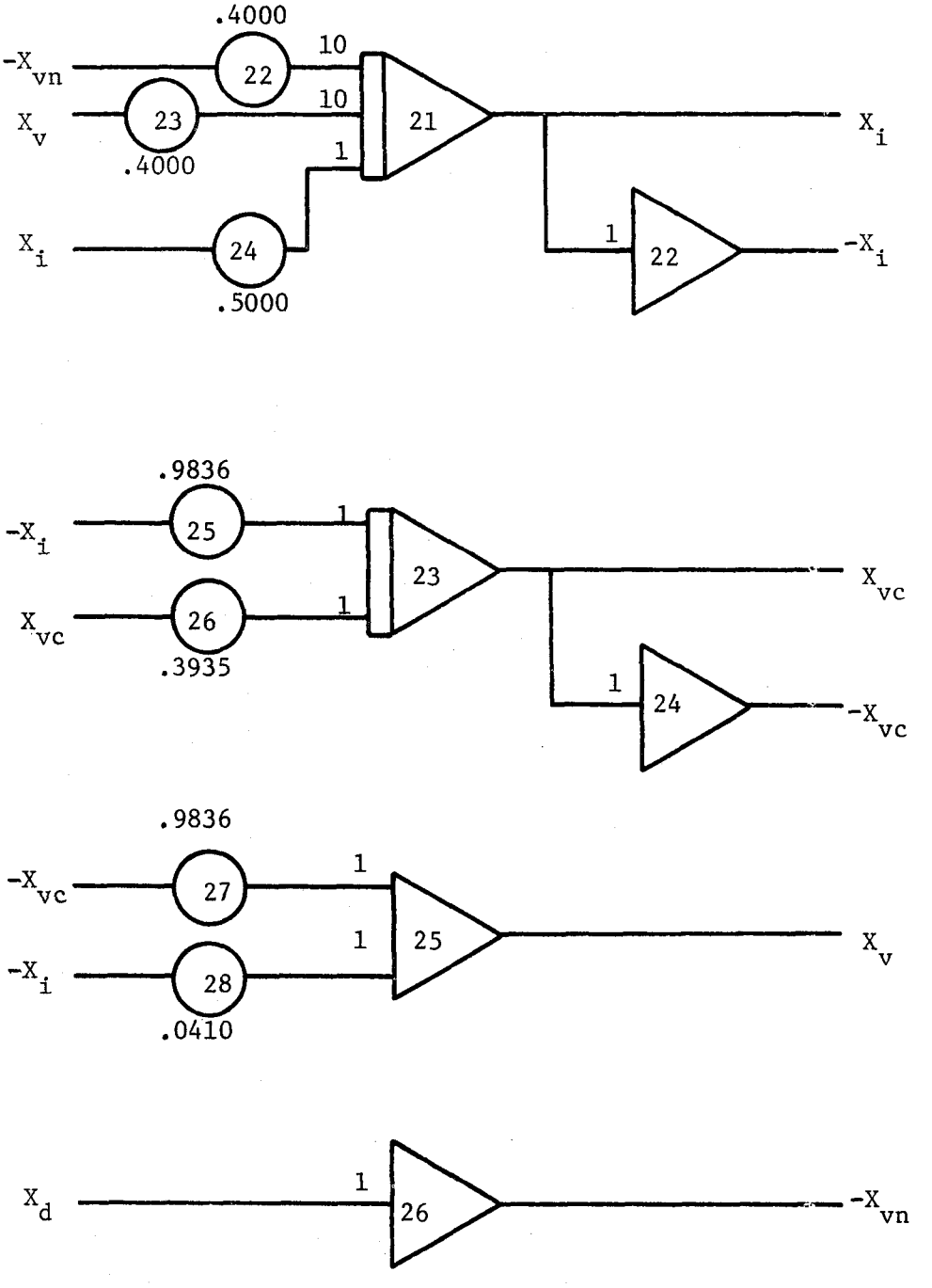

Fig. B.6 Computer diagram of averaged buck power stage.

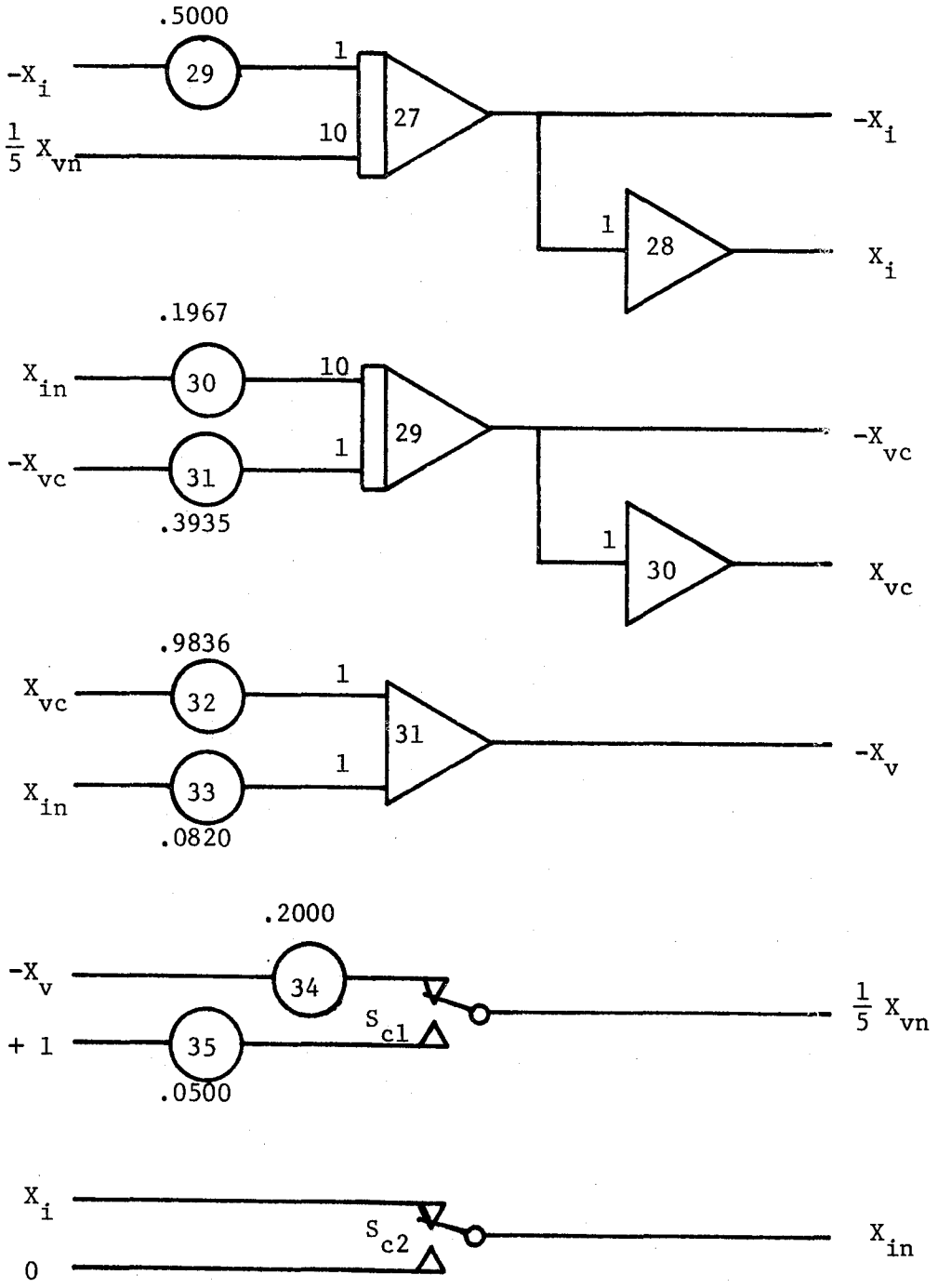

Fig. B.7 Computer diagram of switched buck-boost power stage.

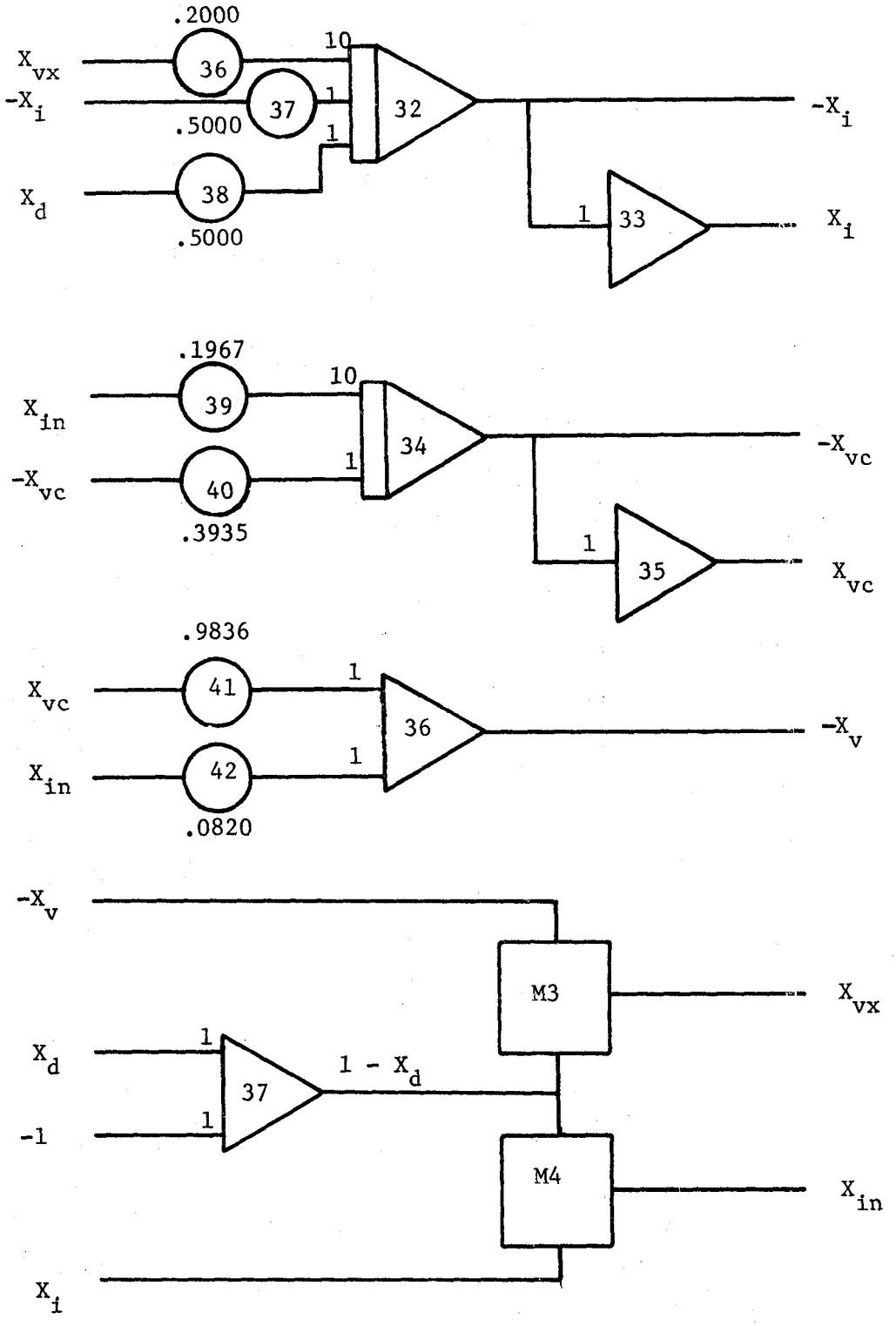

Fig. B.8 Computer diagram of averaged buck-boost power stage.

REFERENCES

1. O. A. Kossov, "Comparative Analysis of Chopper Voltage Regulators with LC Filter," IEEE Trans. Magnetics MAG-4, pp. 712-715, December 1968.
2. L. R. Poulo and S. Greenblatt, "Research Investigations on Feedback Techniques and Methods for Automatic Control," Res. and Dev. Tech. Rep. ECOM-0520-F, pp. 156-165, April 1969.
3. E. E. Landsman, "Modular Converters for Space Power Systems," Power Conditioning Specialists Conf. Record, NASA Goddard Space Flight Center, Greenbelt, Md., April 20-21, 1970, pp. 87-99.
4. W. R. Bennett, "New Results in the Calculation of Modulation Products," Bell System Tech. J. 12, pp. 228-243, April 1933.
5. H. S. Black, Modulation Theory (D. Van Nostrand Co. Inc., Princeton, N. J., 1953), pp. 266-276.
6. H. E. Rowe, Signals and Noise in Communications Systems (D. Van Nostrand Co. Inc., Princeton, N. J., 1965), pp. 257-280.
7. M. Abramowitz and I. Stegun, Handbook of Mathematical Functions (Dover Pub. Inc., New York, 1965), p. 361.
8. B. A. Wells, B. T. Brodie, I. M. H. Bábaá, "Analog Computer Simulation of a dc-to-dc Flyback Converter," Supp. to IEEE Trans. Aerospace AES-3, pp. 399-409, November 1967.